

**The effect of Secoisolariciresinol diglucoside on oxidative stress  
and inflammation in cardiac iron overload**

A thesis presented to  
The Faculty of Graduate Studies  
of  
Lakehead University  
by  
Stephanie Puukila

In partial fulfillment of requirements  
for the degree of  
Master of Science in Biology

June 12, 2012

## **Abstract**

Chronic cardiac iron overload directly correlates with cardiac dysfunction and may ultimately cause heart failure. Although recent studies have suggested that altered calcium homeostasis and increased reactive oxygen species (ROS) play roles in iron overload-induced cardiac dysfunction, the exact mechanism(s) of oxidative stress-mediated cardiac inflammation, matrix remodelling and cell death remain unclear. Here we examined iron-induced cardiac damage in terms of oxidative stress, inflammation and apoptosis in an *in vitro* model of cardiac iron overload using the H9c2 cardiac cells. We also investigated the effect of secoisolariciresinol diglucoside (SDG), a component of flaxseed, on the above mentioned parameters. H9c2 cells were treated with 50  $\mu$ M iron and a pre-treatment of 500  $\mu$ M SDG was performed by dissolving SDG into serum- and antibiotic-free Dulbecco's Modified Eagle's Medium and for each treatment type, cells were incubated for 24 hours. Cardiac iron overload resulted in increased intracellular ROS while SDG treatment prevented this increase, as measured by the H<sub>2</sub>DCFDA assay using flow cytometry. Increased gene expression of inflammatory mediators Tumor Necrosis Factor (TNF)- $\alpha$ , interleukin (IL)-10 and interferon (IFN) $\gamma$ , as well as matrix metalloproteinases (MMP)-2 and 9, and antioxidants glutathione reductase (GSR), superoxide dismutase (SOD)-2 and peroxiredoxin (Prdx)-6 and a decrease in SOD concentration correlated with increased apoptosis as measured by active caspase 3/7 activity and increase in FOXO3. SDG attenuated the increase of gene expression of inflammatory and apoptosis mediators as well as the increase of caspase 3/7 activity caused by iron treatment. SDG also lead to an increase in gene expression of antioxidants

GSR, SOD-2 and Prdx-6 when compared to iron treatment. Cardiac iron overload also resulted in an increase in protein levels of p70S6K1 and a decrease in the AMPK levels. The increase of p70S6 and decrease in AMPK levels was prevented by SDG. Pre-treatment with SDG attenuated the iron-induced increases in oxidative stress, inflammation and apoptosis, suggesting a cardio-protective role for SDG against cardiac iron overload.

## Lay Summary

The Lakehead University Department of Biology's lists its mission statement as: "Faculty and students in the Department of Biology are bound together by a common interest in explaining the diversity of life, the fit between form and function, and the distribution and abundance of organisms." This research project, centered in the realm of the human sciences, aims to understand the mechanisms behind cardiac iron overload in an *in vitro* model and how secoisolariciresinol diglucoside, a component found in flax seed, can act as a natural therapeutic agent capable of protecting cardiac cells during iron overload.

## Acknowledgements

I would like to thank my supervisor, Dr. Neelam Khaper, for her guidance, support and motivation during this project and throughout my undergraduate studies. I would like to thank my committee members, Dr. Schraft and Dr. Yang. I would like to thank Sean Bryan for his guidance and assistance during my time in the lab. I would also like to thank Jessica Abdel-Malak, Anna Laakso, Carli Gurney and Adrian Agostino for their assistance on this project. Finally, I would like to thank all of the people that work in the laboratory for creating an enjoyable work environment. Working in the Northern Ontario School of Medicine research laboratory has been a truly rewarding experience.

## Abbreviations

AP - Activator protein

AMPK - Adenosine monophosphate-activated protein kinase

ATP - Adenosine triphosphate

Atg - Autophagy protein

Bcl - B-cell lymphoma

Bax - B-cell lymphoma-associated X protein

$\beta$ 2M - Beta-2 microglobulin

DED - Death effector domain

DMT - Dimetal transporter

FADD - Fas-associated death domain protein

Fe<sup>3+</sup> - Ferric

Fe<sup>2+</sup> - Ferrous

FOXO - Forkhead box subfamily O

GSR - Glutathione reductase

HFE - Hemochromatosis associated

HJV - Hemojuvelin

H63D - Histidine at position 63

H<sub>2</sub>O<sub>2</sub> - Hydrogen peroxide

°OH – Hydroxyl radical

IFN $\gamma$  - Interferon gamma

ISGs - Interferon-stimulated genes

IL-10 - Interleukin-10

JNK - Jun N-terminal kinases

MRI - Magnetic resonance imaging

mTOR - Mammalian target of rapamycin

MAP1lc3B - Microtubule-associated proteins light chain 3

mtDNA - Mitochondrial DNA

SOD2 - Manganese superoxide dismutase

MMP - Matrix metalloproteinase

MI - Myocardial infarction

NTBI - Non-transferrin bound iron

NF- $\kappa$ B - Nuclear factor-kappaB

LTCC - L-type Ca<sup>2+</sup> channels

p70S6K1 - p70S6 Kinase 1

Prdx6 - Peroxiredoxin 6

PI3K - Phosphoinositide 3-kinase

PARP - Poly (ADP-ribose) polymerase

qPCR - Quantitative polymerase chain reaction

ROS - Reactive oxygen species

RIP - Receptor-interacting protein

SDG - Secoisolariciresinol diglucoside

STAT - Signal transducer and activator of transcription

O<sub>2</sub><sup>•-</sup> - Superoxide anion

SOD - Superoxide dismutase

TfR - Transferrin receptors

TNF- $\alpha$  - Tumor necrosis factor-alpha

TNFR - Tumor necrosis factor receptor

TRADD - Tumor necrosis factor receptor associated death domain

TRAF - Tumor necrosis factor receptor associated factor

# Table of Contents

<b>Lay Summary</b> .....	i
<b>Acknowledgements</b> .....	ii
<b>Abbreviations</b> .....	iii
<b>List of Tables and Figures</b> .....	ix
<b>Introduction</b> .....	1
<i>Iron absorption and transport-Transferrin bound iron</i> .....	1
<i>Iron absorption and transport-Non-transferrin bound iron</i> .....	3
<i>Primary iron overload</i> .....	4
<i>Secondary iron overload</i> .....	5
<i>Cardiac iron overload</i> .....	6
<i>Transport of iron in the heart</i> .....	7
<i>Diagnosis</i> .....	8
<i>Treatment</i> .....	10
<i>Reactive oxygen species</i> .....	11
<i>Inflammation</i> .....	13
<i>Tumor necrosis factor-alpha</i> .....	15
<i>Interleukin 10</i> .....	16
<i>Interferon gamma</i> .....	18
<i>Matrix metalloproteinase</i> .....	18
<i>Antioxidants</i> .....	19

<i>Apoptosis</i> .....	21
<i>Autophagy</i> .....	23
<i>Cell survival</i> .....	24
<i>Secoisolariciresinol diglucoside</i> .....	26
<b>Methods</b> .....	30
<i>H9c2 cardiac cell line</i> .....	30
<i>Ammonium iron (III) citrate preparation</i> .....	30
<i>Secoisolariciresinol diglucoside</i> .....	30
<i>Trypan Blue Exclusion assay</i> .....	30
<i>MTT assay</i> .....	31
<i>Reactive oxygen species indicator assay</i> .....	32
<i>Active caspases 3/7-based apoptosis detection assay</i> .....	33
<i>Superoxide dismutase activity assay</i> .....	34
<i>RNA isolation</i> .....	35
<i>Automated electrophoretic RNA analysis</i> .....	36
<i>cDNA synthesis</i> .....	36
<i>Quantitative real-time polymerase chain reaction</i> .....	36
<i>Total protein assay</i> .....	38
<i>Sodium dodecyl sulfate-polyacrylamide gel electrophoresis</i> .....	39
<i>Electrophoretic transfer</i> .....	40
<i>Protein immunoblot and antibodies</i> .....	40

<i>Chemiluminescent imaging and densitometry</i> .....	41
<i>Statistics</i> .....	41
<b>Results</b> .....	43
<b>Discussion</b> .....	70
<b>Conclusion</b> .....	77
<b>References</b> .....	78

## List of Tables and Figures

**Table 1** Quantitative real-time PCR primers

**Figure 1** The fenton reaction

**Figure 2** The vicious cycle between oxidative stress and inflammation

**Figure 3** Chemical structure of SDG Secoisolariciresinol diglucoside

**Figure 4** Iron overload induces inflammation, oxidative stress and cell death

**Figure 5** Effect of iron on cell viability

**Figure 6** Effect of SDG on iron induced decrease of cell viability

**Figure 7** Effect of SDG on iron-induced oxidative stress in cardiomyocytes

**Figure 8.1** Effect of SDG on iron-induced tumour necrosis factor  $\alpha$  mRNA expression in cardiomyocytes

**Figure 8.2** Effect of SDG on iron-induced interleukin 10 mRNA expression in cardiomyocy

**Figure 8.3** Effect of SDG on iron-induced interferon  $\gamma$  mRNA expression in cardiomyocytes

**Figure 9.1** Effect of SDG on iron-induced matrix metalloproteinase 2 mRNA expression in cardiomyocytes

**Figure 9.2** Effect of SDG on iron-induced matrix metalloproteinase 9 mRNA expression in cardiomyocytes

**Figure 10.1** Effect of SDG on iron-induced glutathione reductase mRNA expression in cardiomyocytes

**Figure 10.2** Effect of SDG on iron-induced peroxiredoxin 6 mRNA expression in cardiomyocytes

**Figure 10.3** Effect of SDG on iron-induced superoxide dismutase 2 mRNA expression in cardiomyocytes

**Figure 11** Effect of iron and SDG on SOD concentration

**Figure 12** Effect of SDG on iron-induced cardiomyocyte apoptosis

**Figure 13.1** Effect of iron and SDG on Caspase 3 protein expression

**Figure 13.2** Effect of iron and SDG on FOXO3 protein expression

**Figure 13.3** Effect of iron and SDG on Bax protein expression

**Figure 13.4** Effect of iron and SDG on Bcl2 protein expression

**Figure 14** Effect of SDG on iron-induced MAP1c3b1 mRNA expression in cardiomyocytes

**Figure 15** Effect of iron and SDG on p70S6 Kinase protein expression

**Figure 16** Effect of iron and SDG on AMPK protein expression

## Introduction

Iron is a transition metal that is essential to almost all eukaryotic cells for cell metabolism and function. Iron is a component of hemoglobin, myoglobin, mitochondrial electron transport chain enzymes, the cytochrome p450 system and many other proteins [1; 2]. The biological importance and toxicity of iron is largely attributable to its ability to undergo oxidation reduction reactions between its ferric  $\text{Fe}^{3+}$  and ferrous  $\text{Fe}^{2+}$  states [1; 3]. However, an over abundance of iron can result in such complications as cardiomyopathy, cirrhosis, and diabetes [1; 3; 4; 5]. Primary iron overload, or hemochromatosis, is a common autosomal recessive disorder whereby mutation of the hemochromatosis associated gene causes impaired feedback inhibition of iron uptake, resulting in maximal absorption [1; 3; 5]. Secondary iron overload typically derives from dietary or transfusional excesses, iron-loading anemias, and chronic liver diseases [2; 4]. As the iron burden on the body increases it outpaces the ability of transferrin to bind to it resulting in increased amounts of labile plasma iron [5] and its deposition in various tissues, including the heart [3].

### *Iron absorption and transport-Transferrin bound iron*

The human body uses about 20 mg of iron per day for hemoglobin synthesis, the production of approximately 200 billion erythrocytes and an additional 4-5 mg for the production of cellular proteins including mitochondrial proteins and muscle myoglobin [1; 2; 6]. Total iron content in normal individuals is relatively fixed, with men (50 mg Fe/kg) having slightly higher iron levels than women (40 mg/kg) [1]. Dietary iron exists

in two main forms: heme iron, ferrous iron from hemoglobin and myoglobin in animal tissue, and non-heme iron, ferric oxides and salts, ferritin, and lactoferrin [7; 8]. Most of the iron in the body is contained in hemoglobin but it can also be stored in hepatocytes and macrophages as ferritin [1; 7]. Iron equilibrium requires carefully controlled and efficient absorption by duodenal enterocytes, release into plasma, transport in plasma by transferrin, storage, release from storage, uptake by erythroblasts for synthesis of heme and recycling from senescent erythrocytes [7]. Iron is delivered to most cells of the body via the blood as ferric iron bound to serum protein transferrin. Transferrin-bound iron is relatively nonreactive. Movement of iron within the body involves a combination of transporters, including transferrin receptors (TfR1 and TfR2), divalent metal transporter 1 (DMT1), ferroportin and a heme receptor [1]. Iron transport requires redox cycling between the ferric ( $\text{Fe}^{3+}$ ) to the ferrous ( $\text{Fe}^{2+}$ ) states, which can be done by several ferric reductases including duodenal-cytochrome b and ferroxidases, such as ceruloplasmin and hephaestin [1; 6; 9]. The most prevalent method for iron transport involves the binding of plasma transferrin-bound iron to TfR1 or TfR2. TfR1 is expressed in all cells while TfR2 is only expressed in hepatocytes, duodenum and erythroid precursors [1; 6]. Transferrin and TfR1/2 complexes are internalized into acidic endosomes where the iron is reduced to  $\text{Fe}^{2+}$  and released into the cytosol by the DMT1. Iron also enters cells by DMT1 transporters, which are  $\text{H}^+$ /divalent metal symporters capable of transporting many other divalent metals. DMT1 and transferrin iron transport systems are regulated in a negative-feedback manner by iron responsive elements [1; 10]. Ferroportin is a divalent iron export protein that is expressed on the surface of enterocytes, macrophages, hepatocytes and placental cells [1; 9]. Ferroportin exports reduced iron into the plasma, whereupon

the iron is oxidized and binds to transferrin [1; 6]. Finally, iron can also be imported as a heme-iron complex into selected tissues such as intestinal enterocytes and reticulo-endothelial macrophages by a heme receptor. Once internalized heme-bound iron is released by heme oxygenase [1]. About 1 mg of iron is lost daily in the stool from sloughed iron-containing duodenal enterocytes and from sloughed skin cells [7; 11]. An average additional 1 mg of iron is lost daily from menstruation in women and bleeding from other causes will further increase iron loss [7].

#### *Iron absorption and transport-Non-transferrin bound iron*

Although cellular iron uptake is tightly regulated elevated body iron does occur under several disease conditions due to excessive intestinal iron absorption or repeated blood transfusions. This leads to surplus iron accumulation in tissues such as liver, pancreas and heart. When transferrin becomes iron-saturated excess free iron resides as non-transferrin bound iron (NTBI) in the blood stream, which is then transported into selected tissues [1]. The actual mechanism of NTBI transport into cells currently remains unclear, particularly since it is clear that certain tissues are more susceptible to NTBI than others. Cardiomyocytes, neurons, beta cells of the pancreas and pituitary cells seem to be popular targets of NTBI. Reduction of  $\text{Fe}^{3+}$  to  $\text{Fe}^{2+}$  by a membrane-associated ferri-reductase system is required for NTBI uptake into excitable cells [1; 10]. At first it was suggested that DMT1 was responsible for NTBI uptake into excitable cells but DMT1 protein expression decreases when iron is elevated in cardiomyocytes and DMT1 is expressed at extremely low levels in most excitable tissue including the heart [1; 12; 13]. Recently it has been suggested that divalent metal transporters L-type  $\text{Ca}^{2+}$  channels

(LTCC) are responsible for the transport of NTBI into cells. Excitable cells and tissues with the greatest risk in iron overload have high duty cycles for LTCC activity [1], supporting the idea that these channels are responsible for cellular uptake of NTBI.

### *Primary iron overload*

Primary iron overload, commonly referred to hemochromatosis, is the most common hereditary genetic disorder affecting Canadians [14]. There are four distinctive subtypes with Type 1, or classical hemochromatosis, being the most common [1; 2; 9]. It is caused by an autosomal recessive disorder mutation of the hemochromatosis associated (*HFE*) gene. A Cys282Tyr mutation on the major intracellular histocompatibility-like protein responsible for heterodimeric protein formation in the endoplasmic reticulum has been identified as a main cause of hemochromatosis. The *HFE* gene is involved with iron absorption of the gastro intestine and facilitates the binding of transferrin, iron's carrier protein in the blood. The Cys282Tyr mutation results in the gene's inability to provide feedback inhibition of iron uptake in the gut wall. The intestines perpetually interpret a strong transferrin signal as if the body were deficient in iron. This leads to maximal iron absorption from ingested foods [1; 3]. Type 1 hemochromatosis can also be caused by a substitution of aspartate for histidine at position 63 (H63D) of the *HFE* gene. The Cys282Tyr mutation is primarily limited to individuals of northern European ancestry with an allele frequency of about 10%, while the H63D mutation occurs at allele frequencies greater than 5% in Mediterranean/ Middle East regions and the Indian subcontinent [1; 3; 15]. Type 2 hemochromatosis, or juvenile hemochromatosis, is also an autosomal recessive inherited disorder. It results in a large amount of iron burdens and

organ damage at a young age, mostly under the age of 30. The disorder is caused by mutations in an iron-regulatory protein hemojuvelin (*HJV* gene). Type 3 is also an autosomal recessive condition caused by a mutation in the transferrin receptor *TfR2*, which normally allows iron to enter a cell. The final type, Type 4, is the only type of primary hemochromatosis that is inherited as an autosomal dominant condition. It is linked to mutations and altered function of the iron exporter ferroportin (specifically the *SLC40A1* gene), the second most common cause of hemochromatosis after mutations in *HFE* [1; 3; 9]. The excess iron is deposited in the cytoplasm of parenchymal cells of various organs and tissues, including the liver, pancreas and heart [16]. Long-standing hemochromatosis can lead to increased complications of heart failure, liver cancer, and cirrhosis. Also, heterozygous individuals have an increased risk for myocardial infarction and cerebrovascular disease [4].

### *Secondary iron overload*

Secondary iron overload is caused by an underlying disease or condition, usually a blood disorder, which results in increased free iron. In patients with secondary iron overload total serum iron levels range from 20 to 60  $\mu\text{M}$ , while normal range is 8-15  $\mu\text{M}$  [1; 6]. It occurs in patients with disorders of erythropoiesis, the process by which red blood cells are produced, which cause hereditary anemias including  $\alpha$ -thalassemia,  $\beta$ -thalassemia and sickle cell anemia [1; 16]. In these patients iron overload occurs because of repeated blood transfusions coupled with increased gastrointestinal iron absorption, leading to conditions similar to those seen in primary iron overload. With blood transfusions iron burden can increase very rapidly through the combined impact of

increased iron absorption and transfusion derived iron (in hemoglobin). Therefore these patients may present with the consequences of iron toxicity to the liver, heart, and pancreas many years earlier than do patients with primary iron overload [16].  $\alpha$ - and  $\beta$ -thalassemias are caused by mutations resulting in defective synthesis of the  $\alpha$ - and  $\beta$ -globin chains of hemoglobin, respectively, and are the most common monogenetic diseases in humans [1]. Individuals with  $\beta$ -thalassemia are characterized by profound anemia, so regular blood transfusions are necessary [16]. Sickle cell anemia is the most common and severe form of sickle cell disease, caused by the homozygous presence of sickle haemoglobin due to a glutamate to valine mutation in the beta-globulin gene (Hgb S) [1; 3]. Patients with sickle cell disease, like individuals with  $\beta$ -thalassemia, require chronic transfusions [4]. Several other clinical disorders are associated with secondary iron overload including sideroblastic anemia, myelodysplastic syndrome, acute myeloid leukemia, congenital dyserythropoietic anemia and chronic renal failure. Sideroblastic anemia is characterized by mitochondrial iron overload in erythroblast and is associated with systemic iron overload, suggesting an important role for mitochondria in cellular iron metabolism [1; 17]. In patients with chronic renal failure and end-stage kidney disease, anemia is common due in part to erythropoietin deficiency that often necessitates therapy with intravenous iron [1; 4]. To prevent iron accumulation caused by blood transfusions the use of intensive chelation therapy is required, starting at the time that there is a commitment to long-term transfusion [16].

#### *Cardiac iron overload*

Iron overload cardiomyopathy is a common cause of cardiovascular deaths worldwide in the second and third decades of life [3; 1]. The amount of myocardial iron accumulation predicted to occur over 20 years, a relevant period for patients with iron overload, is estimated to be about 10 mg of iron per gram of myocardial tissue [1; 18]. In patients with hemochromatosis or thalassemia major cardiovascular disease contributes significantly to their mortality and morbidity [1; 19]. It has been shown to lead to restrictive cardiomyopathy with prominent early diastolic dysfunction that invariably progresses to end-stage dilated cardiomyopathy characterized by impaired systolic function and reduced mean arterial blood pressure often accompanied by arrhythmias including atrioventricular block, conduction defects, bradyarrhythmias, tachyarrhythmias and sudden cardiac death [1; 3; 19; 20]. Iron overload may also facilitate myocardial ischemia-reperfusion injury because of an increased formation of ROS and reduce antioxidant reserve [1; 3]. Iron accumulation occurs initially in the ventricular followed by the atrial myocardium. During the progression of iron overload, iron accumulates in the ventricular wall, the epicardium, the papillary muscles, and the ventricular septum. First degree heart block and supraventricular arrhythmias are correlated with the extent of iron deposition in the atrial myocardium [2; 22]. Although the precise mechanism underlying cardiomyocyte dysfunction induced by iron overload is not entirely clear [1] recent studies suggest that generation of free radicals play an important role.

#### *Transport of iron in the heart*

Recent studies suggest that LTCCs are responsible for the transport of NTBI into the cardiac cells. LTCCs are primarily utilized for the transport of  $\text{Ca}^{2+}$  but they are able to transport many other divalent cations. LTCCs are the only  $\text{Fe}^{2+}$  transporter whose

activity increases with elevated iron, consistent with NTBI uptake in the heart under iron overload conditions [1; 23]. The link between LTCCs and iron uptake in excitable tissues is consistent with the observation that iron uptake is approximately tenfold higher in cardiomyocytes, that have a large amount of LTCCs, than in fibroblasts, that have few LTCCs [1; 24; 25]. Studies with mice using LTCC blockers amlodipine and verapamil reduced intracellular myocardial iron accumulation and reduced oxidative stress while protecting diastolic and systolic cardiac function. Then, cardiac-specific LTCC overexpression caused increases in myocardial iron accumulation and oxidative damage in proportion to the elevated  $\text{Ca}^{2+}$  currents that were, again, reduced with LTCC blockers [1; 10], further supporting the theory of transport of NTBI by LTCCs. Finally, involvement of LTCC in iron transport is also supported by the protective actions of taurine supplementation against myocardial iron accumulation, oxidative damage, and altered cardiac structure and function [1; 20]. NTBI entering cardiomyocytes is effectively trapped in the cytosol, following rapid redox cycling [1].

### *Diagnosis*

The diagnosis of iron overload is based on physical examination with routine screening and monitoring of iron levels. Screening is necessary for the diagnosis of iron overload, and monitoring after the diagnosis has been made is required to manage therapy effectively and prevent iron toxicity. Several biochemical and genetic studies, screening and monitoring tests and direct biopsy are used to assess patients for the presence of iron overload cardiomyopathy [3; 7]. Genetic screening is used to diagnose primary iron overload; genetic screening for the C252Y and H52D mutations for type 1 primary

hemochromatosis is now widely available as well as hemoglobin electrophoresis for the detection of congenital hemoglobinopathies [3]. There are two main tests for serum iron measurement currently used; serum ferritin and serum transferrin saturation. Serum ferritin is non-invasive and inexpensive; making it the most convenient laboratory test used to determine iron overload. A serum ferritin level greater than 200  $\mu\text{g/L}$  in premenopausal women and a serum ferritin level greater than 300  $\mu\text{g/L}$  in men and postmenopausal women is a marker of excess iron [3; 7; 9]. Problems can arise in the accuracy of this test because ferritin is an acute-phase reactant, and serum levels increase in chronic inflammation and infection. Also, serum ferritin levels decrease in vitamin C deficiency [7; 26]. Serum transferrin saturation measures the proportion of transferrin bound to iron and is derived by dividing serum iron by total iron-binding capacity. An indicator of primary iron overload is serum transferrin saturation greater than 45%. This test is only effective in diagnosing secondary iron overload when used in combination with serum ferritin [3; 7]. Imaging studies are used to visualize tissue iron. The widespread use of cardiac magnetic resonance imaging (MRI) measurement has led to an increased detection of myocardial iron overload [3]. MRI measures tissue iron concentration indirectly by detecting the paramagnetic influences of storage iron on the proton resonance behavior of tissue water [7; 27]. MRI is suitable for ongoing assessment of iron levels in the heart and for estimation of total body iron, as well as for serial evaluation of therapy for iron toxicity [7]. Endomyocardial biopsy is not routinely used but can serve as definitive assessment of tissue iron stores while allowing a detailed histological assessment of end-organ damage. However, the distribution of stored iron in

the heart is not homogeneous so the test may not provide a true estimate of iron content. It is also highly invasive and can cause serious complications [7; 3; 28].

### *Treatment*

Currently there are two types of treatment available for patients with iron overload; phlebotomy and chelation therapy. Phlebotomy, the removal of blood from the body, begun early can be expected to result in normal lifespan. Phlebotomy should be continued after primary iron depletion to prevent reaccumulation of iron, with a goal to keep the serum ferritin concentration at 50 ng/mL or less. Usually, patients with primary iron overload are often diagnosed and treated only after iron overload becomes advanced, after damage has occurred. Oxidative stress may persist or rebound during the chronic maintenance phase of phlebotomy therapy in patients with primary iron overload, suggesting that close attention to iron control is necessary [3]. For transfusional iron overload in patients with underlying anemia, phlebotomy is not a feasible form of treatment [7; 16]. Chelation has been shown to improved ventricular function, prevents ventricular arrhythmias and reduces mortality in patients with secondary iron overload [3]. Three iron chelating agents are currently available: subcutaneous iron chelator deferoxamine mesylate (desferrioxamine, DFO, Desferal®) and oral chelators deferasirox (Exjade®) and deferiprone (Ferriprox®) [3; 7]. The primary routes of excretion for all chelators are the urine and stool [7]. Deferoxamine is a hexadentate iron chelator, forming a complex (ferrioxamine) with iron at a 1:1 molar ratio with a stability constant of  $10^{31}$ , but has a very short plasma half-life of 5-10 minutes [7; 16]. A daily dose of 500–1000 mg (20–40 mg/kg/day) can be given over a period of 8–24 h through

subcutaneous infusion via a portable pump [7]. In two thirds of patients with thalassemia major conventional chelation treatment with deferoxamine does not prevent excess cardiac iron deposition, placing them at risk of heart failure and its complications [3]. Deferoxamine is effective and has few major side effects but it has the disadvantages of high cost and difficulties in patient compliance with the subcutaneous infusion regimen [16]. Deferasirox has a longer half-life than deferoxamine at 8-16 hours, making it suitable for once-daily oral administration with 24 hour chelation. It is just as effective as deferoxamine in transfusion-dependent patients but has side effects including gastrointestinal disturbances and rash [7]. Deferiprone has a plasma half-life of 47-134 minutes and therefore must be administered three times daily orally. It is more effective than deferoxamine in the removal of myocardial iron and, in comparison to deferoxamine alone, combination treatment with deferiprone reduced myocardial iron and improved heart and endothelial function in thalassemia major patients with cardiac iron overload [7; 3]. Major side effects include agranulocytosis, musculoskeletal and joint pain, gastric intolerance, and zinc deficiency. The risk of agranulocytosis requires a weekly complete blood count, and serum alanine transaminase should be measured monthly for 3 to 6 months and then every 6 months [7]. Although chelation therapy has been consistently shown to reduce the cardiovascular burden from secondary iron overload, chelation therapy is cumbersome and associated with the toxic side effects described above, thereby setting a limit its impact on possible clinical outcome [3].

*Reactive oxygen species*

Redox reactions are the transfer of electrons from an electron donor to an electron acceptor [29]. Free radicals are formed when a molecule contains one or more unpaired electron(s) in the outermost orbital, making the molecule a highly reactive species [30; 31]. Due to its unique diradical configuration oxygen is a major source of free radicals [30]. Reactive oxygen species (ROS) include free radicals superoxide ( $O_2^{\cdot-}$ ) and hydroxyl ( $\cdot OH$ ), as well as the reactive molecule hydrogen peroxide ( $H_2O_2$ ) [32]. ROS are generated intracellularly by two metabolic sources: the mitochondrial electron-transport chain and oxygen-metabolizing enzymatic reactions, where the mitochondrial electron-transport chain is the major source of ROS in the heart [29; 32]. Mitochondria provide energy in the form of adenosine triphosphate (ATP) to the cell through oxidative phosphorylation, the process by which ATP is formed. Electrons are transferred from NADH or  $FADH_2$  generated through the Krebs cycle flow along the respiratory transport chain through a series of electron transport carriers located on the inner mitochondrial membrane called complexes I, II, III and IV. Normally, only 1% to 2% of electrons leak out to form  $O_2^{\cdot-}$ , and this is scavenged by manganese superoxide dismutase (SOD2). However, under pathophysiologic conditions, the electron transport chain may become uncoupled, leading to increased  $O_2^{\cdot-}$  production [32]. ROS are important for several biological functions; they are required for oxidative burst reaction, which is essential to phagocytes [33], and act as signaling molecules that regulate numerous cellular processes [29]. ROS's role as signaling molecules can also be detrimental in instances of high levels of ROS and can cause significant damage to cellular proteins, membranes and to nucleic acid, leading to single strand breaks and chromosomal alterations [32]. ROS signaling can also lead to high levels of inflammation and even cell death. In iron

overload condition free iron can catalyze the production of hydroxyl radicals through the Fenton reaction (**Figure 1**). The resulting °OH are much more reactive than either O<sub>2</sub><sup>•-</sup>

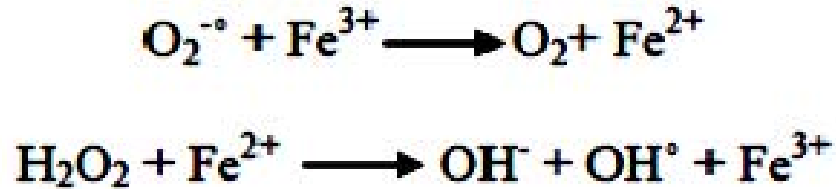


**Figure 1 The Fenton Reaction.** Image and text from Shawky, M. et al. *Oxidative Stress and Cardiac Failure* (2003) [4]. Iron interacts with cellular oxidizing and reducing ROS hydrogen peroxide (H<sub>2</sub>O<sub>2</sub>) and superoxide radical (O<sub>2</sub><sup>•-</sup>) produced from the electron transport chain during ischemia and reperfusion. Iron is able to accept and donate electrons readily by interconverting between Fe<sup>3+</sup> and Fe<sup>2+</sup>, which makes it a useful component of cytochromes, hemoglobin, and enzymes. However, ROS can be converted to hydroxyl radicals (OH<sup>•</sup>) by interacting with Fe<sup>2+</sup> through the Fenton Reaction. OH<sup>•</sup> is highly reactive and it itself can damage many organic molecules.

or H<sub>2</sub>O<sub>2</sub>, causing an increase in damage to structural membranes, enzymes, mitochondria, DNA, and ultimately apoptosis [4]. Numerous studies have shown that ROS activation is increased in the cardiovascular system in response to various stressors and in failing heart [33]. ROS has been shown to be involved in the development of pressure overload hypertrophy [32; 34]. There is also evidence that increased levels of ROS observed following Myocardial infarction (MI) are directly involved in the development of contractile dysfunction and plays a multi-factoral role in myocardial remodelling [32; 35] ROS also play a significant role in tissue necrosis and reperfusion injury [33; 36]. Together, these observations strongly suggest a role for ROS in cardiovascular pathophysiology.

Inflammation, like oxidative stress, can result in both beneficial effects or be detrimental and is implicated in several cardiac disease conditions. Specifically, inflammatory response is an integral component of the host response to tissue injury or host invasion but plays a particularly active role after myocardial infarction [37]. The inflammatory response is mediated by a variety of signaling molecules, particularly inflammatory cytokines. Cytokines are a group of relatively small molecular weight proteins (15–30 kDa) secreted by cells in response to stress. They form a complex network of signals regulating the growth, differentiation, and functions of almost all types of cells, but they are more implicated in the host's immune response to infections and other forms of stresses. Cytokines are classified as pro-inflammatory and anti-inflammatory [38]. Pro-inflammatory cytokines such as tumor necrosis factor-alpha (TNF- $\alpha$ ), a major contributor to cardiac inflammation, are elaborated soon after MI injury and can acutely regulate myocyte survival/apoptosis and trigger additional cellular inflammatory response [37]. Recent studies suggest that cytokines not only induce ROS production but also are themselves induced by ROS in what can be called the 'vicious cycle' (**Figure 2**) of redox-cytokine interaction [37; 39; 40]. In studies on isolated adult rat cardiomyocytes exposed to TNF- $\alpha$ , researchers have shown an increase in ROS and in events leading to oxidative stress [38; 41]. ROS can act as a messenger molecule, initiating pathways and transcription factors, which can lead to an increase of cytokines cascade [37]. Thus, this 'vicious cycle' that indicates perpetual increases in inflammation and oxidative stress appears to have significant effects on the development and progression of cardiovascular disease and ultimately heart failure.

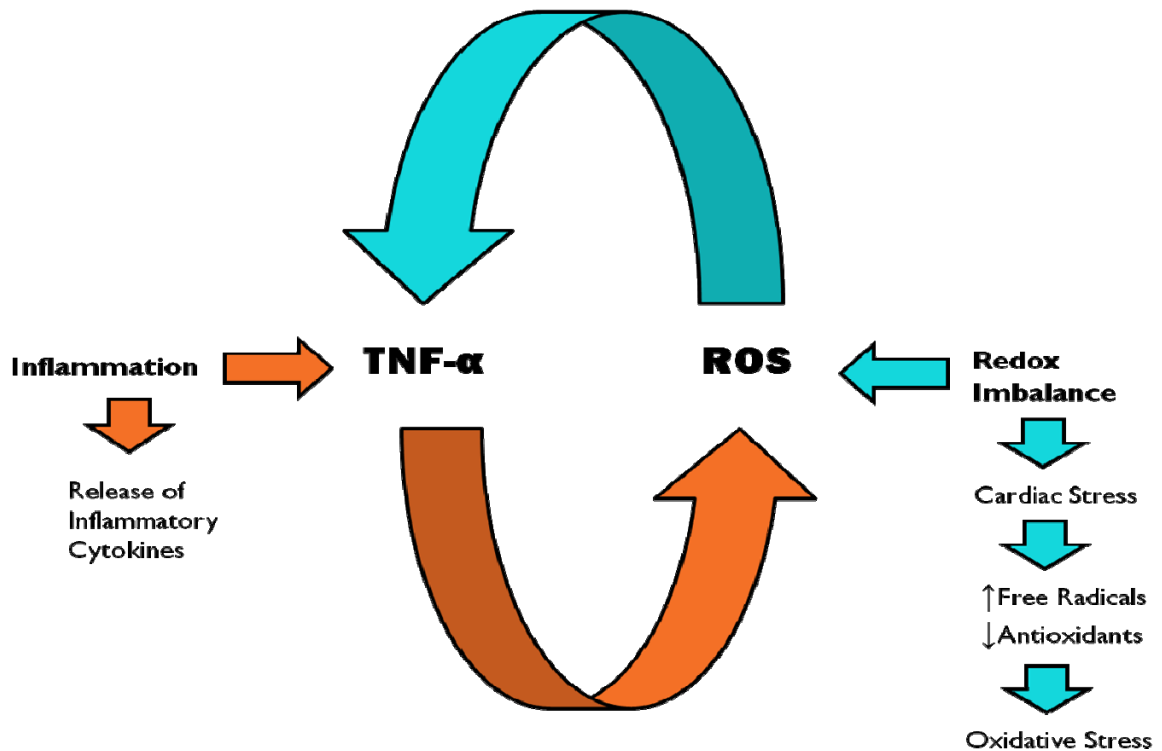


**Figure 2 The vicious cycle between oxidative stress and inflammation.** There is evidence of a ‘vicious cycle’ between oxidative stress and inflammation. In redox imbalance there is cardiac stress which can lead to an increase in free radicals and a decrease in antioxidant, then leading to oxidative stress. Oxidative stress increases inflammation and TNF- $\alpha$  level. An increase in inflammation causes the release of more inflammatory cytokines. Inflammatory cytokines, particularly TNF- $\alpha$ , can cause an increase in the level of ROS, continuing the cycle of oxidative stress and inflammation, leading to cellular stress and damage.

### *Tumor necrosis factor-alpha*

TNF- $\alpha$  is a key cytokine that has been shown to play important physiological and pathological roles in the heart. It can stimulate antigen presentation, adhesion molecule expression on endothelial cells, inflammatory cell activity and expression of matrix-degrading enzymes [38; 42; 43; 44]. It belongs to a family of structurally related

cytokines, the TNF superfamily, which includes more than 20 different ligands. TNF- $\alpha$  initiates activation of intercellular pathways by binding to TNF receptors, which are found on a variety of cell types [38]. There are two types of TNF- $\alpha$  receptors isolated so far [38; 43; 44; 45; 46]. TNFR1 seems to be ubiquitous while TNFR2 seems to be more restricted to cells of hematopoietic origin [38; 47]. Binding of TNF- $\alpha$  to TNFR1 will induce binding of TNFR-associated death domain (TRADD) to the inner membrane portion of TNFR1. TRADD will then recruits and binds to molecules Fas-associated death domain protein (FADD), receptor-interacting protein (RIP) and TNFR-associated factor 2 (TRAF2). TRAF2 and RIP stimulate pathways leading to activation of transcription factor nuclear factor-kappaB (NF- $\kappa$ B) and of jun N-terminal kinases/activating protein-1 (JNK/AP-1), whereas FADD mediates activation of apoptosis by binding to a death effector domain (DED) [42; 48]. NF- $\kappa$ B can cause the expression of more inflammatory cytokines, including TNF- $\alpha$ , while JNK/AP-1 can lead to the release of ROS from the mitochondria [42]. The source of TNF- $\alpha$  in the heart is not fully understood. Activation of the immune system after myocardial injury may be responsible for the release of cytokines in the injured myocardium, failing heart may be the source of TNF- $\alpha$  production, in which elevated serum levels of TNF- $\alpha$  represent spillover of cytokines that were produced within the myocardium, leading to the secondary activation of the immune system, or decreased cardiac output in heart failure may lead to the elaboration of TNF- $\alpha$  due to an under-perfusion of systemic tissue that allows translocation of endotoxins, which activates cytokine production [38; 49; 50].

*Interleukin 10*

Anti-inflammatory cytokines also play a role in the inflammatory response in the heart. Interleukin-10 (IL-10), demonstrates potent anti-inflammatory properties through inhibiting the production of various pro-inflammatory cytokines including TNF- $\alpha$  [51; 52]. The biological activities of IL-10 are dependent on two receptors that bind IL-10 with high affinity, IL-10R1, and low affinity, IL-10R2 [38]. The IL-10/IL-10R interaction activates the tyrosine kinase Jak1 and Tyk2, which activates the cytoplasmically localized inactive signal transducer and activator of transcription (STAT) protein 1,3 and 5, and results in the translocation and gene activation [38; 53; 54]. IL-10 appears to be a neutralizing component of inflammation and serves to reduce both duration and magnitude of the process. Studies with IL-10 gene deficient mice showed an overproduction of inflammatory cytokines and the development of chronic inflammation disease [38; 54; 56]. It acts as an anti-inflammatory cytokine by inhibiting the synthesis of a number of cytokines such as interferon gamma (IFN $\gamma$ ), IL-2, and TNF- $\alpha$ . As mentioned earlier, TNF- $\alpha$  is transcriptionally controlled by NF- $\kappa$ B and it was suggested that IL-10 may exert a significant part of its anti-inflammatory properties by inhibiting this transcription factor [38]. There is also evidence that IL-10 can act as an antioxidant by inhibiting the release of ROS [38; 57; 58]. Recently, studies have shown that improvement in cardiac function after dexamethasone, growth hormone, or steroid treatment has been associated with an increase in IL-10 content. Also, studies in rats have shown a significant decrease in IL-10 content after 4, 8, and 16 weeks of MI [38; 51; 59; 60; 61]. Recent evidence has shown an importance in the ratio between TNF- $\alpha$  and IL-10. Studies on isolated cardiomyocytes have shown that exposure to IL-10/ TNF- $\alpha$  in the ratio of 1 was found to be consistent with normal healthy myocytes. At an IL-10/ TNF- $\alpha$

ratio of 1, IL-10 treatment was able to antagonize the deleterious effects of TNF- $\alpha$  with respect to generation of ROS, antioxidant enzymes, and lipid peroxidation [38; 51; 62]. In MI-induced rats, where the cardiac function was also depressed, there is a significant decrease in the IL-10/ TNF- $\alpha$  ratio [38; 51]. A higher IL-10/ TNF- $\alpha$  does not provide any additional protection, emphasizing an optimal ratio of 1 for IL-10/ TNF- $\alpha$  [38].

### *Interferon gamma*

IFN $\gamma$  is an important pro-inflammatory cytokine in immune reactions, however its role occurs to be much larger. Besides its immunologic activity [63; 64] IFN $\gamma$  is involved in atherogenesis, inflammation and apoptosis [63; 65; 66; 67; 68]. It acts through its specific receptor composed of two subunits: IFN $\gamma$  R1 (ligand binding) and R2 (signal transduction). IFN $\gamma$  binds to cell surface receptors and activates members of the JAK kinase family. Activated JAK kinases phosphorylate the STAT family of transcription factors. STAT proteins homo-or heterodimerize and form complexes with other transcription factors to activate transcription of IFN-stimulated genes (ISGs) [69; 70; 71]. It is through the activation of ISGs that IFN $\gamma$  is capable of inducing a wide range of cellular processes including inflammation and apoptosis. ISGs can act as a transcription factor, resulting in increased inflammation, or induce death inducing ligands, resulting in apoptosis [69].

### *Matrix metalloproteinase*

Matrix metalloproteinases (MMPs) are synthesized in inflammation and participate in tissue remodeling and the destructive effects of cardiovascular diseases

associated with enhanced oxidative stress [72]. MMPs are generally secreted in an inactive form but can be readily activated within minutes of ischemia by ROS, cytokines and hypoxia. ROS and cytokines stimulate transcription factors NF- $\kappa$ B, Ets, and AP-1 to stimulate MMP expression. [37; 73; 74; 75]. MMP2 and MMP9 are the two major remodelling proteins in the heart and are known to play key roles in various cardiac disease states [76]. MMP2 and 9 specialize in the degradation of type IV collagen, the major structural component of basement membranes. A previous study demonstrated that H9c2 cardiomyoblasts exposed to oxidative stress exhibited increased MMP2 activity, leading to cleavage and activation of the apoptotic protein, glycogen synthase kinase-3 $\beta$  [72]. It has also been shown that MMP2 and MMP9 are robustly increased during various stages of congestive heart failure. Furthermore, studies have shown that MMP9 has a major role in ventricular remodelling associated with endothelial and myocyte apoptosis [77]. Hearts expressing highest levels of MMP-2 and MMP-9 proteins also have a high amount of collagen deposition and impaired diastolic function [37; 78].

### *Antioxidants*

An antioxidant is a molecule capable of inhibiting the oxidation of other molecules, removing free radical intermediates and inhibiting other oxidation reactions, thus they play a protective role against oxidative stress damage. They do this by being oxidized themselves, so antioxidants are often reducing agents. There are many studies showing that both enzymatic and non-enzymatic antioxidants offer protection in different pathophysiological conditions, where ROS are known to be involved [30]. There are a number of antioxidants that are naturally found in the heart, including glutathione

reductase (GSR), manganese superoxide dismutase (SOD2) and peroxiredoxin (Prdx)6. GSR is important for maintaining reduced glutathione (GSH) levels. GSH is a multifunctional tripeptide that directly or indirectly regulates a number of biological processes, such as DNA synthesis, ion transport, enzyme activity, transcription, signal transduction, and antioxidant defenses [30; 79; 80; 81; 82; 83]. It is used as a reducing agent for enzymes that detoxify lipid or oxygen radicals as well as a scavenger of radicals in the aqueous portion of the cell, thereby protecting protein thiol groups [30; 84]. As well as the reduced state, glutathione can exist as an oxidized state (GSSG). Studies have shown that GSH depletion and accumulation of its oxidized form, glutathione disulfide (GSSG), occur in the heart muscle within minutes of initiating oxidative stress [79; 85]. The change in GSH status elicited by oxidative stress is due to an increased cellular demand for GSH. In GSH the thiol group of cysteine is able to donate a reducing equivalent ROS and thus becomes reactive itself. It readily reacts with another reactive GSH to form GSSG. In order to act as an antioxidant GSSG must be converted back to GSH. GSR readily reduces GSSG to GSH in oxidative stress conditions, making it a good indicator of oxidative stress [30; 79; 81; 83; 86]. Superoxide dismutase (SOD) catalyzes the dismutation of  $O_2^{\circ-}$  to  $H_2O_2$  and  $O_2$ . Previous studies have shown that SOD offers protection against ischemia-reperfusion injury [30; 87; 88; 89]. SOD2 is a nuclear-encoded homotetrameric enzyme, mitochondria-localized that is the primary defense against mitochondrially generated ROS [29; 90]. Prdx6 is a member of a relatively new family of antioxidant enzymes that is involved in redox regulation [91]. Prdx6 is the only mammalian 1-Cys member of the peroxiredoxin superfamily that is expressed in all the vital organs, including the heart [91; 92]. Prdx6 antioxidant activity lies in its ability to

reduce H<sub>2</sub>O<sub>2</sub> and hydroperoxides into water and alcohol, respectively [91; 93]. Studies have shown that mice with a targeted mutation of Prdx6 are susceptible to oxidative stress and mouse hearts devoid of Prdx6 were indeed susceptible to ischemia-reperfusion injury [91; 94].

### *Apoptosis*

Apoptosis is a tightly regulated program of cell death. It is required for normal organ development, control of cell number and deletion of harmful, nonfunctional and abnormal cells. Apoptotic cells are characterized by cell shrinkage, plasma membrane blebbing, chromatin condensation and DNA fragmentation [95]. Increase in apoptosis plays a major role in the development of various cardiovascular disorders and heart failure [96; 97]. Iron overload has been linked to cardiomyocyte loss due to apoptosis and enhanced apoptosis in iron-overload cardiomyopathy could be linked to altered mitochondrial function [20; 98; 99]. Apoptosis is activated in cardiac myocytes by multiple stressors that are commonly seen in cardiovascular disease such as increased oxidative stress and cytokine production [97; 100; 101; 102]. Different stressors induce different pathways of apoptosis. ROS is believed to initiate the intrinsic pathway, which is apoptosis initiated by an intracellular stressor. The first step is the activation of pro-apoptotic proteins in the cytoplasm, including B-cell lymphoma (Bcl)-2-associated X protein (Bax). Bax binds to and opens channels on the mitochondria surface allowing the release of cytochrome c. Anti-apoptotic proteins, such as Bcl-2, can prevent the release of cytochrome c by binding to and forming a heterodimer with Bax, preventing the opening of mitochondrial channels. In oxidative stress there is a decrease in ratio of Bcl-2/Bax,

which leads to the release of cytochrome c [96; 97]. Cytochrome c, once released into the cytosol, binds to apoptotic protease activating factor (Apaf)-1, leading to a conformational change. Cytochrome c/Apaf-1 then recruits and activates initiator caspase caspase-9, creating an apoptosome [97; 103; 104]. The apoptosome cleaves and activates effector caspases caspase-3 and -7. Activated effector caspases translocate to the nucleus, then cleave the DNA repairing enzyme, poly (ADP-ribose) polymerase (PARP) and activate endonucleases which cleave DNA, culminating in apoptotic cell death [96; 97; 103; 105]. Apoptosis initiated by stressors from outside the cell is referred to as extrinsic apoptosis, such as TNF- $\alpha$ . It begins with the binding of TNF- $\alpha$  to previously mentioned death domains TNFR1 and/or Fas. TNFR1 will then bind and activate intracellular FADD, while Fas first binds to and activates TRADD, which in turn binds to FADD. Activated FADD binds to pro-caspase 8 leading to cleavage and activation of initiator casepase caspase-8. Caspase-8 has two roles: it can cleave and activate caspase-3, resulting in apoptosis, or initiate the release of cytochrome c by the mitochondria, causing intrinsic apoptosis [97; 106]. As mentioned earlier, ISGs are able to activate death domains, including Fas and TNFR1. This activation also leads to activation of caspase-8 and ultimately apoptosis, suggesting a role for IFN $\gamma$  in cell death [69]. Apoptosis is mediated by many transcription factors, including the forkhead box subfamily O (FOXO) family. Besides apoptosis, FOXOs mediate many aspects of physiology, including stress response and metabolism [107]. FOXOs are ubiquitous in most cell types, where FOXO3 is commonly expressed in cardiomyocytes [108]. Some studies have shown that FOXO3 can have beneficial effects on cardiomyocytes by preventing cardiac hypertrophy [108; 107]. However, FOXO3 can also act as a pro-apoptotic transcription factor and has

shown to be a promoter of the *Fas* gene [109]. FOXO3's mechanism of action depends on cell type and types of stressor, so its exact effects in cardiovascular disease and damage remains an active area of research.

### *Autophagy*

As stated, cardiac myocytes responses to various stressors, such as excess iron and/or oxidative stress, includes molecular modifications, inflammation and remodeling, thus ultimately leading to various cardiac disorders including hypertrophy, arrhythmias, MI and heart failure. Autophagy, a catabolic pathway for bulk turnover of long-lived proteins and organelles via lysosomal degradation, is a cellular response to these stressors. Autophagy is initiated by the formation of a single membrane structure, possibly derived from the sarcoplasmic/endoplasmic reticulum. Fusion of the tips of the isolation membrane results in the formation of a double-membrane structure known as the autophagosome, which surrounds portions of the cytoplasm and organelle. Autophagosomes undergo a series of maturation steps and finally fuse with the lysosome called the autophagolysosome, in which the sequestered contents and the inner membranes of autophagosomes are degraded by the lysosomal hydrolases [110; 111; 112; 113]. Autophagy can promote cell survival by generating free amino acids and fatty acids required to maintain function during nutrient-limiting conditions, or by removing damaged organelles and intracellular pathogens [110; 114; 115; 116]. Autophagy might also promote cell death through excessive self-digestion and degradation of essential cellular constituents [110; 117; 118; 119]. In the heart, autophagy is upregulated in response to ischemia/reperfusion [97; 120; 121]. However, the functional significance of

increased autophagy in the heart is not clear; autophagy has been reported to protect against cell death as well be the cause of cell death [97; 121; 122; 123]. During ischemia, oxygen and nutrient supplies are decreased, causing activation of adenosine monophosphate-activated protein kinase (AMPK) and inactivation of mammalian target of rapamycin (mTOR), which in turn leads to autophagy for cell survival. Also, beclin 1, a promoter of autophagy, is negatively regulated by interaction with Bcl-2 [121; 124; 125; 126]. In reperfusion AMPK is inactive while mTOR is activated, the opposite of what is seen in ischemia. Instead, expression of beclin 1 is markedly upregulated. Bcl-2 is degraded by the ubiquitin–proteasome system, which is activated during oxidative stress. The combination of upregulation of beclin 1 and downregulation of Bcl-2 during the reperfusion phase stimulates the activity of beclin 1, thereby stimulating autophagic cell death [121; 124; 126; 127]. Recent studies suggest that there is cross talk between autophagy and apoptosis. Autophagy protein (Atg)5, an essential autophagy protein, has been reported to activate apoptosis. It was found that over expression of Atg5 increased the cell's susceptibility to apoptosis following stimulation with several death triggers. Death stimulation resulted in cleavage of Atg5, and truncated Atg5 induced cytochrome c release and apoptosis. Over expression of Bcl-2 protected against Atg5-mediated mitochondrial dysfunction. This suggests that Atg5 can serve as a molecular switch between autophagy and apoptosis [97; 128]. Another study reported that Atg5 associated with FADD to mediate IFN $\gamma$ -induced cell death [97; 129].

*Cell survival*

In condition distress, cells may promote cell survival pathways in order to compensate with the stressor, leading to increased cellular growth, proliferation and differentiation [130]. Enlargement of cardiomyocytes has been reported to result from an increase in protein content and activation of p70S6 Kinase 1 (p70S6K1). p70S6K1 plays a major role in regulating the phosphorylation of 40S ribosomal S6 protein and selective translation of a family of mRNAs that contain an oligopyrimidine tract at the 5'-transcriptional start site [130; 131]. p70S6K1 is activated through the phosphoinositide 3-kinase (PI3K) pathway. PI3K catalyzes addition of a phosphate group to the 3' position of the sugar ring in a phosphoinositide. Its products act on multiple downstream effectors that interact with Src homology-2 and pleckstrin homology domains of serine/threonine and tyrosine kinases. It is these kinases that contribute to phosphorylation and activation of p70S6K1 [130]. Studies have shown treatment with H<sub>2</sub>O<sub>2</sub> activates PI3K and thus p70S6K1 in cardiomyocytes. Activated p70S6K1 also lead to increased cardiomyocyte size, supporting the theory that activation of p70S6K1 plays an important role in cardiomyocyte hypertrophy [130]. Mammalian target of rapamycin (mTOR) can also be a regulator of p70S6K1 in stress conditions. Activation of mTOR is regulated by energy metabolism by adenosine monophosphate-activated protein kinase (AMPK). AMPK reserves cellular energy content and serves as a key regulator of cell survival or death in response to pathological stress. The precise role that AMPK plays in cardiac metabolism remain incompletely understood. AMPK may play a role in altering cardiac myocyte morphology and proliferation. The main AMPK activator, LKB1, is in fact a tumor suppressor gene. Activated AMPK inhibits mTOR signaling and cell growth and proliferation [132; 133; 134]. Recent evidence indicates that AMPK-mediated

modification of gene expression leads to cardiac protection from anoxia and ischemia [132; 135; 136]. Another study showed that in cardiac muscle cells resveratrol, an antioxidant found in red wine, induced activation of AMPK and inhibited the occurrence of cell death caused by treatment with H<sub>2</sub>O<sub>2</sub> [137]. More research is required to better understand the role of cardiac AMPK in energy metabolism.

### *Secoisolariciresinol diglucoside*

Secoisolariciresinol diglucoside (SDG) is an antioxidant phytochemical present in flaxseed. After ingestion, SDG is converted to secoisolariciresinol, which is further metabolised to the mammalian lignans enterodiol and enterolactone. A growing body of evidence suggests that SDG metabolites may provide health benefits due to their weak oestrogenic or anti-oestrogenic effects, antioxidant activity, ability to induce phase 2 proteins and/or inhibit the activity of certain enzymes [138; 139; 140; 141; 142]. The chemical structure of SDG, as well as Secoisolariciresinol (SECO) and Nordihydroguaiaretic acid (NDGA) are shown in Figure 3. SDG has been shown

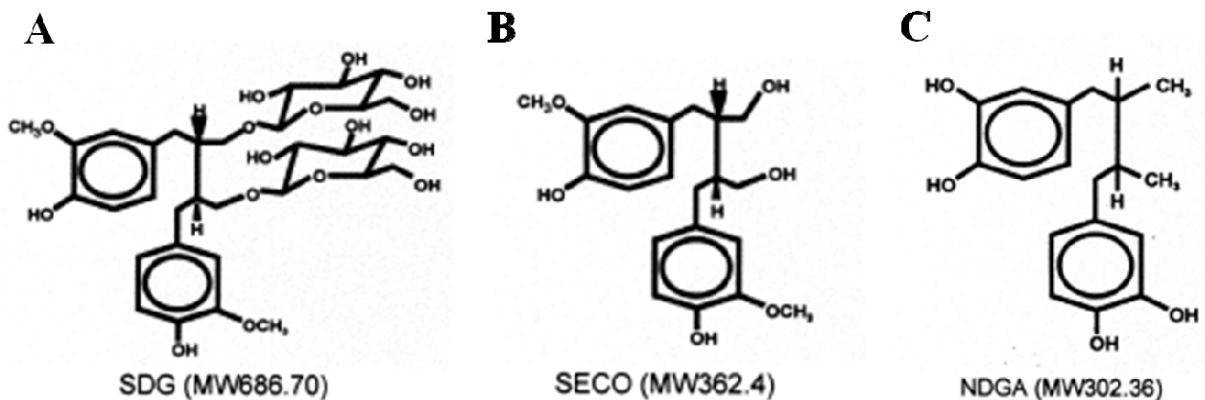


**Figure 3 Chemical structure of SDG Secoisolariciresinol diglucoside.** Image and text from Prasad, K. *Molecular and Cellular Biochemistry* (2000). The chemical structure and molecular

weight of Secoisolariciresinol diglucoside (SDG) (A), Secoisolariciresinol (SECO) (B), and Nordihydroguaiaretic acid (NDGA) (C). Antioxidant activity of SDG could be due to the structural similarity of the aglycone SECO with known antioxidant NDGA.

to decrease the production of inflammatory mediators and scavenge ROS to reduce oxidative stress. *In vitro* studies have shown that SDG and its metabolites, SECO, EL and ED, possess antioxidant activity and were effective in preventing lipid peroxidation of liver homogenate [143]. There have been multiple studies on the effect of SDG on cardiovascular health. SDG prevents the development of hypercholesterolemic atherosclerosis, induces angiogenesis-mediated cardioprotection and prevents the development of type 1 diabetes. SDG treatment reduced the development of hypercholesterolemic atherosclerosis by causing a decrease in serum cholesterol, LDL-C, and lipid peroxidation product and an increase in HDL-C and antioxidant reserve in rabbits fed a high cholesterol diet [144]. SDGs effect on arterial pressures in anesthetized rats was investigated. SDG in the doses of 3, 5, and 10 mg/kg produced dose-dependent reductions in systolic, diastolic, and mean arterial pressures [145]. The angiogenic properties of SDG were investigated in three different models. First, in an *in vitro* model, human coronary arteriolar endothelial cells treated with SDG showed a significant increase in tubular morphogenesis. Second, in an *ex vivo* ischemia/reperfusion model, SDG-treated showed an increased level of aortic flow and functional recovery. Also, SDG reduced infarct size compared and also decreased cardiomyocyte apoptosis. Third, in an *in vivo* myocardial infarction model, SDG increased capillary density and myocardial function as evidenced by increased fractional shortening and ejection fraction [146]. To study the effects SDG had on diabetes diabetic prone BioBreeding rats were used as a human type I diabetes model. SDG prevented the development of diabetes by

approximately 71%; prevention in development of diabetes by SDG was associated with a decrease in serum and pancreatic-MDA and an increase in antioxidant reserve [144]. Currently, there have been no studies to date investigating the role of SDG in abrogating oxidative stress-induced cardiac damage in an iron overload model.

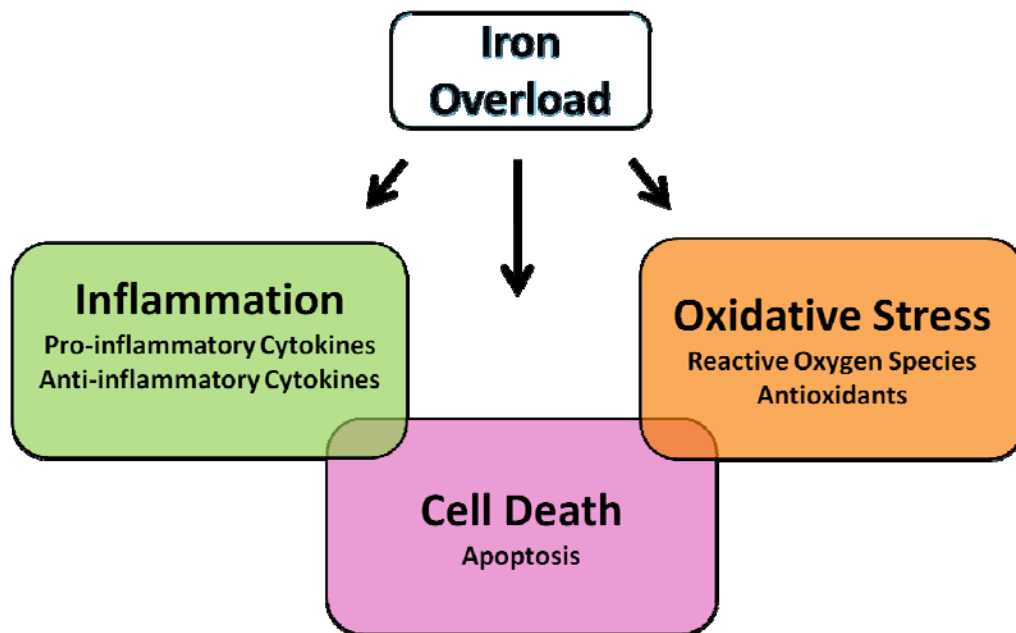


**Figure 4 Iron overload induces inflammation, oxidative stress and cell death.** Excess iron has been attributed to an increase in cellular inflammation, oxidative stress and death. Free iron causes the expression of inflammatory cytokines leading to inflammation. Iron can also cause the formation of reactive oxygen species causing oxidative stress. Excess iron can cause cell death by leading to an increase in apoptosis. Reactive oxygen species and inflammatory cytokines can also contribute to apoptosis. The increase in inflammation, oxidative stress and cell death caused by iron overload is associated with cardiac dysfunction and may ultimately cause heart failure.

As previously stated, the mechanism/s of iron induced cardiac damage, as well as SDG in an iron overload model are not fully understood. In this study we hypothesize increase oxidative stress and inflammation in cardiac iron overload will correlate with increased apoptosis (**Figure 4**), and pre-treatment with SDG may attenuate these effects.

To better understand the mechanism/s of cardiac damage in an iron overload model as well, as protection by SDG, multiple markers of oxidative stress, inflammation, remodelling, cell death and cell survival were investigated.

## Methods

### *H9c2 cardiac cell line*

Rat cardiac cells (H9c2) were obtained from the American Type Culture Collection (Manassas, VA) and grown in Dulbecco's Modified Eagle's Medium (DMEM) (Sigma-Aldrich, St. Louis, MO), fetal calf serum (Hyclone, Pittsburgh, PA) and penicillin-streptomycin (Invitrogen, Carlsbad, CA). All H9c2 cells were cultured at 37 °C, 5 % CO<sub>2</sub> and used for experimentation upon reaching approximately 95 % confluence. All experiments were completed with cultures between passage 34 and 57.

### *Ammonium iron (III) citrate preparation*

Different concentrations of iron (0.1, 1, 10, 50, 100, 200 and 300 µM) iron solution was prepared by dissolving ammonium iron (III) citrate (Sigma-Aldrich, St. Louis, MO) into serum- and antibiotic-free DMEM. Treatment cells were incubated for 24 hours at 37°C.

### *Secoisolariciresinol diglucoside*

Different concentrations of Secoisolariciresinol diglucoside (SDG) (10, 50, 100, and 500 µM) was prepared by dissolving SDG into serum- and antibiotic-free DMEM. Treatment cells were incubated for 24 hours at 37°C. SDG was provided by Dr Prasad at the University of Saskatchewan.

### *Trypan Blue Exclusion assay*

The diazo dye, Trypan Blue ((3Z,3'Z)-3,3'-[(3,3'-dimethylbiphenyl-4,4'-diyl)di(1Z)hydrazin-2-yl-1-ylidene]bis(5-amino-4-oxo-3,4-dihydronaphthalene-2,7-disulfonic acid), is a stain used to discern living from dead cells. It is cell-impermeable and penetrates only damaged, non-viable cells with compromised membrane integrity. Viable cell counts were performed via automated Trypan Blue Exclusion assay using a Vi-Cell XR Cell Viability Analyzer (Beckman Coulter), wherein 0.5 mL of diluted, trypsinized cell suspensions were loaded, mixed with Trypan Blue reagent, and live/dead cell counts accessed via 50 individual sub-samples measured using the Vi-Cell XR Cell Viability Analyzer software. The total viable cell count was used when passaging or standardizing cell samples for experimentation.

#### *MTT assay*

The MTT (3-(4,5-dimethylthiazol-2-yl)-2,5-diphenyltetrazolium bromide) assay is used as a quantitative index of activity of mitochondrial and cytosolic dehydrogenases, which, in living cells, reduce the yellow tetrazolium salt to produce a purple formazan dye that can be measured spectrophotometrically [261]. In the present studies the MTT assay was used to measure cell viability. Cells were seeded onto sterile flatbottom 96-well plates (Corning) and incubated overnight to achieve the desired confluence. Plated cells were subjected to iron, SDG or SDG pre-treatment followed by iron treatments in serum- and antibiotic-free media. With  $t = 4$  hours of treatment time remaining, MTT reagent (Thiazolyl Blue Tetrazolium Bromide; Sigma, St. Louis, MO, USA) was added to wells to achieve a final concentration of 10 % (v/v), and cells were incubated at 37 °C for an additional 4 hours, during which time the MTT reagent was converted to purple

formazan crystals in living cells according to their metabolic activity. Following this, the incubation media was aspirated and 50  $\mu$ L of dimethylsulfoxide per well was added to solubilise the formazan crystals. Following 10 minutes of agitation on a Belly Dancer shaker (Stovall, Greensboro, NC, USA) at its highest setting, absorbance was measured spectrophotometrically at a wavelength of 490 nm (650 nm correction wavelength) using a PowerWave XS Microplate Spectrophotometer (BioTek, Winooski, VT, USA). Viability of treated wells was assessed relative to control wells, which were considered to represent 100 % viability.

#### *Reactive oxygen species indicator assay*

CM-H2DCFDA (5 - (and -6) – chloromethyl - 2', 7' - dichlorodihydrofluorescein diacetate, acetyl ester) is used as a cell-permeable indicator of ROS. This molecule remains non-fluorescent until the acetate groups are removed by intracellular esterases as oxidation occurs within the cell. In addition, esterase cleavage of the lipophilic blocking groups yields a charged form of the dye that is much better retained by cells than the parent compound. Moreover, the chloromethyl derivative of H2DCFDA used here allows for covalent binding to intracellular components, permitting even longer retention within the cell. Cells were seeded onto sterile flat-bottom 25 cm<sup>2</sup> culture flasks (Corning) and grown overnight to achieve the desired confluence. Cells were subjected to iron, SDG or SDG pre-treatment followed by iron treatments in serum- and antibiotic-free media. Following this the cells were washed with PBS and stained for 30 minutes with CM-H2DCFDA (Molecular Probes, Eugene, OR, USA) under standard incubation conditions. Stained cells were washed with PBS and detached from the flask using trypsin and

suspended in PBS for flow cytometric analysis using the FL1-H channel of a BD FACSCalibur Flow Cytometer (BD Biosciences) supported by BD CellQuest Pro Software. A minimum of  $1 \times 10^4$  gated events were acquired per trial. Mean fluorescence (specifically: geometric mean fluorescence) was understood to be directly proportional to levels of intracellular ROS. In early experiments, a  $H_2O_2$  control was also analyzed to aid in calibrating the flow cytometer for this assay.

#### *Active caspases 3/7-based apoptosis detection assay*

The cell permeable, carboxyfluorescein-labeled fluoromethyl ketone peptide inhibitor, fluorochrome inhibitors of caspases (FLICA), covalently binds to a reactive cysteine residue that resides on the large subunit of an active caspase heterodimer, thereby inhibiting further enzymatic activity. The bound labeled reagent is retained within the cell, while any unbound reagent will diffuse out of the cell and is washed away. The green fluorescent signal is a direct measure of the amount of active caspase-3 and caspase-7 present in the cell at the time the reagent was added. Active caspase-3/7 activity was assessed via flow cytometric analysis of control and treated cells that were stained with FLICAI using the CaspaTag Caspase-3/7 In Situ Assay kit (Chemicon International, Temecula, CA, USA). Cells were seeded onto sterile flat-bottom  $25 \text{ cm}^2$  culture flasks (Corning) and grown overnight to achieve the desired confluence. Cells were subjected to iron, SDG or SDG pre-treatment followed by iron treatments in serum- and antibiotic-free media. Following the treatment the cells were washed with wash buffer and suspended via trypsinization in PBS to achieve  $1 \times 10^7$  cells / mL.  $10 \text{ }\mu\text{L}$  of freshly prepared FLICA reagent was added to  $290 \text{ }\mu\text{L}$  of cell suspension, mixed gently

and incubated at 37 °C for 1 hour in the absence of light (mixing gently twice during this incubation). Following several wash and count steps, samples were immediately analyzed via flow cytometry with a BD FACSCalibur Flow Cytometer (BD Biosciences) supported by BD CellQuest Pro Software on the FL1-H (FLICA) channel, acquiring a minimum of  $1 \times 10^4$  gated events per trial.

#### *Superoxide dismutase activity assay*

Superoxide dismutases (SODs) catalyze the dismutation of the superoxide radical ( $O_2^-$ ) into  $H_2O_2$  and elemental oxygen ( $O_2$ ) which diffuses into the intermembrane space or mitochondrial matrix, providing an important defense against the toxicity of superoxide radicals [268]. In the Superoxide Dismutase Assay (Trevigen, Helgerman Ct. Gaithersburg, MD, USA), ions generated from the conversion of xanthine to uric acid and  $H_2O_2$  by xanthine oxidase, converts nitro-blue tetrazolium chloride (NBT) to NBT-diformazan, which absorbs light at 550 nm. SOD reduces superoxide ion concentrations, thereby lowering the rate of NBT-diformazan formation, which can thus be used to measure the SOD activity present in an experimental sample [269]. Cells were seeded onto sterile 150 cm<sup>2</sup> culture flasks (Corning) and grown overnight to achieve the desired confluence. Cells were subjected to iron, SDG or SDG pre-treatment followed by iron treatments in serum- and antibiotic-free media. Immediately following challenge, pelleted cell samples were lysed and their total protein quantitated via *DC* Protein Assay (Bio-Rad), being careful to keep protein samples cold to prevent degradation. Samples were assayed as per the kit's instructions and absorbance read at 550 nm using a PharmaSpec UV-1700 Visible Spectrophotometer (Shimadzu, Columbia, MD, USA). The SOD

activity was measured by calculating absorbance at 330 seconds subtracted by absorbance at 30 seconds, where greater SOD activity would be evidenced by less change in absorbance over time. These values were converted to SOD units per volume by reference to an SOD inhibition curve, generated as per the kit's instructions.

### *RNA isolation*

RNA isolation was performed using the Aurum Total RNA Mini kit (Bio-Rad) in accordance with the manufacturer's instructions using certified RNase-free barrier tips (Ambion, Foster City, CA, USA). Cells were seeded onto sterile 25 cm<sup>2</sup> culture flasks (Corning) and grown overnight to achieve the desired confluence. Cells were subjected to iron, SDG or SDG pre-treatment followed by iron treatments in serum- and antibiotic-free media. Adherent cells were washed once with PBS and detached via trypsinization. Following centrifugation (500 × g for 5 min at 4 °C), cells were washed with PBS and lysed using the provided lysis and binding buffer containing components for stabilization of RNA and inhibition of RNase activity. Lysates were placed in RNase-free microfuge tubes (Ambion) and RNA was extracted using a silica membrane spin column. Upon loading the RNA onto the column, genomic DNA was digested with an RNase-free DNase enzyme and, following washes to remove degraded genomic DNA, salts, and other cellular components, an elution buffer of low ionic strength was used to collect the pure RNA from the column. Aliquots were stored at -80 °C unless being used immediately, in which case they were kept on ice and separated into stock and sample aliquots, the latter used for RNA quantitation.

### *Automated electrophoretic RNA analysis*

The concentration and integrity of extracted RNA was assessed using the Experion RNA StdSens kit (Bio-Rad) on an Experion Automated Electrophoresis Station (Bio-Rad) supported by Experion software for Windows (Bio-Rad), in accordance with the manufacturer's instructions. Briefly, 1  $\mu$ L aliquots of denatured RNA samples and ladder were loaded onto a microfluidic chip comprised of channels that, once primed with a gel matrix, allowed for the separation, staining, detection, and data analysis of samples by via measurement of the 18 and 28 S rRNA peaks. Only high-quality (i.e. 9+ RNA quality index, as per automatic Experion software calculation) RNA samples were used for subsequent gene expression analysis.

### *cDNA synthesis*

First strand complementary DNA (cDNA) synthesis reactions were performed using a RevertAid H Minus First Strand cDNA Synthesis kit (Fermentas, Flamborough, ON, Canada) in accordance with the manufacturer's instructions. This kit features reverse transcriptase with a point mutation that completely eliminates RNase H activity and, in concert with the kit's RNase inhibitor, helps prevent RNA degradation during cDNA synthesis. Briefly, RNA samples were mixed with oligo(dT)<sub>18</sub> primers and the other kit components and incubated at 42 °C for 1 hour before terminating the reaction by heating at 70 °C for 5 minutes. The resultant products were stored at -20 °C unless being used immediately, in which case they were kept on ice.

### *Quantitative real-time polymerase chain reaction*

Quantitative real-time PCR (qPCR) was performed using primers for various genes (SABiosciences, Frederick, MD, USA) and SYBR Green RT<sup>2</sup> qPCR Master Mix (SABiosciences) via iQ5 Multicolor Real-Time PCR Detection System (Bio-Rad) in accordance with the manufacturer's instructions. Briefly, 10  $\mu$ L of 2x Master Mix was pipetted into the wells of a sterile 96-well PCR plate (Bio-Rad). Primer was added to nuclease-free ddH<sub>2</sub>O at a ratio of 1  $\mu$ L primer to 8  $\mu$ L ddH<sub>2</sub>O, and then 9  $\mu$ L of the mix was pipetted into the wells of the PCR plate, followed by 1  $\mu$ L cDNA template. The PCR plate was sealed with optical film (Bio-Rad). Following iQ5 calibration, qPCR analysis of triplicate samples was performed using a two-step cycling program involving an initial single cycle of 95 °C for 10 min (required to activate the DNA polymerase), followed by 40 cycles of 95 °C for 15 seconds and 60 °C for 1 minute. Following the qPCR reaction, a first derivative dissociation curve was performed as a quality control measure. Briefly, the reaction was heated to 95 °C for 1 min, cooled to 65 °C for 2 min, then ramped from 65 to 95 °C at a rate of 2 °C per minute. The formation of a single peak at temperatures greater than 80 °C indicated the presence of a single PCR product in the reaction mixture. Gene of interest expression was normalized to the housekeeping gene  $\beta$ 2-microglobulin.

**Table 1 Quantitative real-time PCR primers.** These primer sets were used as per manufacturer's instructions, as described above.

Gene name	UniGene #	RefSeq Accession #	Band Size (bp)	Reference Position	Source
Tumour necrosis factor- $\alpha$	Rn.2275	NM_012675	59	1642	SABiosciences
Interleukin-10	Rn.9868	NM_012854	102	34	SABiosciences
Interferon- $\gamma$	Rn.10795	NM_138880	71	275	SABiosciences
Matrix metalloproteinase 2	Rn.6422	NM_031054	164	2775	SABiosciences
Matrix metalloproteinase 9	Rn.10209	NM_031055	138	2883	SABiosciences
Glutathione reductase	Rn.19721	NM_053906	101	1182	SABiosciences
Peroxiredoxin 6	Rn.42	NM_053576	118	587	SABiosciences
Superoxide dismutase 2	Rn.10488	NM_017051	143	553	SABiosciences
Microtubule-associated proteins 1 light chain 3B	Rn.41412	NM_022867	158	308	SABiosciences
B2-microglobulin	Rn.1868	NM_012512	128	119	SABiosciences

### *Total protein assay*

Cell samples for use in immunoblotting were lysed using Nonidet P40 (NP-40) (Roche Diagnostics, Germany) buffer containing 150 mM NaCl, 1% NP-40, 50 mM Tris (pH 8.0) and protease inhibitors phenylmethylsulfonyl fluoride, leupeptin, aprotinin and pepstatin. Inhibitors were added immediately prior to NP-40 buffer application. Upon addition of ice-cold lysis buffer to pelleted cell samples, the crude lysate was pipetted up and down repeatedly. Lysates were vortexed, incubated on ice for 10 minutes, vortexed again and incubated on ice for a further 10 minutes. Lysates were then centrifuged for 12 minutes at  $1 \times 10^4$  rpm to remove cellular debris. Supernatant was collected and stored at  $-80\text{ }^{\circ}\text{C}$ . Protein lysates were quantitated via a detergent-compatible, colourimetric,

Lowry-based protein assay. Using the *DC* Protein Assay (Bio-Rad)'s 'microplate' method, which requires 5  $\mu$ L of protein lysate, full-strength and 1/10-strength samples were measured alongside a range of bovine serum albumin (BSA; Fisher) standard concentrations from 0.2-1.5 mg / mL. Following a 15-minute colour-development period, standard and sample absorbance was measured spectrophotometrically at a wavelength of 750 nm using a PowerWave XS Microplate Spectrophotometer (BioTek). Microsoft Excel for Macintosh was used to create a standard curve from the BSA standards, and the equation of the line of best fit (minimum accepted  $R^2 = 0.99$ ) was used to calculate the sample protein concentrations. Stock sample lysates were kept on ice to minimize degradation during the course of the assay.

#### *Sodium dodecyl sulfate-polyacrylamide gel electrophoresis*

Immediately following quantitation, 2x SDS sample loading buffer containing  $\beta$ -mercaptoethanol (Sigma-Aldrich) was added to the sample lysates, which were then placed in a 100 °C water bath for 5 minutes (with punctured tube lids to alleviate pressure) and then on ice for an additional 5 minutes. Boiled lysates were quick-spun and loaded into 10 % sodium dodecyl sulfate-polyacrylamide gels at 50  $\mu$ g per well (Bio-Rad Mini PROTEAN 3 Cell System apparatus was used). 3-5  $\mu$ L of HiMark™ Pre-stained protein standard (Invitrogen) or Precision Plus Kaleidoscope (Bio-Rad) protein standard was loaded alongside the sample wells. Empty wells were partially filled with 2x SDS loading buffer to ensure even migration across the gel. The electrophoresis apparatus was filled with 1x Running buffer (standard 1x Running buffer was prepared from a 10x stock). Gels were run at 80 V for 20 minutes or until the sample front cleared the stacking

gel, followed by 100 V until the appropriate kDa range had migrated to the centre of the resolving gel, as indicated by reference to the protein standard indicator.

#### *Electrophoretic transfer*

Immediately upon completion of sodium dodecyl sulfate-polyacrylamide gel electrophoresis (to prevent protein band dissociation), gels were removed from the electrophoresis assembly, their edges trimmed and orientation marks added (i.e. diagonal edge cut at top-left), and then were soaked in 1x Transfer buffer for ~10 minutes for equilibration (standard 1x transfer buffer was prepared from a 10x stock). Polyvinylidene fluoride transfer membrane (Pierce, Rockford, IL, USA) was soaked in methanol for ~15 minutes. The transfer cassette was assembled as per the manufacturer's instructions, filled with 1x Transfer buffer, and the transfer was performed at 100 V for 1 hour 30 minutes on ice with ddH<sub>2</sub>O ice blocks.

#### *Protein immunoblot and antibodies*

Following electrophoretic transfer membranes were stained with Ponceau S solution (Bio-Rad) for 5-10 minutes to verify transfer efficiency (i.e. substantial Ponceau S staining of the membranes), and Ponceau S stain was removed by successive washes in ddH<sub>2</sub>O. The membranes were then soaked in Tris-buffered saline containing 0.1 % Tween-20 detergent (TBST) (Sigma) for 3x 5 minutes (protein side up) to wash and equilibrate them before being blocked with 5 % BSA solution for 1hour 30 minutes at room temperature or 16 hours at 4 °C. Blocked membranes were incubated with 1:1000 primary antibody in 5% BSA on a Belly Dancer shaker (Stovall) for 1hour 30 minutes at

room temperature or ~14 hours at 4 °C.  $\beta$ -actin, Bax and Bcl 2 antibodies were purchased from Santa Cruz Biothechnology, Santa Cruz, CA. Caspase 3, AMPK, FOXO3 and p70S6K1 antibodies from Cell Signaling Technology, New England. Membranes were then washed in TBST 3x 10 minutes. Following this step, 1:5000 HRP-conjugated goat anti-rabbit or anti-mouse IgG secondary antibodies (Pierce) in 5 % BSA solution were used to probe the membrane on a shaker for 1 hour 30 minutes at room temperature. Following this step, membranes were again washed with TBST 3x 10 minutes. Following chemiluminescent imaging, membranes were stripped for re-blotting.

#### *Chemiluminescent imaging and densitometry*

Enhanced chemiluminescence (ECL) utilizes horseradish peroxidase enzyme (HRP) attached to the molecule of interest through labeling an immunoglobulin that specifically recognizes the molecule. Standard ECL was performed to detect protein-banding patterns on the immunoblots by virtue of the HRP-conjugated secondary antibodies. Chemiluminescent immunoblots were detected via 10-minute High-Sensitivity Chemiluminescent exposures using a Chemidoc XRS imager (Bio-Rad) supported by Quantity One software for Windows (Bio-Rad). Brief Epi-White exposures were also collected in order to interpret chemiluminescent banding patterns with the membranes' visible protein ladders. Blots were analyzed via densitometry using the Quantity One software, with reference to  $\beta$ -actin control.

#### *Statistics*

Data were presented as mean  $\pm$  standard error of the mean (SEM), and all data presented here represents  $n \geq 3$  independent experiments. Statistical analyses were performed using GraphPad Prism software. One-way ANOVA with post hoc Tukey's test were utilized when possible with  $p < 0.05$  considered significant. Asterisks are used herein to denote significance according to the following scheme: \*/# =  $p < 0.05$ ; \*\*/## =  $p < 0.01$ ; \*\*\*/### =  $p < 0.001$ .

## Results

### *Effect of iron and SDG on cell viability*

H9c2 cells were subjected to various concentrations of iron treatment (0.1, 1, 10, 50, 100, 200 and 300  $\mu\text{M}$  iron) for 24 hours at 37 °C, 5 %  $\text{CO}_2$ . Cell viability was assessed via the colourimetric MTT assay, wherein MTT reagent was added to cultures at  $t = 20$  hours and incubated for the remaining 4 hours before analysis at  $t = 24$  hours. All seven iron concentrations induced a significant decrease in cell viability (0.1  $\mu\text{M}$  iron decreased  $19.10 \pm 10.31\%$ ,  $p < 0.001$ ; 1  $\mu\text{M}$  iron decreased  $21.51 \pm 9.76\%$ ,  $p < 0.001$ ; 10  $\mu\text{M}$  iron decreased  $29.14 \pm 15.51\%$ ,  $p < 0.001$ ; 50  $\mu\text{M}$  iron decreased  $39.12 \pm 9.28\%$ ,  $p < 0.001$ ; 100  $\mu\text{M}$  iron decreased  $39.03 \pm 12.04\%$ ,  $p < 0.001$ ; 200  $\mu\text{M}$  iron decreased  $70.47 \pm 5.51\%$ ,  $p < 0.001$  and 300  $\mu\text{M}$  iron decreased  $70.19 \pm 4.99\%$ ,  $p < 0.001$ ) when compared to control (**Figure 5**). 50  $\mu\text{M}$  iron treatment was chosen for all further experiments because it was the lowest iron concentration that induced appreciable decrease in cell viability. To determine if SDG will negatively affect cell viability cells were treated with various concentrations of SDG (10, 50, 100 and 500  $\mu\text{M}$  SDG) for 24 hours. Cells were pre-treated for 24 hours with all four SDG concentrations in addition to 24 hour treatment with 50  $\mu\text{M}$  iron. Only 100  $\mu\text{M}$  SDG caused a small but significant decrease in cell viability ( $13.29 \pm 7.38\%$ ,  $p < 0.001$ ) when compared to control (**Figure 6**). 500  $\mu\text{M}$  SDG treatment with and without iron treatment was the only SDG treatment that did not cause a significant decrease in cell viability when compared to control but did cause an increase in viability when compared to just iron treatment (SDG increased  $25.15 \pm 34.04\%$ ,  $p < 0.001$ ; SDG + iron increased  $18.87 \pm 13.91\%$ ,  $p < 0.01$ ) (**Figure 6**), so 500  $\mu\text{M}$  SDG treatment was chosen for further experiments.

#### *Effect of SDG on iron-induced oxidative stress in H9c2 cardiomyocytes*

Iron-induced oxidative stress was investigated in cultured H9c2 cells. Intracellular ROS levels were assessed using the CM-H<sub>2</sub>DCFDA assay and measured via flow cytometry. 24-hour treatment with 50  $\mu$ M iron caused a significant increase ( $44.52 \pm 4.37\%$ ,  $p < 0.01$ ) in ROS generation (**Figure 7**) as indicated by increased mean FL1 fluorescence versus control. These data indicate a pronounced elaboration of ROS resulting from iron treatment of the H9c2 cells. Given the observed iron-induced ROS elaboration, the potential protective antioxidant effect of SDG was investigated. 24-hour pre-treatment with 500  $\mu$ M SDG abrogated the significant increase in iron-induced ROS generation, relegating it to near control levels (**Figure 7**). This finding indicates that the observed iron-induced increase in ROS was attenuated by pre-treatment with SDG.

#### *Effect of SDG on iron-induced inflammatory cytokine expression in H9c2 cardiomyocytes*

The effect of iron on the expression of tumour necrosis factor (TNF)- $\alpha$ , interleukin (IL)-10, and interferon (IFN)- $\gamma$  was investigated via qPCR. Iron treatment caused significant increases in TNF- $\alpha$  ( $3.23 \pm 0.34$  fold,  $p < 0.001$ ) (**Figure 8.1**), IL-10 ( $1.10 \pm 0.44$  fold,  $p < 0.05$ ) (**Figure 8.2**), and IFN- $\gamma$  ( $3.39 \pm 0.90$  fold,  $p < 0.01$ ) (**Figure 8.3**) versus control. These data indicate greatly enhanced expression of key inflammatory mediators in response to iron treatment. Pre-treatment with SDG abrogated the significant increase in iron-induced TNF- $\alpha$  and IL-10 expression, maintaining it at near-normal, control levels (**Figure 8.1, 8.2**). IFN- $\gamma$  expression significantly decreased when treated with SDG and iron when compared to iron treated cells ( $1.56 \pm 0.69$  fold,  $p < 0.05$ )

(**Figure 8.3**). These data indicate that SDG can abrogate the iron-induced increased expression of inflammatory cytokines.

*Effect of SDG on iron-induced matrix metalloproteinase expression in H9c2 cardiomyocytes*

Since oxidative stress and inflammation are demonstrably linked to matrix degradation and cardiac remodelling, the expression of matrix metalloproteinases (MMP)-2 and -9 was investigated via qPCR. Iron treatment caused significant increases in MMP-2 ( $1.83 \pm 0.50$  fold,  $p < 0.01$ ) (**Figure 9.1**) and MMP-9 ( $1.76 \pm 0.19$  fold,  $p < 0.001$ ) (**Figure 9.2**) versus control. These data indicate that these endopeptidases were activated upon iron treatment, suggesting extracellular matrix changes under these conditions. Pre-treatment with SDG abrogated the significant increase in iron-induced MMP-2 and -9 expression, maintaining it at near control levels (**Figure 9.1, 9.2**).

*Effect of SDG on iron-induced antioxidant enzyme expression in H9c2 cardiomyocytes*

To investigate potential cellular antioxidant responses to the observed iron-induced increase in oxidative stress, the expression of glutathione reductase (GSR), peroxiredoxin (Prdx)-6 and superoxide dismutase (SOD)2 was investigated via quantitative real-time PCR (qPCR). Iron treatment caused significant increases in GSR ( $1.95 \pm 0.68$  fold,  $p < 0.05$ ) (**Figure 10.1**), Prdx-6 ( $6.69 \pm 0.38$  fold,  $p < 0.001$ ) (**Figure 10.2**) and SOD2 ( $2.66 \pm 0.22$  fold,  $p < 0.001$ ) (**Figure 10.3**) versus control. These data indicate a robust antioxidant response to the observed iron-induced increase in ROS. Pre-treatment with SDG abrogated the significant increase in iron-induced GSR expression,

maintaining it at control levels (**Figure 10.1**). Prdx6 expression levels were similar to the control when cells were treated with just SDG. When treated with SDG and iron combined Prdx6 expression increased significantly ( $2.45 \pm 1.13$  fold,  $p < 0.05$ ) when compared to the control but decreased significantly ( $p < 0.01$ ) when compared to just iron treatment (**Figure 10.2**). SOD2 expression increased when cells were treated with just SDG (**Figure 10.3**) when compared to control ( $5.75 \pm 0.62$  fold,  $p < 0.001$ ) and iron treatment ( $3.09 \pm 0.62$  fold;  $p < 0.01$ ). When cells were treated with SDG and iron SOD2 expression was similar to the control. These findings suggest that there was an iron-induced increase in antioxidant expression.

#### *Effect of iron and SDG on SOD concentration*

To further investigate potential cellular antioxidant responses the concentration of SOD in iron and SDG treated cells was measured via the Superoxide Dismutase assay. Iron and SDG treatment caused a decrease in SOD concentration ( $54.88 \pm 11.83\%$ ,  $p < 0.05$  and  $79.61 \pm 5.11\%$ ,  $p < 0.01$  respectively) when compared to the control, while combined treatment with SDG and iron lead to an increase in SOD concentration when compared to the control and iron treated sample ( $43.79 \pm 29.14\%$ ,  $p < 0.001$  and  $221.69 \pm 17.41\%$ ,  $p < 0.001$  respectively) (**Figure 11**). This finding suggests that iron-induced decrease in SOD activity can be abrogated by treatment with SDG.

#### *Effect of SDG on iron-induced H9c2 cardiomyocyte apoptosis*

To investigate the potential cytotoxicity of the observed iron-induced ROS elaboration, the activity of apoptotic proteins, caspases 3 and 7, was assessed using the

CaspaTag assay and measured via flow cytometry. Iron caused a significant increase ( $40.86 \pm 11.56\%$ ,  $p < 0.01$ ) in apoptosis (**Figure 12**) as indicated by increased mean FL1 fluorescence versus control. These data indicate that this concentration of iron was cytotoxic to the H9c2 cells, suggesting its feasibility as a model of cardiac iron overload. Given the observed SDG-mediated prevention of iron-induced ROS elaboration, the potential cytoprotective effect of SDG was investigated. Pre-treatment with SDG abrogated the significant increase in iron-induced apoptosis, maintaining it at near control levels (**Figure 12**). This finding suggests that iron-induced activation of effector caspases can be attenuated by treatment with SDG.

#### *Effect of iron and SDG on Caspase 3 and FOXO3 activity and Bax/Bcl2 ratio*

To further investigate the iron-induced apoptosis Caspase 3, Forkhead box O3 (FOXO3), Bax, and Bcl2 protein expression was assessed via immunoblotting. Caspase 3, FOXO3 and Bax protein expression was significantly increased after 24 hour iron treatment ( $3.55 \pm 1.53$  fold,  $p < 0.01$ ,  $0.88 \pm 0.20$  fold,  $p < 0.01$  and  $4.68 \pm 1.80$  fold,  $p < 0.01$  respectively) when compared to control (**Figure 13.1, 13.2, 13.3**). Pre-treatment with SDG abrogated the significant increase in iron-induced Caspase 3, FOXO3 and Bax protein expression, maintaining it at near control levels (**Figure 13.1, 13.2, 13.3**). Bcl2 protein expression did not change significantly after 24 hour iron treatment when compared to control (**Figure 13.4**). Pre-treatment with SDG lead to a significant increase in Bcl2 protein expression when compared to control and iron treatment ( $10.82 \pm 4.37$  fold,  $p < 0.01$  and  $9.29 \pm 4.37$  fold,  $p < 0.05$  respectively) (**Figure 13.4**). These findings further suggest SDG was effective in attenuating iron-induced cell death.

#### *Effect of SDG on iron-induced MAP1lc3b1 expression in cardiomyocytes*

Expression of Microtubule-associated proteins 1 light chain 3B (MAP1lc3b1), a gene involved in autophagy, was investigated via qPCR. Iron treatment caused significant increase in MAP1lc3b1 ( $1.59 \pm 0.30$  fold,  $p < 0.01$ ) (**Figure 14**). Pre-treatment with SDG abrogated the significant increase in iron-induced MAP1lc3b1 expression, maintaining it at near control levels (**Figure 14**), suggesting that SDG can abrogate the iron-induced increased expression of autophagy gene MAP1lc3b1.

#### *Effect of iron and SDG on p70S6K1 protein expression*

Cardiac hypertrophy in response to oxidative stress has been reported to result from an increase in protein content and activation of p70S6 Kinase 1 (p70S6K1). p70S6K1 protein expression was assessed via immunoblotting and was significantly increased ( $4.17 \pm 2.26$  fold,  $p < 0.05$ ) after 24 hour iron treatment when compared to control (**Figure 15**). Pre-treatment with SDG abrogated the significant increase in iron-induced p70S6K1 protein expression, maintaining it at near control levels (**Figure 15**). This finding suggests SDG can prevent iron-induced increases in p70S6K1 protein expression.

#### *Effect of iron and SDG on AMPK protein expression*

AMP-activated protein kinase (AMPK) reserves cellular energy content and serves as a key regulator of cell survival in response to pathological stress. AMPK protein expression was assessed via immunoblotting and protein expression and was significantly

decreased after iron treatment ( $1.30 \pm 0.27$  fold,  $p < 0.05$ ) when compared to control levels (**Figure 16**). Pre-treatment with SDG abrogated the significant decrease in iron-induced AMPK protein expression, maintaining it at near control levels (**Figure 16**). This finding suggests iron overload can lead to a decrease in AMPK and cell survival, and this decrease in protein expression can be prevented by SDG.

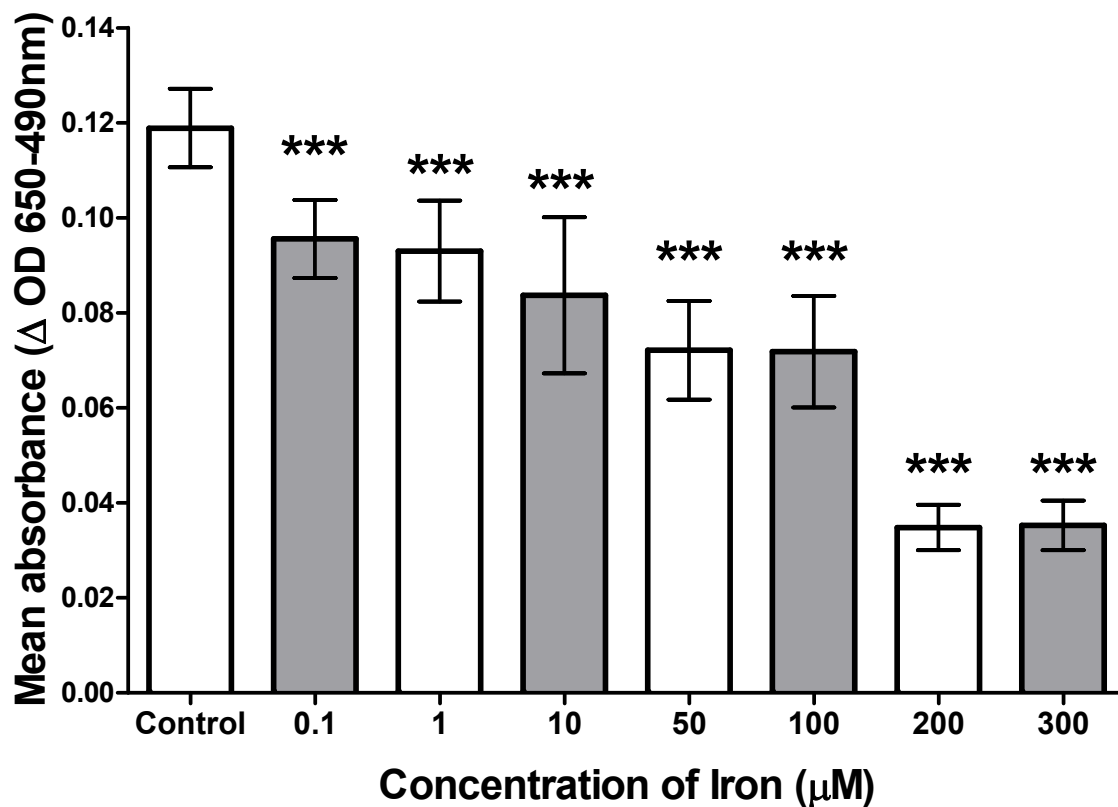


**Figure 5 Effect of iron on cell viability.** The effect of iron on the viability of H9c2 cells was assessed via measurement of mitochondrial dehydrogenase activity (MTT assay). Cells were treated in medium containing 0.1, 1, 10, 50, 100, 200 and 300 μM iron. Bars represent mean ± SEM of 3 independent experiments. Data is expressed as mean absorbance (\*\*\* =  $p < 0.001$  versus control).

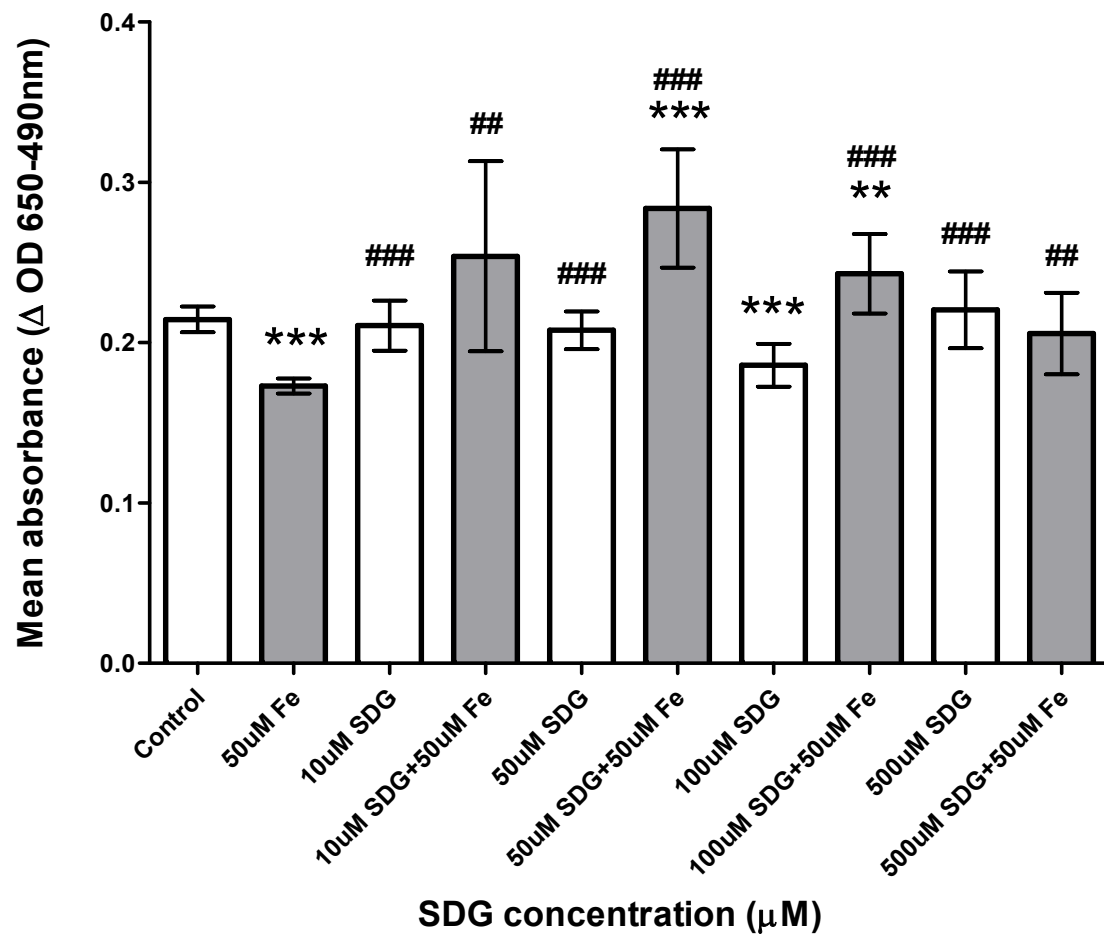


**Figure 6 Effect of SDG on iron induced decrease of cell viability.** The effect of iron and SDG on the viability of H9c2 cells was assessed via measurement of mitochondrial dehydrogenase activity (MTT assay). Cells were treated in medium containing 50  $\mu$ M iron and/or 500  $\mu$ M SDG. Bars represent mean  $\pm$  SEM of 3 independent experiments. Data is expressed as mean absorbance (\*\* =  $p < 0.01$  versus control; \*\*\* =  $p < 0.001$  versus control; ## =  $p < 0.01$  versus iron; ### =  $p < 0.001$  versus iron).

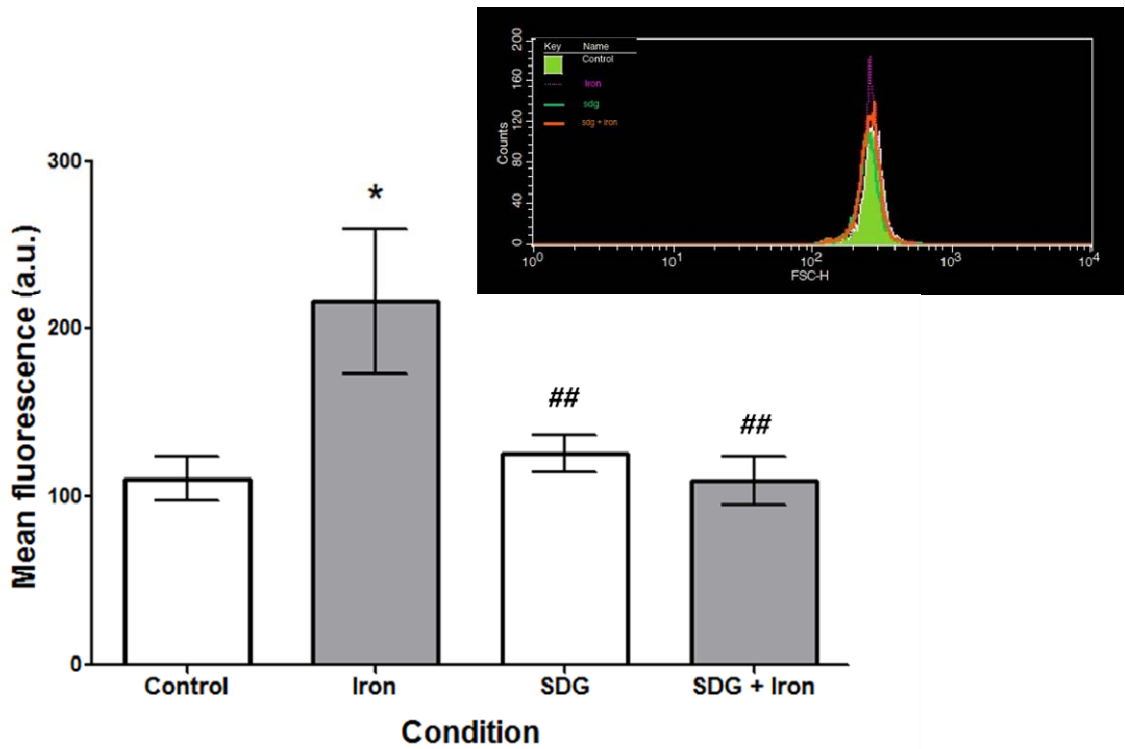


**Figure 7 Effect of SDG on iron-induced oxidative stress in cardiomyocytes.** The effect of iron and SDG on intracellular ROS levels in H9c2 cells was assessed via fluorescent detection of oxidation-induced esterase activity (CM-H2DCFDA assay), and analyzed via flow cytometry. Cells were treated in medium containing 50  $\mu$ M iron and/or 500  $\mu$ M SDG. Bars represent mean  $\pm$  SEM of 3 independent experiments. Data is expressed as mean fluorescence arbitrary units (a.u.) (\* =  $p < 0.05$  versus control; ## =  $p < 0.01$  versus iron)

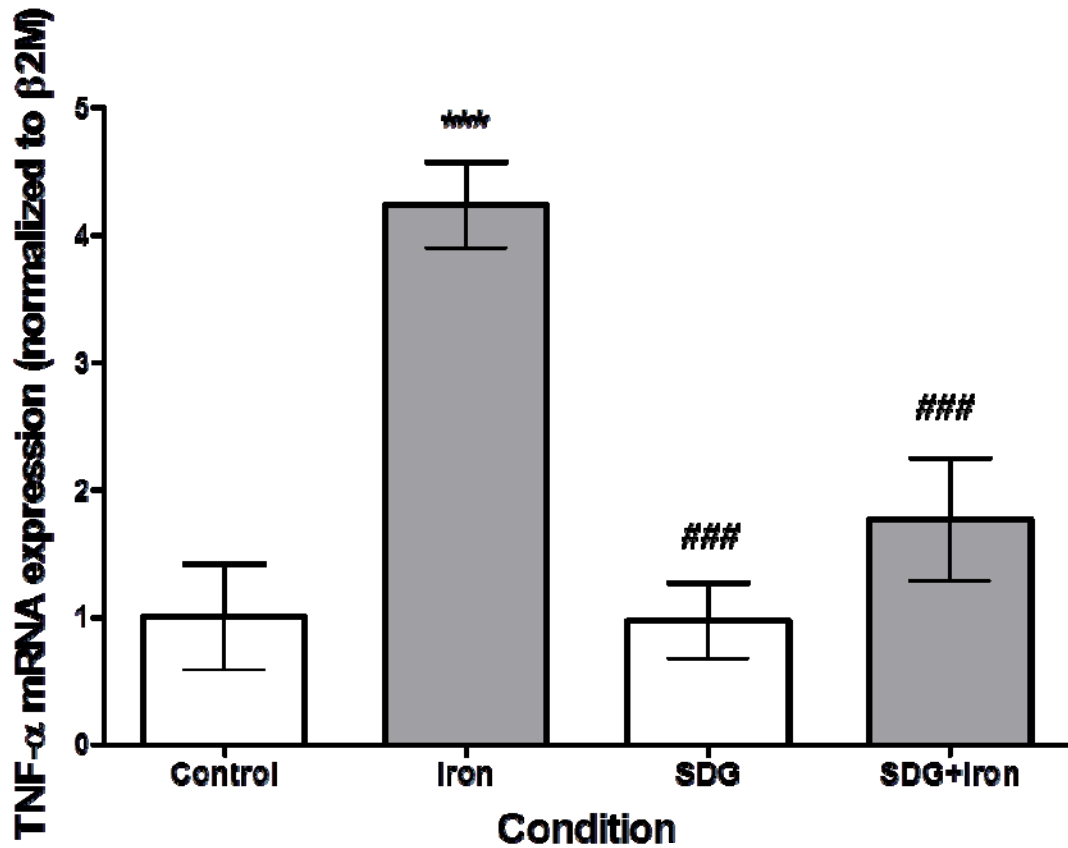
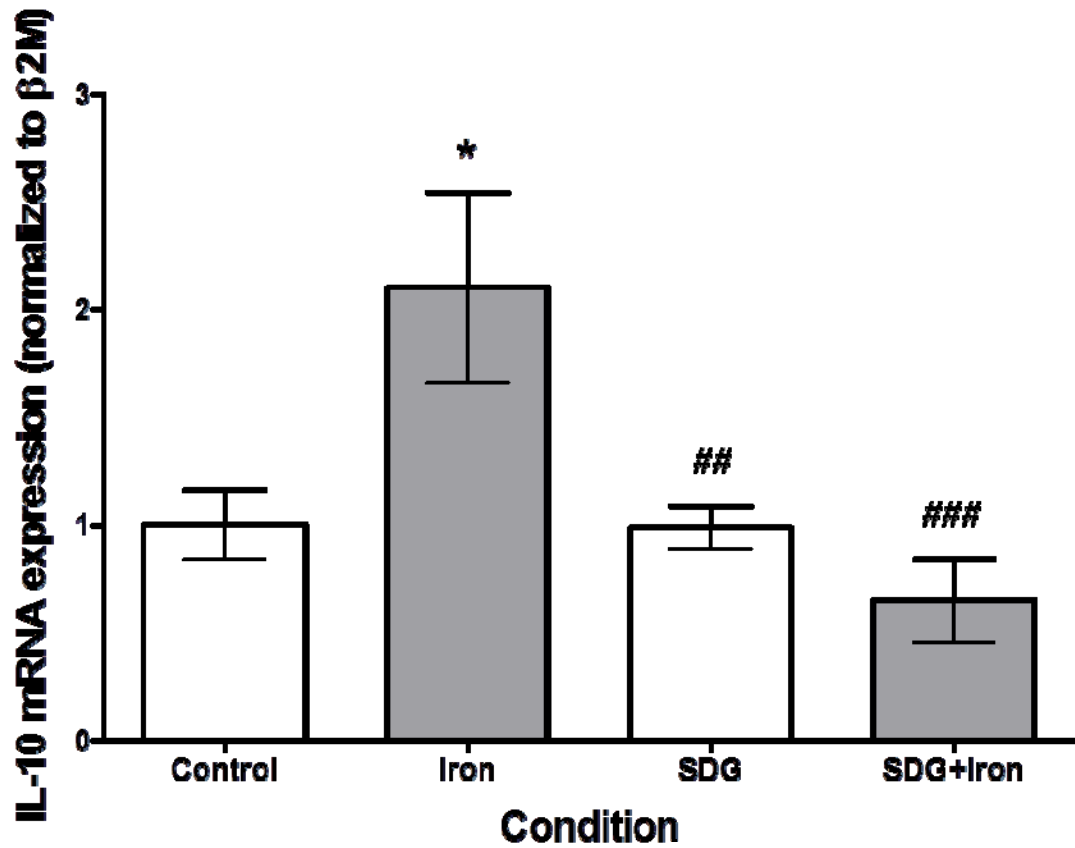
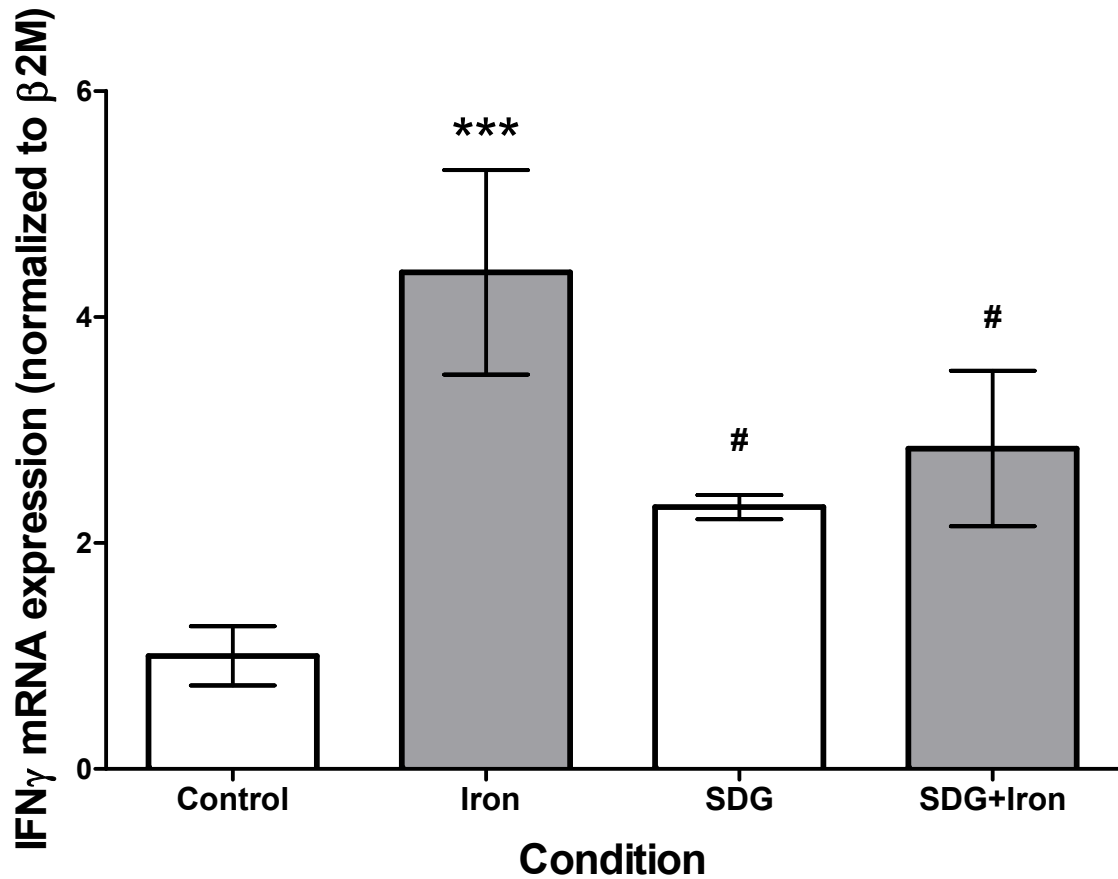


Figure 8.1 Effect of SDG on iron-induced tumour necrosis factor  $\alpha$  mRNA expression in H9c2 cardiomyocytes. The effect of iron and SDG on TNF- $\alpha$  mRNA expression in H9c2 cells was assessed via qPCR. Cells were treated in medium containing 50  $\mu$ M iron and/or 500  $\mu$ M SDG. Real-time PCR was performed and results were normalized to  $\beta$ 2M and normal expression standardized to the control. Bars represent mean  $\pm$  SEM of 3 independent experiments (\*\*\*) =  $p < 0.001$  versus control; ### =  $p < 0.001$  versus iron).



**Figure 8.2 Effect of SDG on iron-induced interleukin 10 mRNA expression in H9c2 cardiomyocytes.** The effect of iron and SDG on IL-10 mRNA expression in H9c2 cells was assessed via qPCR. Cells were treated in medium containing 50 μM iron and/or 500 μM SDG. Real-time PCR was performed and results were normalized to β2M and normal expression standardized to the control. Bars represent mean ± SEM of 3 independent experiments (\* =  $p < 0.05$  versus control; ### =  $p < 0.001$  versus iron; \*\* =  $p < 0.01$  versus iron).



**Figure 8.3 Effect of SDG on iron-induced interferon  $\gamma$  mRNA expression in H9c2 cardiomyocytes.** The effect of iron and SDG on IFN- $\gamma$  mRNA expression in H9c2 cells was assessed via qPCR. Cells were treated in medium containing 50  $\mu$ M iron and/or 500  $\mu$ M SDG. Real-time PCR was performed and results were normalized to  $\beta$ 2M and normal expression standardized to the control. Bars represent mean  $\pm$  SEM of 3 independent experiments (\*\*\*) =  $p < 0.001$  versus control; # =  $p < 0.05$  versus iron).

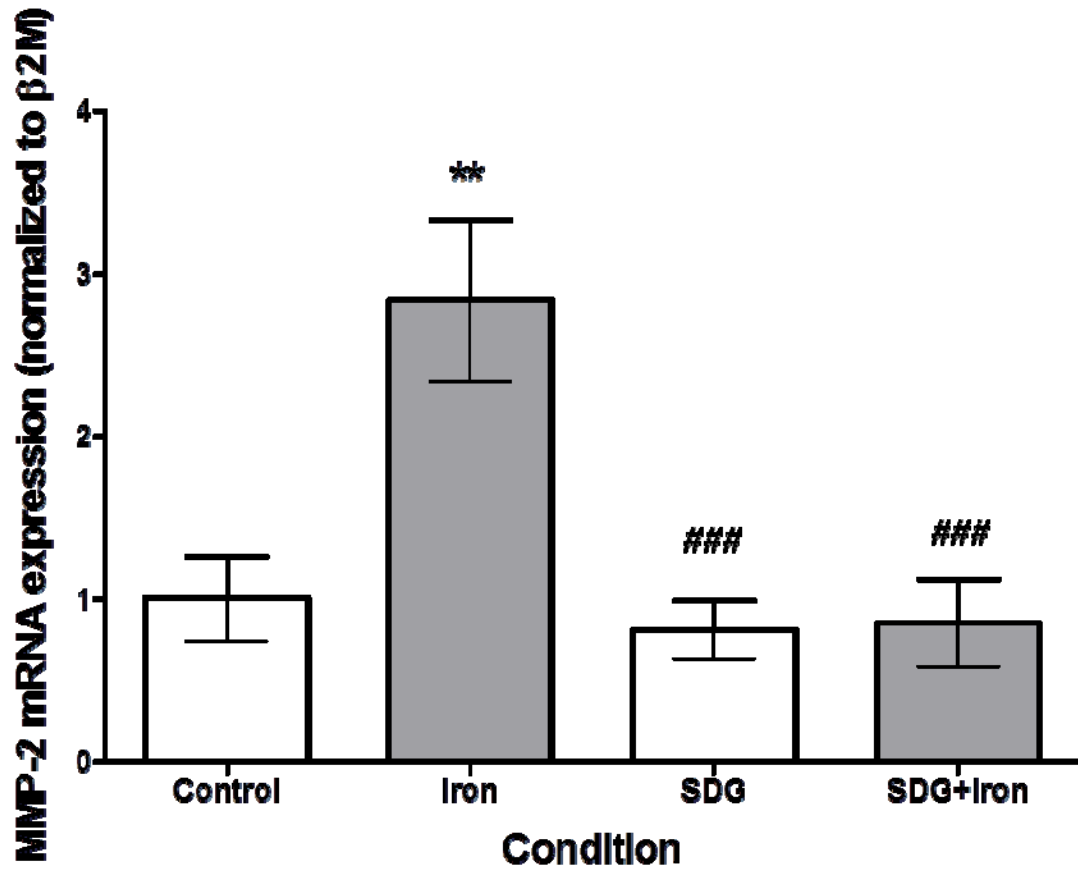
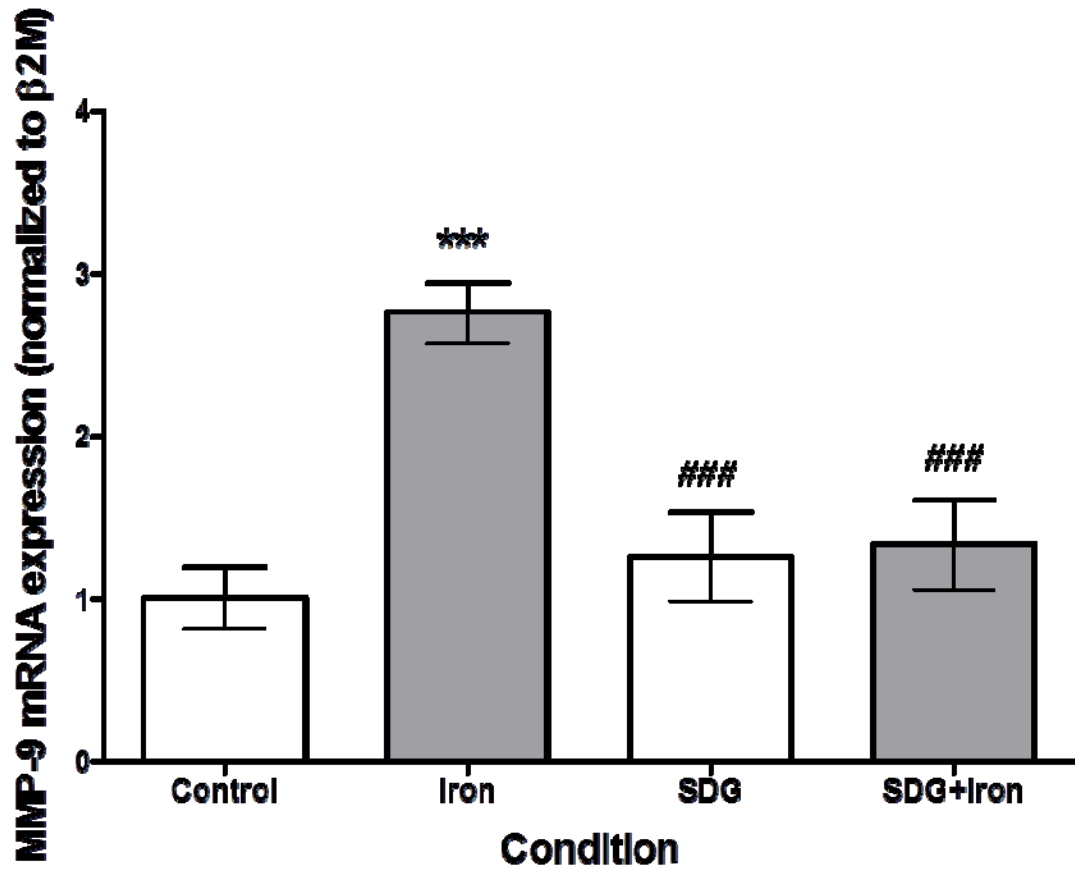
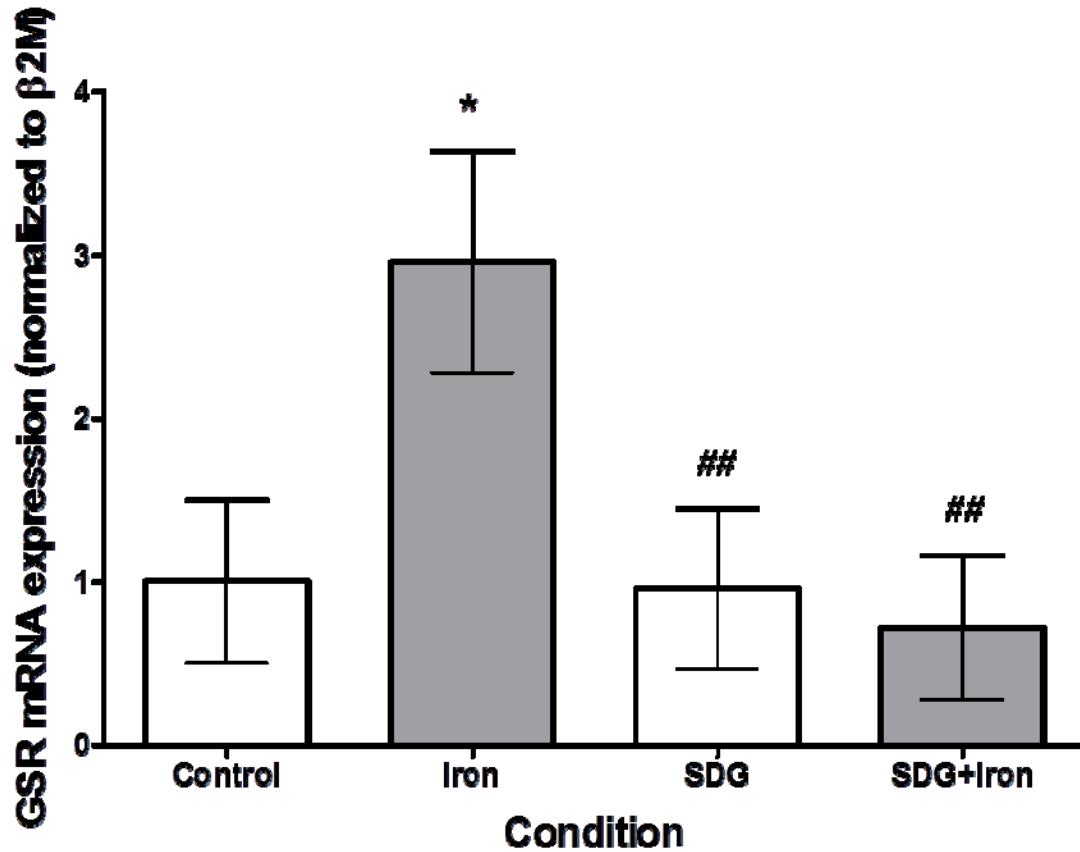


Figure 9.1 Effect of SDG on iron-induced matrix metalloproteinase 2 mRNA expression in H9c2 cardiomyocytes. The effect of iron and SDG on MMP-2 mRNA expression in H9c2 cells was assessed via qPCR. Cells were treated in medium containing 50  $\mu$ M iron and/or 500  $\mu$ M SDG. Real-time PCR was performed and results were normalized to  $\beta$ 2M and normal expression standardized to the control. Bars represent mean  $\pm$  SEM of 3 independent experiments (\*\* =  $p < 0.01$  versus control; ### =  $p < 0.001$  versus iron).



**Figure 9.2** Effect of SDG on iron-induced matrix metalloproteinase 9 mRNA expression in H9c2 cardiomyocytes. The effect of iron and SDG on MMP-9 mRNA expression in H9c2 cells was assessed via qPCR. Cells were treated in medium containing 50  $\mu$ M iron and/or 500  $\mu$ M SDG. Real-time PCR was performed and results were normalized to  $\beta$ 2M and normal expression standardized to the control. Bars represent mean  $\pm$  SEM of 3 independent experiments (\*\*\*) =  $p < 0.001$  versus control; ### =  $p < 0.001$  versus iron).



**Figure 10.1** Effect of SDG on iron-induced glutathione reductase mRNA expression in H9c2 cardiomyocytes. The effect of iron and SDG on GSR mRNA expression in H9c2 cells was assessed via qPCR. Cells were treated in medium containing 50 μM iron and/or 500 μM SDG. Real-time PCR was performed and results were normalized to β2M and normal expression standardized to the control. Bars represent mean ± SEM of 3 independent experiments (\* =  $p < 0.05$  versus control; ## =  $p < 0.01$  versus iron).

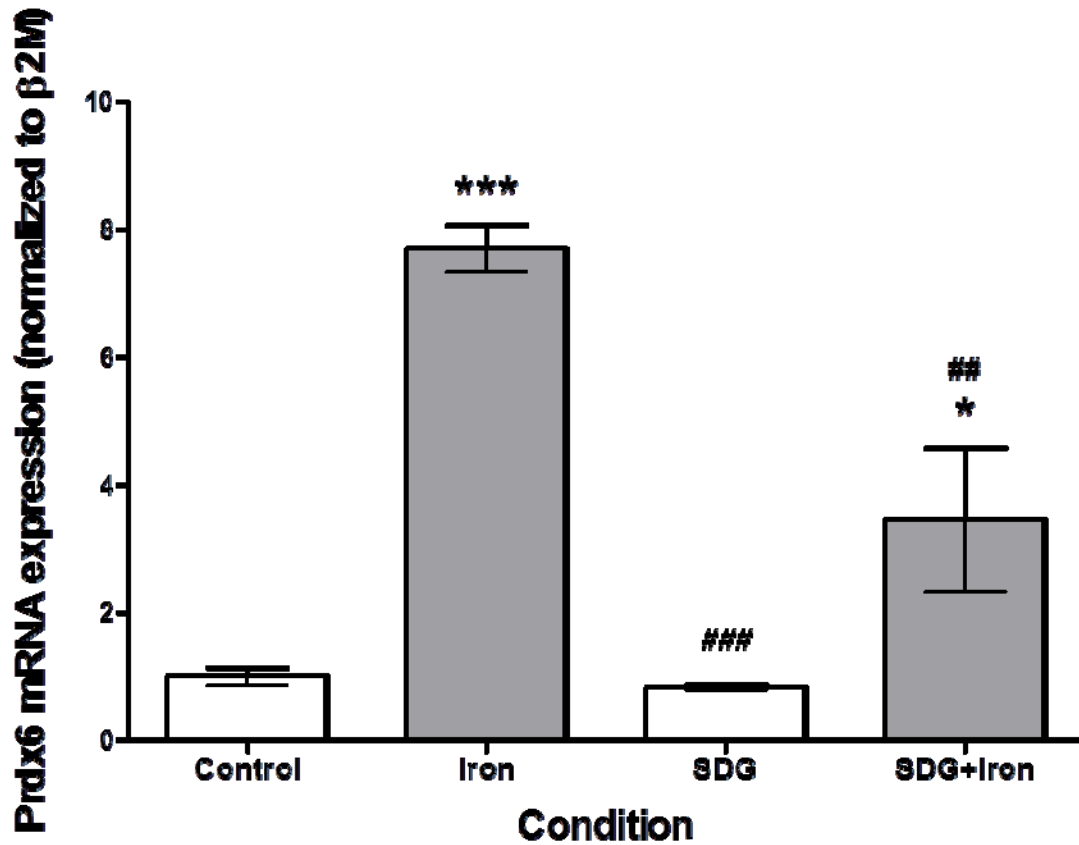


**Figure 10.2 Effect of SDG on iron-induced peroxiredoxin 6 mRNA expression in H9c2 cardiomyocytes.** The effect of iron and SDG on Prdx6 mRNA expression in H9c2 cells was assessed via qPCR. Cells were treated in medium containing 50  $\mu M$  iron and/or 500  $\mu M$  SDG. Real-time PCR was performed and results were normalized to  $\beta 2M$  and normal expression standardized to the control. Bars represent mean  $\pm$  SEM of 3 independent experiments (\*\*\*) =  $p < 0.001$  versus control; \* =  $p < 0.05$  versus control; ### =  $p < 0.001$  versus iron; ## =  $p < 0.01$  versus iron).

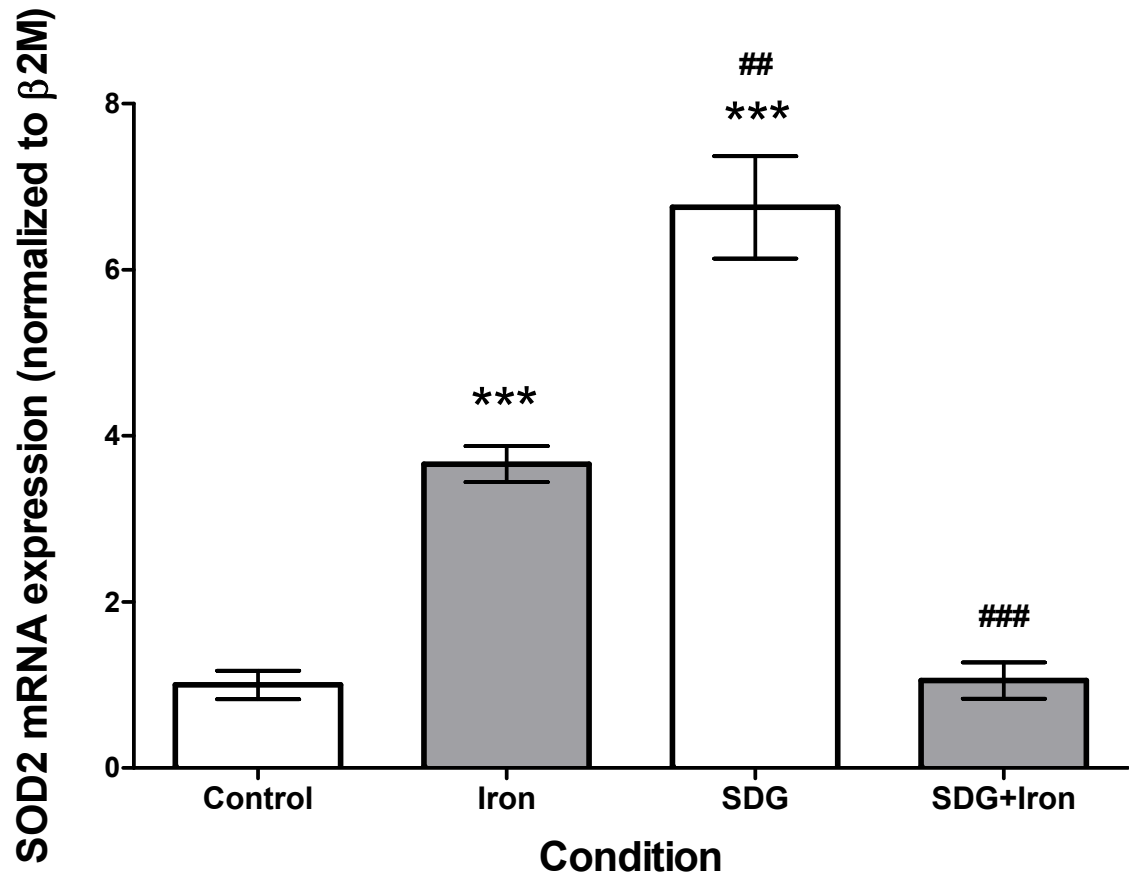


**Figure 10.3 Effect of SDG on iron-induced superoxide dismutase 2 mRNA expression in H9c2 cardiomyocytes.** The effect of iron and SDG on SOD2 mRNA expression in H9c2 cells was assessed via qPCR. Cells were treated in medium containing 50 μM iron and/or 500 μM SDG. Real-time PCR was performed and results were normalized to β2M and normal expression standardized to the control. Bars represent mean ± SEM of 3 independent experiments (\*\*\*) =  $p < 0.001$  versus control; ### =  $p < 0.001$  versus control; ## =  $p < 0.01$  versus iron).

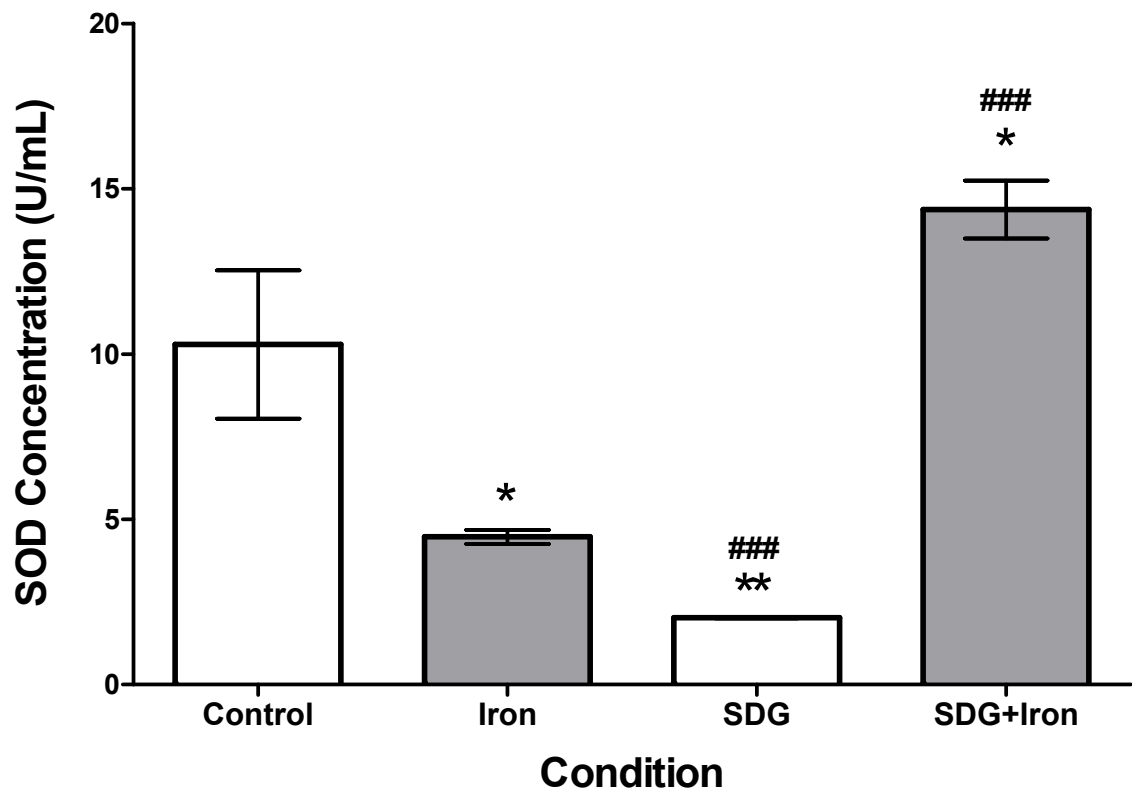


**Figure 11 Effect of iron and SDG on SOD concentration in H9c2 cardiomyocytes.** The effect of iron and SDG on SOD activity in H9c2 cells was assessed via a colourimetric SOD activity assay. Cells were treated in medium containing 50  $\mu$ M iron and/or 500  $\mu$ M SDG. Bars represent mean  $\pm$  SEM of 3 independent experiments (\*\* =  $p < 0.01$  versus control; \* =  $p < 0.05$  versus control; ### =  $p < 0.001$  versus iron).

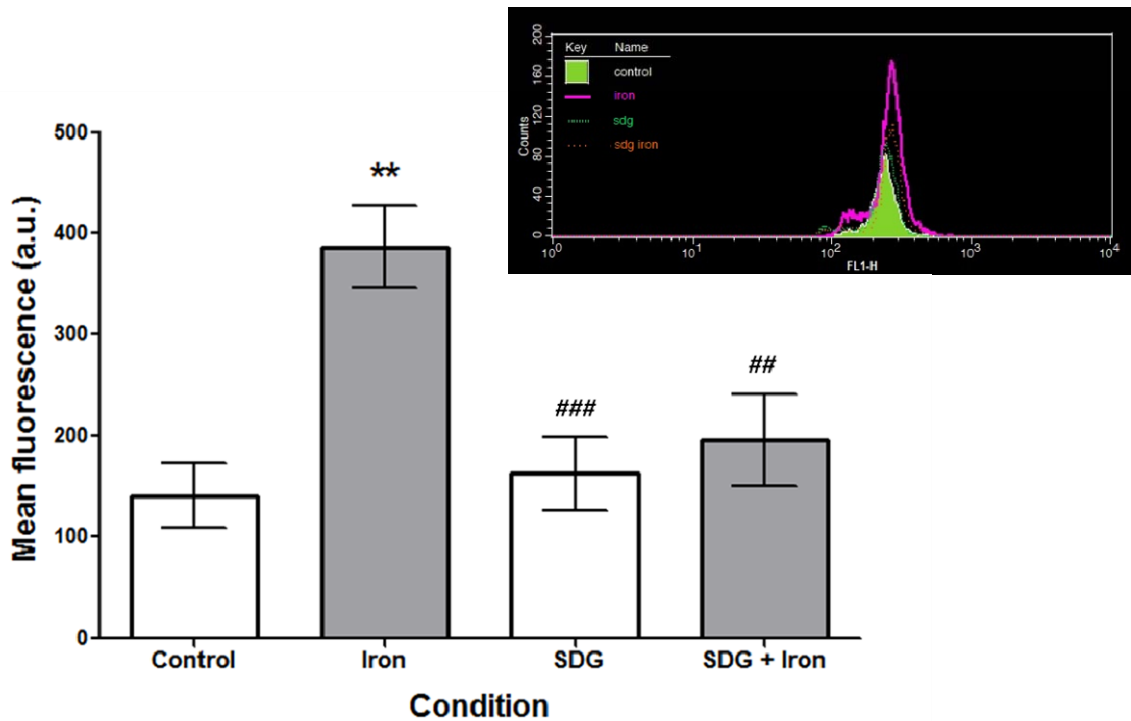


**Figure 12 Effect of SDG on iron-induced H9c2 cardiomyocyte apoptosis.** The effect of iron and SDG on H9c2 cellular apoptosis was assessed via the fluorescent detection of active caspase-3 and -7 (CaspTag 3/7 assay), and analyzed via flow cytometry. Cells were treated in medium containing 50  $\mu\text{M}$  iron and/or 500  $\mu\text{M}$  SDG. Bars represent mean  $\pm$  SEM of 3 independent experiments. Data is expressed as mean fluorescence arbitrary units (a.u.) (\*\* =  $p < 0.01$  versus control; ### =  $p < 0.001$  versus iron; ## =  $p < 0.01$  versus iron).

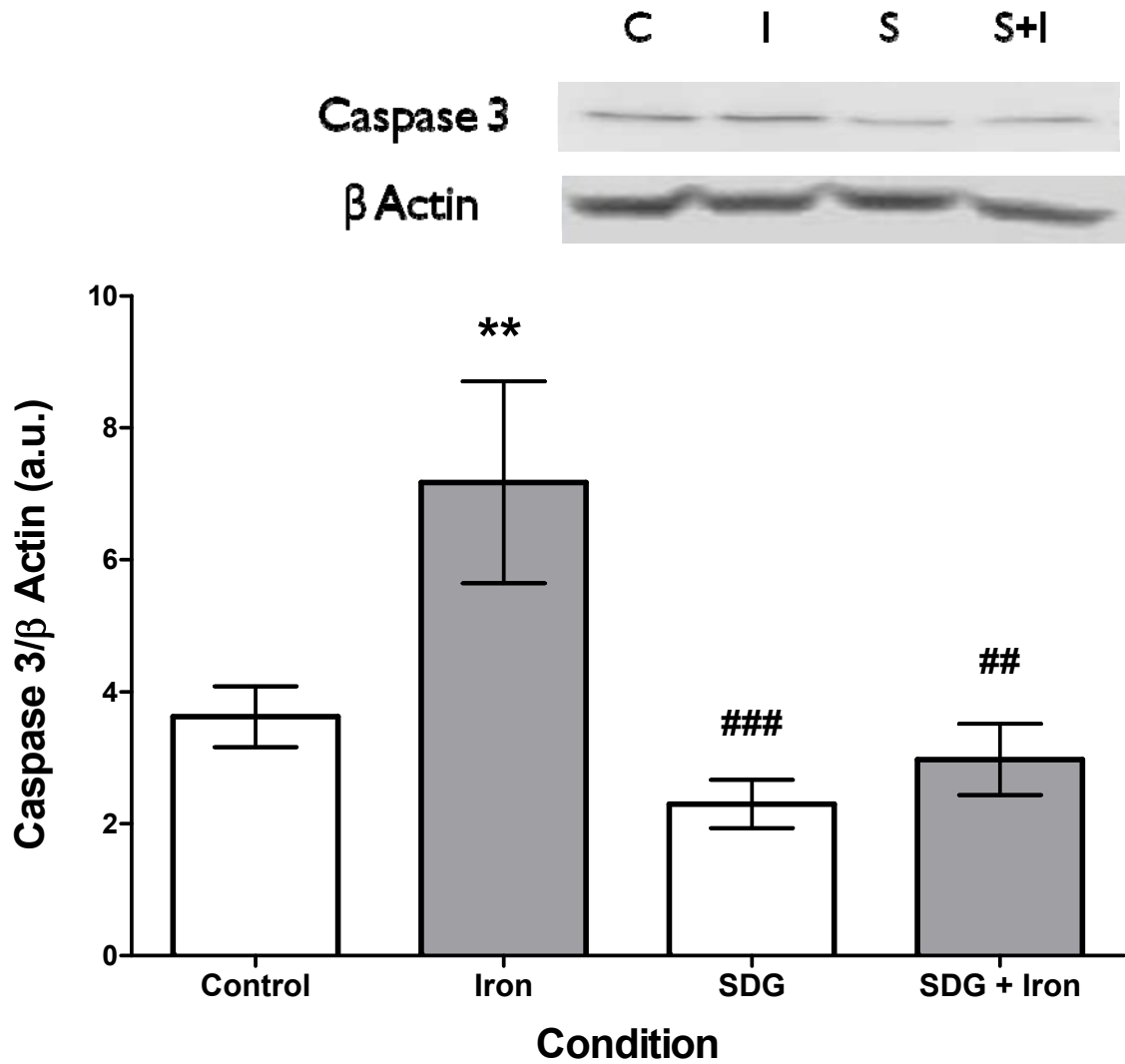


**Figure 13.1** Effect of iron and SDG on Caspase 3 protein expression in H9c2 cardiomyocytes. The effect of iron and SDG on Caspase 3 protein expression in H9c2 cells was assessed via immunoblotting, where C = control, I = iron, S = SDG and S+I = SDG + iron. Bars represent mean  $\pm$  SEM of 4 independent experiments (\*\* =  $p < 0.01$  versus control; ### =  $p < 0.001$  versus iron; ## =  $p < 0.01$  versus iron).

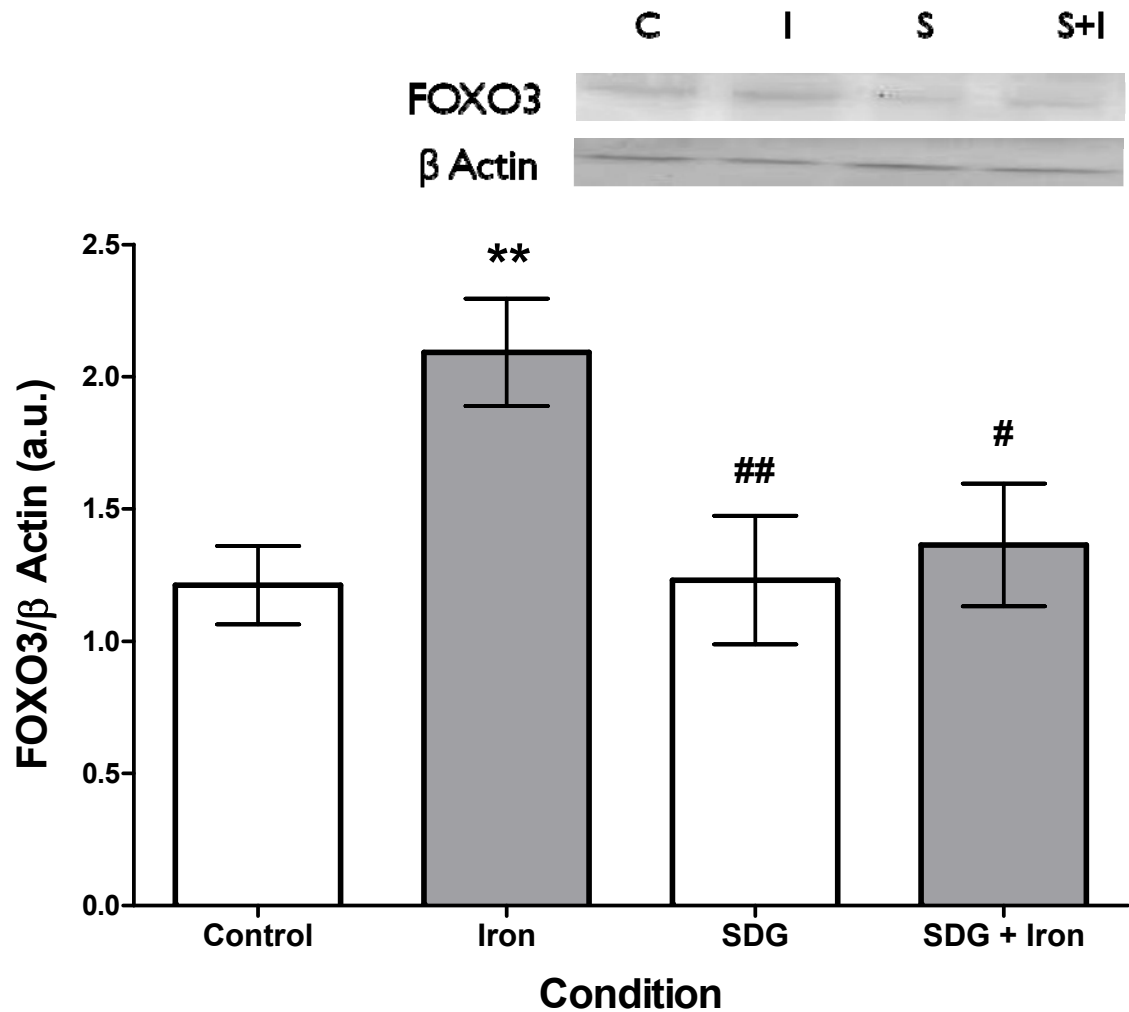


**Figure 13.2 Effect of iron and SDG on FOXO3 protein expression in H9c2 cardiomyocytes.**

The effect of iron and SDG on FOXO3 protein expression in H9c2 cells was assessed via immunoblotting, where C = control, I = iron, S = SDG and S+I = SDG + iron. Bars represent mean  $\pm$  SEM of 3 independent experiments (\*\* =  $p < 0.01$  versus control; ## =  $p < 0.01$  versus iron; # =  $p < 0.05$  versus iron).

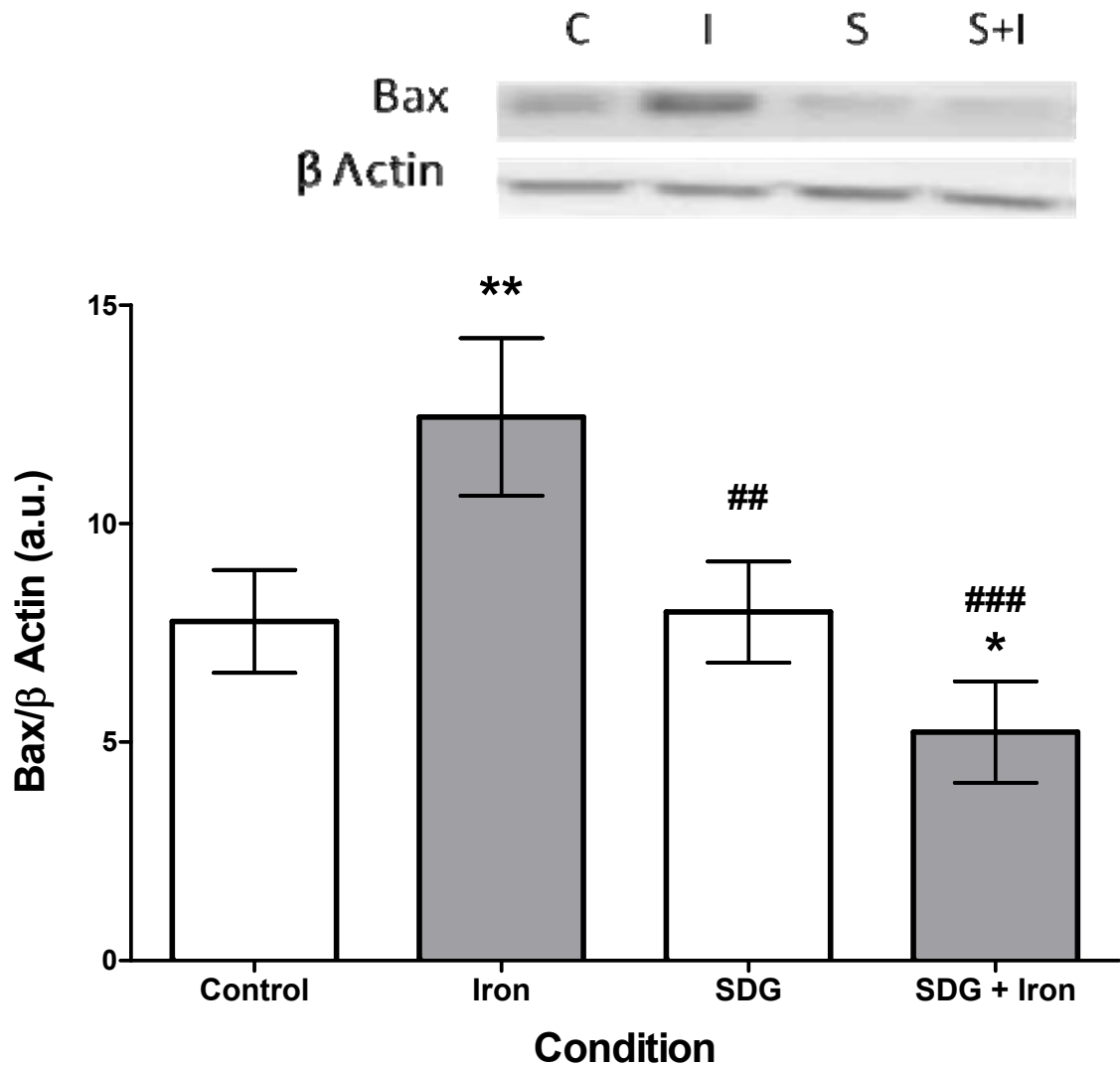


**Figure 13.3** Effect of iron and SDG on Bax protein expression in H9c2 cardiomyocytes. The effect of iron and SDG on Bax protein expression in H9c2 cells was assessed via immunoblotting, where C = control, I = iron, S = SDG and S+I = SDG + iron. Bars represent mean  $\pm$  SEM of 4 independent experiments (\*\* =  $p < 0.01$  versus control; \* =  $p < 0.05$  versus control; ### =  $p < 0.001$  versus iron; ## =  $p < 0.01$  versus iron).

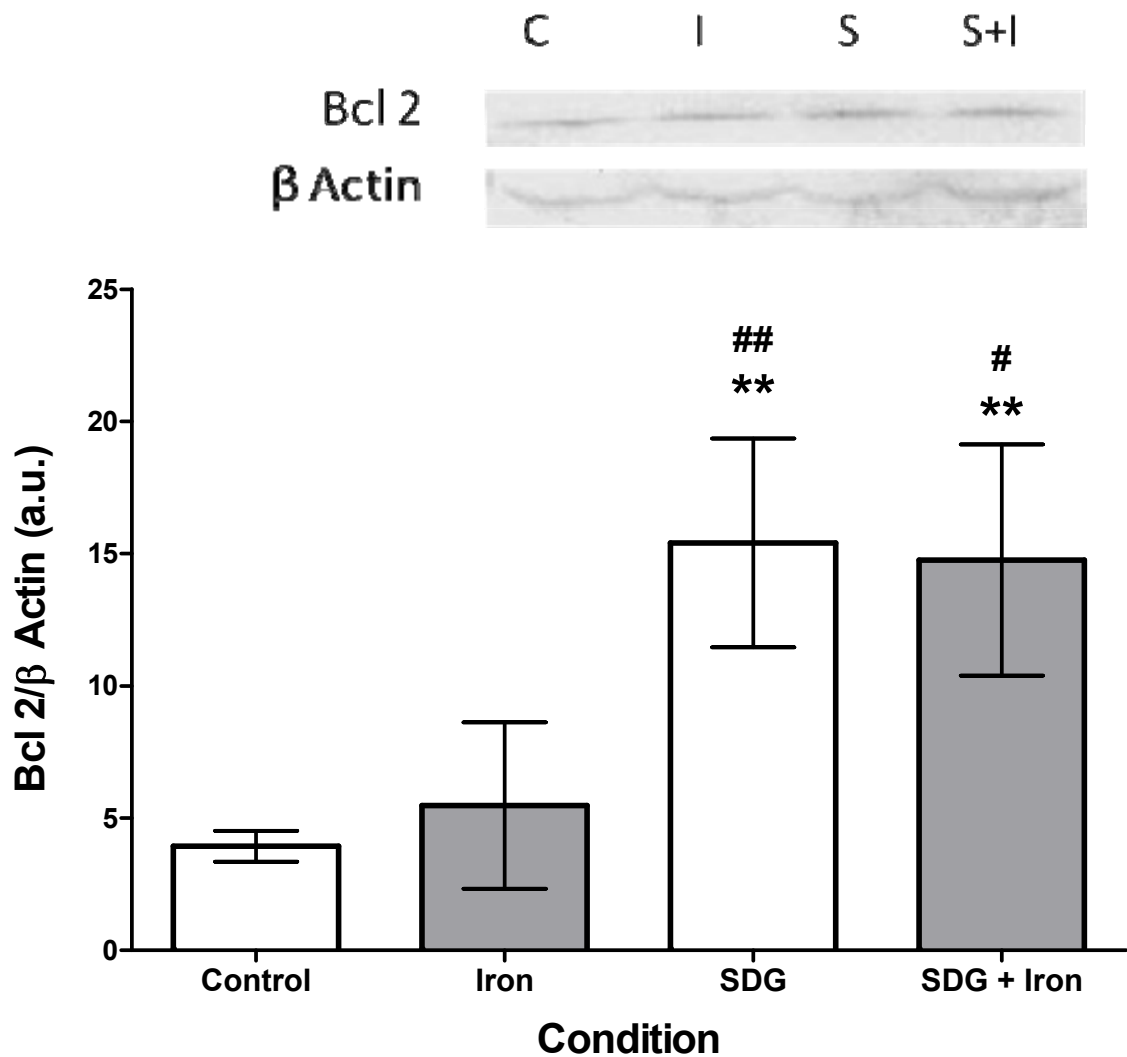


**Figure 13.4 Effect of iron and SDG on Bcl2 protein expression in H9c2 cardiomyocytes.** The effect of iron and SDG on Bcl2 protein expression in H9c2 cells was assessed via immunoblotting, where C = control, I = iron, S = SDG and S+I = SDG + iron. Bars represent mean  $\pm$  SEM of 4 independent experiments (\*\* =  $p < 0.01$  versus control; ## =  $p < 0.01$  versus iron; # =  $p < 0.05$  versus iron).

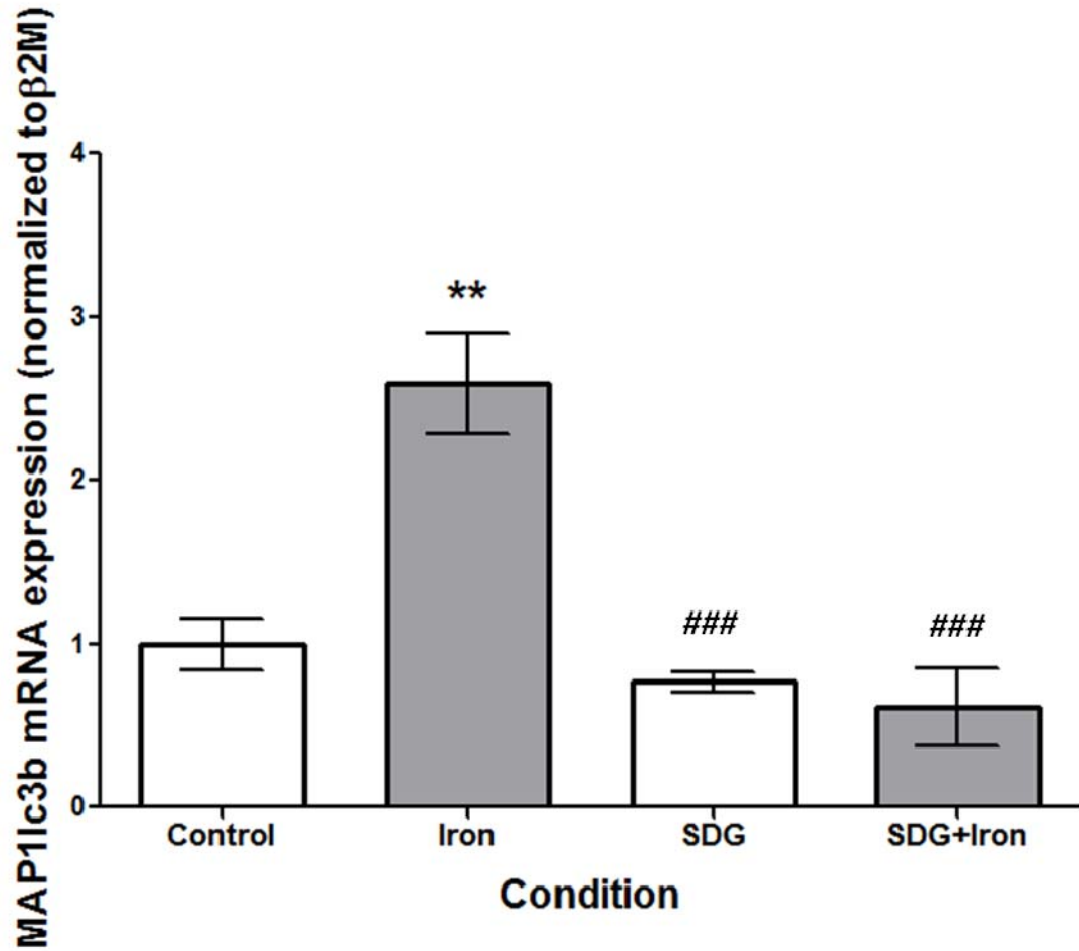


**Figure 14 Effect of SDG on iron-induced MAP1c3b1 mRNA expression in H9c2 cardiomyocytes.** The effect of iron and SDG on MAP1lc3b mRNA expression in H9c2 cells was assessed via qPCR. Cells were treated medium containing 50 μM iron and/or 500 μM SDG. Real-time PCR was performed and results were normalized to β2M and normal expression standardized to the control. Bars represent mean ± SEM of 3 independent experiments (\*\* =  $p < 0.01$  versus control; ### =  $p < 0.001$  versus iron).

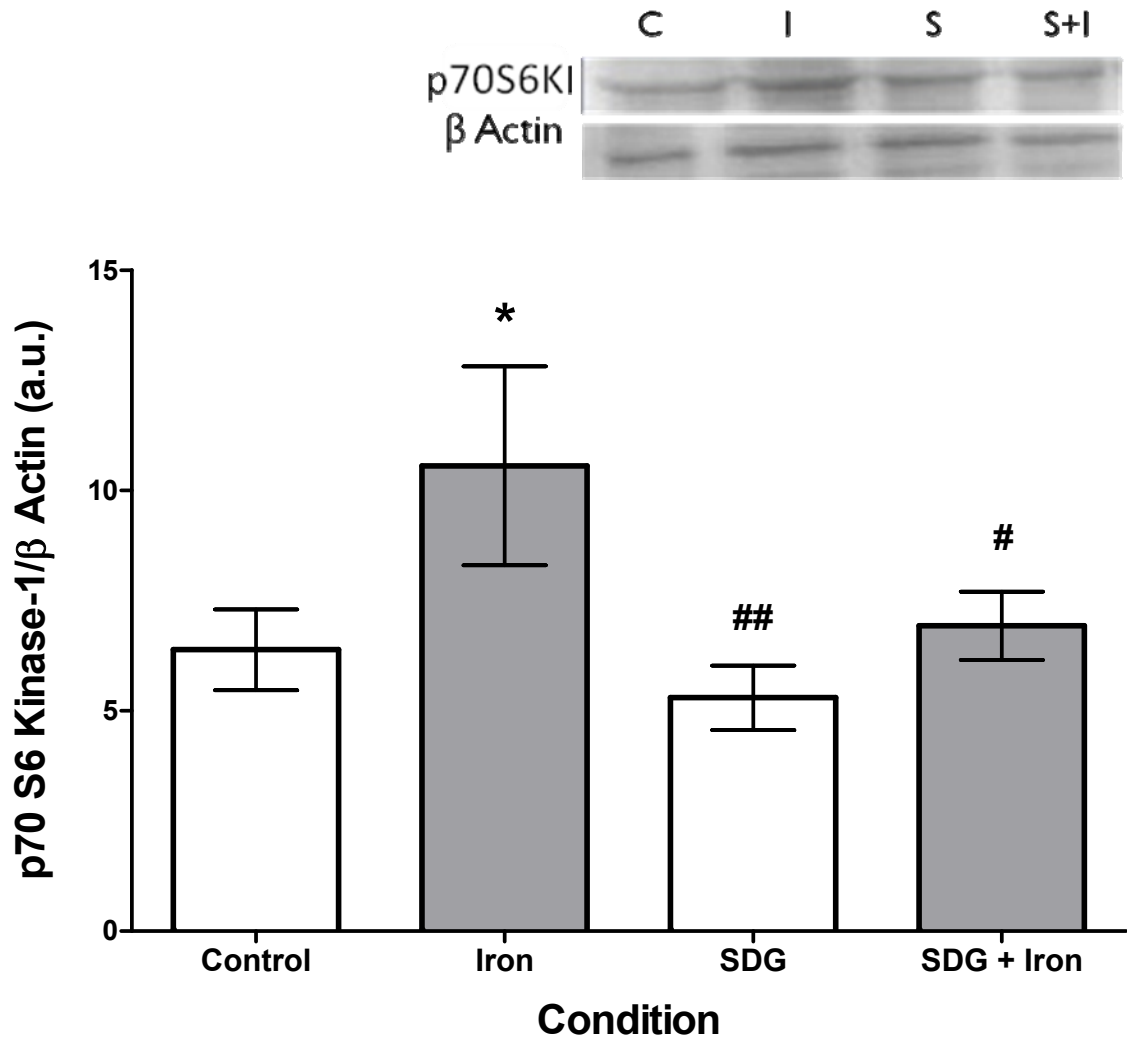


**Figure 15 Effect of iron and SDG on p70S6 Kinase protein expression in H9c2 cardiomyocytes.** The effect of iron and SDG on p70S6 Kinase protein expression in H9c2 cells was assessed via immunoblotting, where C = control, I = iron, S = SDG and S+I = SDG + iron. Bars represent mean  $\pm$  SEM of 3 independent experiments (\* =  $p < 0.05$  versus control; ## =  $p < 0.01$  versus iron; # =  $p < 0.05$  versus iron).

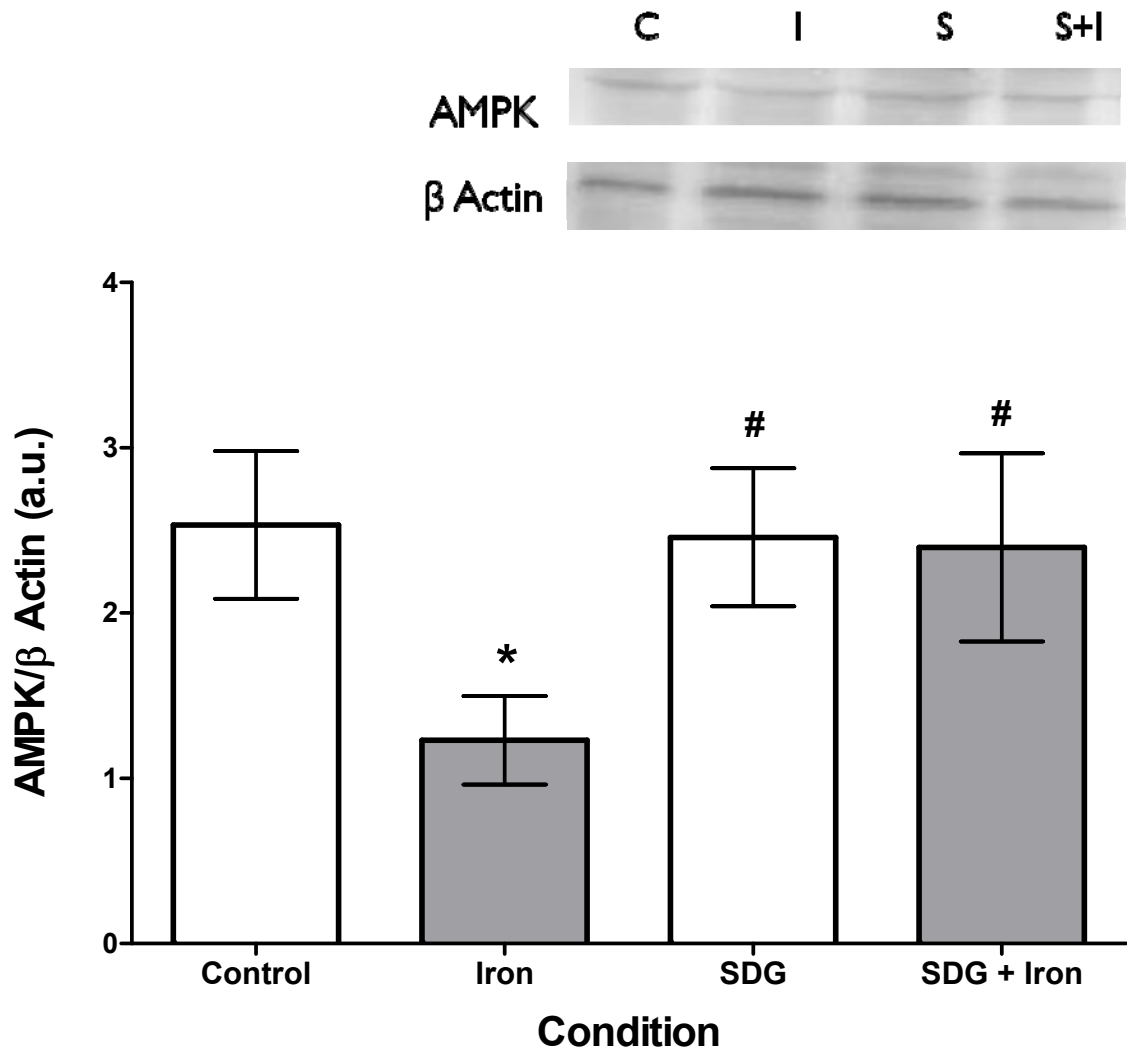


**Figure 16 Effect of iron and SDG on AMPK protein expression in H9c2 cardiomyocytes.** The effect of iron and SDG on AMPK protein expression in H9c2 cells was assessed via immunoblotting, where C = control, I = iron, S = SDG and S+I = SDG + iron. Bars represent mean  $\pm$  SEM of 3 independent experiments (\* =  $p < 0.05$  versus control; # =  $p < 0.05$  versus iron).

## Discussion

Iron overload cardiomyopathy, resulting from primary or secondary iron overload disorders, is responsible for considerable cardiovascular morbidity and mortality [10; 147; 148; 149; 150]. A recent study suggested that free iron in the plasma enters cardiac cells via L-type  $\text{Ca}^{2+}$  channels as reduced iron,  $\text{Fe}^{2+}$  [1; 10].  $\text{Fe}^{2+}$  can then lead to the formation of ROS via the Fenton Reaction by interacting with oxygen species produced in the electron transport chain in the mitochondria, interconverting between  $\text{Fe}^{2+}$  and  $\text{Fe}^{3+}$  to generate further ROS [4; 5; 151]. Currently, treatment options are limited; the only options for patients are phlebotomy and chelation therapy, both can cause detrimental side effects, be expensive, inconvenient and are sometimes ineffective [3; 7; 16]. Secoisolariciresinol diglucoside is an antioxidant present in flaxseed and is known to decrease the production of inflammatory mediators and the superoxide anion. Previous studies have shown that SDG prevents the development of hypercholesterolemic atherosclerosis, induces angiogenesis-mediated cardioprotection [140; 145; 146], and prevents the development of type 1 and type 2 diabetes [140; 144; 145; 152]. We investigated the effects of iron overload on oxidative stress, inflammation and apoptosis in H9c2 cells. Furthermore, we also investigated if SDG can abrogate the unfavourable effects of iron overload.

Iron overload in H9c2 cells resulted in a decrease in cell viability as measured via the MTT assay, a commonly used method of measuring toxicity *in vitro*. After 24 hours all seven iron concentrations induced a significant decrease in cell viability. Based on the

results obtained 50  $\mu\text{M}$  iron treatment was chosen for all further experiments because it was the lowest iron concentration that induced an appreciable decrease in viability but there were still enough viable cells to perform further experiments. Cells were treated with different concentrations of SDG for 24 hours to investigate if SDG had any detrimental effects on cell viability as well as if there was any protection when combined with 50  $\mu\text{M}$  iron. 500  $\mu\text{M}$  SDG treatment in the presence or absence of iron treatment was the only SDG concentration that did not cause a significant decrease in cell viability when compared to control or each other but did cause an improvement in viability when compared to iron treatment alone. These data suggests pre-treatment with 500  $\mu\text{M}$  SDG prevents the decrease in oxidative phosphorylation caused by iron treatment leading to higher metabolic activity and more viable cells.

Iron-mediated damage likely involves the role of mitochondrially generated ROS. Previous studies using the same cell line found that iron overload causes progressive loss of intact mitochondrial DNA (mtDNA), decreased expression of respiratory chain subunits encoded by mitochondrial, but not nuclear, DNA, and diminished respiratory function. They also reported that iron-mediated cytotoxicity involves ROS generated by the mitochondrion itself because cells lacking mtDNA are remarkably tolerant of iron overload [153]. In our study ROS production was shown to increase in 50  $\mu\text{M}$  iron treated cells as shown with the CM-H<sub>2</sub>DCFDA assay. The increase in levels of ROS in excess iron is likely to be caused by the Fenton reaction, as mentioned earlier. Pre-treatment with SDG abrogated the significant increase in iron-induced ROS generation, relegating it to near control levels. This suggests SDG can work as an antioxidant and scavenge ROS produced by increased iron.

A significant relationship exists between oxidative stress and inflammation in cardiovascular diseases leading to heart failure whereby increased ROS has been shown to promote pro-inflammatory mediator expression [38; 51; 154]. Cardiovascular diseases are associated with inflammation and cytokine modulation [37; 154], and chronic heart failure is often characterized by elevated pro-inflammatory cytokine expression [37; 38; 154; 155]. For an indicator of inflammation mRNA expression of inflammatory mediators, TNF- $\alpha$ , IL-10 and IFN $\gamma$ , was assessed via qPCR. Previous studies have shown that there is an increase in pro-inflammatory TNF- $\alpha$  expression in the failing myocardium [155]. Among its many effects, TNF- $\alpha$  is an initiator of the extrinsic apoptotic pathway [42]. IL-10 is an anti-inflammatory cytokine known to down-regulate the production of TNF- $\alpha$ , and it has similarly been detected in failing myocardium [52; 58; 156]. Under iron overload conditions, H9c2 cells feature significantly higher expression of pro and anti-inflammatory cytokines. Taken together, these data indicate a strong inflammatory response in iron overload. Pre-treatment with SDG abrogated the significant increase in iron-induced TNF- $\alpha$  and IL-10 expression, maintaining it at near control levels, while IFN- $\gamma$  expression significantly decreased when treated with SDG and iron when compared to iron treated cells. These data suggest SDG is capable of preventing the increase in inflammation in iron treated cells.

Matrix metalloproteinases participate in tissue remodelling in cardiovascular diseases associated with enhanced oxidative stress [72]. MMP-2 and MMP-9 are the two major remodelling proteins in the heart and are known to play key roles in various cardiac disease states [76]. A previous study demonstrated that H9c2 cardiomyoblasts exposed to oxidative stress exhibited increased MMP2 activity, leading to cleavage and activation of

the apoptotic protein, glycogen synthase kinase-3 $\beta$  [72]. It has also been shown that MMP-9 is robustly increased during various stages of congestive heart failure [77]. Furthermore, studies have shown that MMP-9 has a major role in ventricular remodelling associated with endothelial and myocyte apoptosis [77]. In the present iron overload condition, we demonstrated increased mRNA expression of both MMP-2 and -9, which corresponded with increased oxidative stress and inflammation. This observation is consistent with the significant cardiac damage caused by iron overload, whereby matrix remodelling plays a role in cardiovascular pathophysiology. Pre-treatment with SDG abrogated the significant increase in iron-induced MMP-2 and -9 expressions, maintaining it at near control levels.

Antioxidants scavenge ROS to achieve cellular redox balance. Previous studies have reported the levels of antioxidants, SOD and GSH, to be increased while GPx to be decreased in cardiac iron overload [157; 158; 159]. GSR is important for maintaining the reduced glutathione levels, and SOD2 catalyzes the dismutation of superoxide anion to H<sub>2</sub>O<sub>2</sub> [145]. Prdx6 is involved in redox regulation and decomposes H<sub>2</sub>O<sub>2</sub>, hydroperoxide and peroxynitrite; and its expression is increased in response to H<sub>2</sub>O<sub>2</sub> [160; 161]. In the present study, we too have shown an increase in antioxidant expression in response to iron, indicating a robust antioxidant response to the observed iron-induced elaboration of ROS. However, although these results indicate significant pro- and antioxidant redox changes in response to iron, a net oxidizing effect is likely given that this concentration of iron was cytotoxic to the H9c2 cells. This is further supported with pre-treatment with SDG plus iron treatment, which was near normal control levels. Interestingly, treatment with just SDG caused a significant increase in SOD2 expression when compared to

control and iron treatment, respectively. Antioxidant changes in cardiac iron overload was also investigated by measuring the concentration of SOD. Iron treatment caused a decrease in SOD concentration, which was abrogated by pre-treatment with SDG. In fact, pre-treatment with SDG caused an increase in SOD concentration when compared to control and iron. This further suggests that iron- induced cytotoxicity is ROS related, and that it can be prevented with SDG treatment. Taken together, these findings support the conceptual feasibility of this model of cardiac iron overload in terms of it being an iron-catalyzed, oxidative stress-driven process and that SDG pre-treatment can abrogate iron induced oxidative stress.

Apoptosis is a regulated program of cell death that can be caused by high levels of ROS and is mediated by death receptors in the plasma membrane, the mitochondria, and the endoplasmic reticulum. Two independent pathways may lead to cardiomyocyte apoptosis; intrinsic and extrinsic apoptosis. Both pathways end with the cleavage and activation of executioner caspases 3 and 7 [96; 97]. We showed a significant increase in activated caspase 3/7 in iron treated cells. Pre-treatment with SDG abrogated the significant increase in iron-induced apoptosis, maintaining it at near control levels. To further investigate the iron-induced apoptosis, Caspase 3, FOXO3, Bax, and Bcl2 protein expression was assessed via immunoblotting. FOXO3 acts as a transcription factor known to play important roles in the regulation of apoptosis, while Bax can open mitochondrial channels leading to the release of cytochrome c [96; 97; 107]. Caspase 3, FOXO3 and Bax protein expression was significantly increased after 24 hour iron treatment when compared to control. Pre-treatment with SDG abrogated the significant increase in iron-induced Caspase 3, FOXO3 and Bax protein expression. Bcl2 protein

expression did not change significantly after 24 hour iron treatment when compared to control. Pre-treatment with SDG lead to a significant increase in Bcl2 protein expression when compared to control and iron treatment. Taken together, these data indicate concomitant iron-induced increases in apoptosis and a better understanding into the mechanism of action of SDG in preventing apoptosis caused by iron overload.

Autophagy is the lysosomal degradation of proteins and organelles. In the heart, autophagy functions predominantly as a pro-survival pathway during cellular stress by removing protein aggregates and damaged organelles. When severely triggered the autophagic machinery may lead to cell death [97; 110]. Microtubule-associated proteins light chain 3 (MAP1lc3B) is a major constituent of the autophagosome, making it a reliable marker for autophagy [162]. mRNA expression of MAP1lc3B, measured via qPCR, was significantly increased with iron treatment. Pre-treatment with SDG abrogated the significant increase in iron-induced MAP1lc3b1expression, maintaining it at near control levels. The precise role of autophagy in cardiac iron overload remains to be explored.

Cardiac hypertrophy occurs in response to oxidative stress, which involves activation of p70S6K1 [130]. p70S6K1 protein expression was assessed via immunoblotting and was significantly increased after 24 hour iron treatment when compared to control. Pre-treatment with SDG abrogated the significant increase in iron-induced p70S6K1 protein expression, maintaining it at near-normal, control levels. This suggests that iron overload may play a role in cardiac hypertrophy that can be prevented by pre-treatment with SDG. AMPK reserves cellular energy content and serves as a key regulator of cell survival in response to pathological stress. AMPK protein expression

was assessed via immunoblotting and protein expression and was found to be significantly decreased after iron treatment when compared to control levels. Pre-treatment with SDG abrogated the significant decrease in iron-induced AMPK protein expression. This suggests SDG can promote cell survival in cardiac iron overload.

We found that iron treatment of cardiac H9c2 cells caused increased oxidative stress, inflammation and cell death. This was observed by measuring increases in ROS, inflammatory cytokine expression, expression of antioxidants and remodelling proteins, apoptosis, autophagy and hypertrophy markers and decreases in cell survival proteins. SDG abrogated the observed increases in cellular damage and promoted cell survival, suggesting an impressive, heretofore unknown cardioprotective role for this flaxseed antioxidant in cardiac iron overload condition.

## Conclusion

Cardiac iron overload directly correlates with cardiac dysfunction and may ultimately cause heart failure. Cardiac dysfunction is likely caused by a combination of oxidative stress and inflammation, which can lead to cell death. SDG is an antioxidant phytochemical present in flax seeds that has been shown to prevent the development of hypercholesterolemic atherosclerosis, induce angiogenesis-mediated cardioprotection and prevent the development of Type 1 diabetes. Here we investigated the role of SDG on markers of oxidative stress, inflammation, cell death and autophagy. The results of these *in vitro* studies demonstrated that H9c2 rat cardiac cell were susceptible to iron overload, as evidenced by redox and inflammatory imbalance, increased remodeling and antioxidant expression, and increased apoptosis. Pre-treatment with SDG abrogated the detrimental effects of iron overload, suggesting a possible role for SDG as a cardioprotective agent in iron overload condition

## References

- [1] Oudit, G. Y., Trivieri, M. G., Khaper, N., Liu, P. P., & Backx, P. H. (2006). Role of L-type Ca<sup>2+</sup> channels in iron transport and iron-overload cardiomyopathy. *Journal of Molecular Medicine (Berlin, Germany)*, 84(5), 349-364.
- [2] Andrews, N. C. (1999). Disorders of iron metabolism. *The New England Journal of Medicine*, 341(26), 1986-1995.
- [3] Murphy, C. J., & Oudit, G. Y. (2010). Iron-overload cardiomyopathy: Pathophysiology, diagnosis, and treatment. *Journal of Cardiac Failure*, 16(11), 888-900.
- [4] Shawky M., Khaper N., & Liu P. (2003). Oxygen free radicals, iron, and cytokines in heart failure: From bench to bedside. *Oxidative Stress and Cardiac Failure. Armk, NY: Futura Publishing Co., Inc.* 129-151.
- [5] Esposito, B., Breuer, W., Sirankapracha, P., Pootrakul, P., & Hershko, C. (2003). Labile plasma iron in iron overload: Redox activity and susceptibility to chelation. *Blood*, 102(7), 2670-2677.
- [6] Hentze, M. W., Muckenthaler, M. U., & Andrews, N. C. (2004). Balancing acts: Molecular control of mammalian iron metabolism. *Cell*, 117(3), 285-297.
- [7] Shander, A., Cappellini, M. D., & Goodnough, L. T. (2009). Iron overload and toxicity: The hidden risk of multiple blood transfusions. *Vox Sanguinis*, 97(3), 185-197.
- [8] Sharp, P., & Srail, S. (2007). Molecular mechanisms involved in intestinal iron absorption. *World Journal of Gastroenterology*, 13(35), 4716-4724.

- [9] Pietrangelo, A. (2004). Hereditary hemochromatosis--a new look at an old disease. *The New England Journal of Medicine*, 350(23), 2383-2397.
- [10] Oudit, G., Sun, H., Trivieri, M., Koch, S., & Dawood, F. (2003). L-type Ca<sup>2</sup> channels provide a major pathway for iron entry into cardiomyocytes in iron-overload cardiomyopathy. *Nature Medicine*, 9(9), 1187-1194.
- [11] Ganz, T. (2007). Molecular control of iron transport. *Journal of the American Society of Nephrology*, 18(2), 394-400.
- [12] Gunshin, H., Allerson, C., Polycarpou Schwarz, M., Rofts, A., & Rogers, J. (2001). Iron-dependent regulation of the divalent metal ion transporter. *FEBS Letters*, 509(2), 309-316.
- [13] Ke, Y., Chen, Y., Chang, Y., Duan, X., & Ho, K. (2003). Post-transcriptional expression of DMT1 in the heart of rat. *Journal of Cellular Physiology*, 196(1), 124-130.
- [14] MediaFocus guide. Preview of the Medifocus Guidebook on:Hereditary Hemochromatosis Updated September 14, 2010; Medifocus.com
- [15] Rochette, J., Pointon, J., Fisher, C., Perera, G., & Arambepola, M. (1999). Multicentric origin of hemochromatosis gene (HFE) mutations. *American Journal of Human Genetics*, 64(4), 1056-1062.
- [16] Britton, R., Leicester, K., & Bacon, B. (2002). Iron toxicity and chelation therapy. *International Journal of Hematology*, 76(3), 219-228.
- [17] Bottomley S. (2001). Iron overload in sideroblastic and other non-thalassemic

- anemias. In: Barton JC, Edwards CQ (eds) Hemochromatosis: genetics, pathophysiology, diagnosis, and treatment. Cambridge University Press, Cambridge, 442–467.
- [18] Tsushima, R. G., Wickenden, A. D., Bouchard, R. A., Oudit, G. Y., Liu, P. P., & Backx, P. H. (1999). Modulation of iron uptake in heart by L-type Ca<sup>2</sup> channel modifiers: Possible implications in iron overload. *Circulation Research*, 84(11), 1302-1309.
- [19] Brittenham, G. M., Griffith, P. M., Nienhuis, A. W., McLaren, C. E., Young, N. S., Tucker, E. E., et al. (1994). Efficacy of deferoxamine in preventing complications of iron overload in patients with thalassemia major. *The New England Journal of Medicine*, 331(9), 567-573.
- [20] Oudit, G., Trivieri, M., Khaper, N., Husain, T., Wilson, G., Liu, P., et al. (2004). Taurine supplementation reduces oxidative stress and improves cardiovascular function in an iron-overload murine model. *Circulation*, 109(15), 1877-1885.
- [21] Wood, J. (2008). Cardiac iron across different transfusion-dependent diseases. *Blood Reviews*, 22 Suppl 2, S14-S21.
- [22] Buja, L. M., & Roberts, W. C. (1971). Iron in the heart. etiology and clinical significance. *The American Journal of Medicine*, 51(2), 209-221.
- [23] Templeton, D., & Liu, Y. (2003). Genetic regulation of cell function in response to iron overload or chelation. *Biochimica Et Biophysica Acta*, 1619(2), 113-124.
- [24] Randell, E. W., Parkes, J. G., Olivieri, N. F., & Templeton, D. M. (1994). Uptake of

non-transferrin-bound iron by both reductive and nonreductive processes is modulated by intracellular iron. *Journal of Biological Chemistry*, 269(23), 16046-16053.

- [25] Parkes, J. G., Olivieri, N. F., & Templeton, D. M. (1997). Characterization of Fe<sup>2+</sup> and Fe<sup>3+</sup> transport by iron-loaded cardiac myocytes. *Toxicology*, 117(2-3), 141-151.
- [26] Porter, J. (2001). Practical management of iron overload. *British Journal of Haematology*, 115(2), 239-252.
- [27] Jensen, P. (2004). Evaluation of iron overload. *British Journal of Haematology*, 124(6), 697-711.
- [28] Olson, L. J., Edwards, W. D., Holmes, D. R., Miller, F. A., Nordstrom, L. A., & Baldus, W. P. (1989). Endomyocardial biopsy in hemochromatosis: Clinicopathologic correlates in six cases. *Journal of the American College of Cardiology*, 13(1), 116-120.
- [29] Sarsour, E., Kumar, M., Chaudhuri, L., Kalen, A., & Goswami, P. (2009). Redox control of the cell cycle in health and disease. *Antioxidants Redox Signalling*, 11(12), 2985-3011.
- [30] Khaper, N., Palace, V., Hill, M., Kumar, D., & Singal, P. (1999). Heart failure: A failed adaptation to oxidative stress. *Adaptation Biology and Medicine*, (2), 13-28.
- [31] Singal, P., Hill, M. F., Ganguly, N. K., Khaper, N., Krishenbaum, L. A., & Pichardo, J. (1996). Role of oxidative stress in heart failure subsequent to myocardial infarction. *L'information Cardiologique*, 20(9), 343-362.
- [32] Byrne, J., Grieve, D., Cave, A., & Shah, A. (2003). Oxidative stress and heart

- failure. *Archives Des Maladies Du Coeur Et Des Vaisseaux*, 96(3), 214-221.
- [33] Giordano, F. (2005). Oxygen, oxidative stress, hypoxia, and heart failure. *The Journal of Clinical Investigation*, 115(3), 500-508.
- [34] Chien, K. (1999). Stress pathways and heart failure. *Cell*, 98(5), 555-558.
- [35] Khaper, N., & Singal, P. (1997). Effects of afterload-reducing drugs on pathogenesis of antioxidant changes and congestive heart failure in rats. *Journal of the American College of Cardiology*, 29(4), 856-861.
- [36] Asimakis, G., Lick, S., & Patterson, C. (2002). Postischemic recovery of contractile function is impaired in SOD2( -/-) but not SOD1( -/-) mouse hearts. *Circulation*, 105(8), 981-986.
- [37] Nian, M., Lee, P., Khaper, N., & Liu, P. (2004). Inflammatory cytokines and postmyocardial infarction remodeling. *Circulation Research*, 94(12), 1543-1553.
- [38] Kaur, K., Dhingra, S., Slezak, J., Sharma, A., Bajaj, A., & Singal, P. (2009). Biology of TNFalpha and IL-10, and their imbalance in heart failure. *Heart Failure Reviews*, 14(2), 113-123.
- [39] Meldrum, D. R., Dinarello, C. A., Cleveland, J. C., Cain, B. S., Shames, B. D., Meng, X., et al. (1998). Hydrogen peroxide induces tumor necrosis factor alpha-mediated cardiac injury by a P38 mitogen-activated protein kinase-dependent mechanism. *Surgery*, 124(2), 291-6.
- [40] Nakamura, K., Fushimi, K., Kouchi, H., Mihara, K., Miyazaki, M., Ohe, T., et al. (1998). Inhibitory effects of antioxidants on neonatal rat cardiac myocyte hypertrophy induced by tumor necrosis factor-alpha and angiotensin II. *Circulation*, 98(8), 794-799.

- [41] Kaul, N., Siveskiiliskovic, N., Hill, M., Slezak, J., & Singal, P. (1993). Free-radicals and the heart. *Journal of Pharmacological and Toxicological Methods*, 30(2), 55-67.
- [42] Han, D., Ybanez, M., Ahmadi, S., Yeh, K., & Kaplowitz, N. (2009). Redox regulation of tumor necrosis factor signaling. *Antioxidants Redox Signalling*, 11(9), 2245-2263.
- [43] Idriss, H. T., & Naismith, J. H. (2000). TNF alpha and the TNF receptor superfamily: Structure-function relationship(s). *Microscopy Research and Technique*, 50(3), 184-195.
- [44] Banner, D., Darcy, A., Janes, W., Gentz, R., & Schoenfeld, H. (1993). Crystal-structure of the soluble human 55 kd tnf receptor-human tnf-beta complex - implications for tnf receptor activation. *Cell*, 73(3), 431-445.
- [45] Loetscher, H., Pan, Y. C., Lahm, H. W., Gentz, R., Brockhaus, M., Tabuchi, H., et al. (1990). Molecular cloning and expression of the human 55 kd tumor necrosis factor receptor. *Cell*, 61(2), 351-359.
- [46] Smith, C. A., Davis, T., Anderson, D., Solam, L., Beckmann, M. P., Jerzy, R., et al. (1990). A receptor for tumor necrosis factor defines an unusual family of cellular and viral proteins. *Science*, 248(4958), 1019-1023.
- [47] Vandenamee, P., Declercq, W., Beyaert, R., & Fiers, W. (1995). Two tumour necrosis factor receptors: Structure and function. *Trends in Cell Biology*, 5(10), 392-399.
- [48] Chen, G., & Goeddel, D. (2002). TNF-R1 signaling: A beautiful pathway. *Science*, 296(5573), 1634-1635.

- [49] Kapadia, S., Dibbs, Z., Kurrelmeyer, K., Kalra, D., Seta, Y., Wang, F., et al. (1998). The role of cytokines in the failing human heart. *Cardiology Clinics*, 16(4), 645-56, viii.
- [50] Rauchhaus, M., Coats, A., & Anker, S. (2000). The endotoxin-lipoprotein hypothesis. *Lancet*, 356(9233), 930-933.
- [51] Kaur, K., Sharma, A., Dhingra, S., & Singal, P. (2006). Interplay of TNF-alpha and IL-10 in regulating oxidative stress in isolated adult cardiac myocytes. *Journal of Molecular and Cellular Cardiology*, 41(6), 1023-1030.
- [52] Bolger, A., Sharma, R., von Haehling, S., Doehner, W., Oliver, B., Rauchhaus, M., et al. (2002). Effect of interleukin-10 on the production of tumor necrosis factor-alpha by peripheral blood mononuclear cells from patients with chronic heart failure. *The American Journal of Cardiology*, 90(4), 384-389.
- [53] Moore, K., Malefyt, R., Coffman, R., & O'Garra, A. (2001). Interleukin-10 and the interleukin-10 receptor. *Annual Review of Immunology*, 19(1), 683-765.
- [54] Finbloom, D. S., & Winestock, K. D. (1995). IL-10 induces the tyrosine phosphorylation of tyk2 and Jak1 and the differential assembly of STAT1 alpha and STAT3 complexes in human T cells and monocytes. *The Journal of Immunology*, 155(3), 1079-1090.
- [55] van der Poll, T., Marchant, A., Buurman, W. A., Berman, L., Keogh, C. V., Lazarus, D. D., et al. (1995). Endogenous IL-10 protects mice from death during septic peritonitis. *The Journal of Immunology*, 155(11), 5397-5401.
- [56] Standiford, T. J., Strieter, R. M., Lukacs, N. W., & Kunkel, S. L. (1995).

Neutralization of IL-10 increases lethality in endotoxemia. cooperative effects of macrophage inflammatory protein-2 and tumor necrosis factor. *The Journal of Immunology*, 155(4), 2222-2229.

- [57] Pezzilli, R., Billi, P., Miniero, R., & Barakat, B. (1997). Serum interleukin-10 in human acute pancreatitis. *Digestive Diseases and Sciences*, 42(7), 1469-1472.
- [58] Haddad, J., & Fahlman, C. (2002). Redox- and oxidant-mediated regulation of interleukin-10: An anti-inflammatory, antioxidant cytokine? *Biochemical and Biophysical Research Communications*, 297(2), 163-176.
- [59] Adamopoulos, S., Parissis, J., Paraskevaidis, I., Karatzas, D., Livanis, E., Georgiadis, M., et al. (2003). Effects of growth hormone on circulating cytokine network, and left ventricular contractile performance and geometry in patients with idiopathic dilated cardiomyopathy. *European Heart Journal*, 24(24), 2186-2196.
- [60] El Azab, S. R., Rosseel, P. M. J., de Lange, J. J., Groeneveld, A. B. J., van Strik, R., van Wijk, E. M., et al. (2002). Dexamethasone decreases the pro- to anti-inflammatory cytokine ratio during cardiac surgery. *British Journal of Anaesthesia*, 88(4), 496-501.
- [61] Giomarelli, P., Scolletta, S., Borrelli, E., & Biagioli, B. (2003). Myocardial and lung injury after cardiopulmonary bypass: Role of interleukin (IL)-10. *The Annals of Thoracic Surgery*, 76(1), 117-123.
- [62] Dhingra, S., Sharma, A., Singla, D., & Singal, P. (2007). p38 and ERK1/2 MAPKs

mediate the interplay of TNF-alpha and IL-10 in regulating oxidative stress and cardiac myocyte apoptosis. *American Journal of Physiology.Heart and Circulatory Physiology*, 293(6), H3524-H3531.

- [63] Dabek, J., Kulach, A., Wilczok, T., Mazurek, U., Jakubowski, D., & Gasior, Z. (2007). Transcriptional activity of genes encoding interferon gamma (IFNgamma) and its receptor assessed in peripheral blood mononuclear cells in patients with cardiac syndrome X. *Inflammation*, 30(3-4), 125-129.
- [64] Zhang, P., Chen, Z., Chen, F., Li, M., & Fan, J. (2004). Expression of IFN-gamma and its receptor alpha in the peripheral blood of patients with chronic hepatitis C. *Chinese Medical Journal*, 117(1), 79-82.
- [65] Deb, D., Sassano, A., Lekmine, F., Majchrzak, B., Verma, A., Kambhampati, S., et al. (2003). Activation of protein kinase C delta by IFN-gamma. *The Journal of Immunology*, 171(1), 267-273.
- [66] Allione, A., Bernabei, P., Bosticardo, M., Ariotti, S., Forni, G., & Novelli, F. (1999). Nitric oxide suppresses human T lymphocyte proliferation through IFN-gamma-dependent and IFN-gamma-independent induction of apoptosis. *The Journal of Immunology*, 163(8), 4182-4191.
- [67] Pestka, S. (1997). The interferon receptors. *Seminars in Oncology*, 24(3), 918-940.
- [68] Haus, O. (2000). The genes of interferons and interferon-related factors: Localization and relationships with chromosome aberrations in cancer. *Archivum Immunologiae Et Therapiae Experimentalis*, 48(2), 95-100.
- [69] Chawla Sarkar, M., Lindner, D. J., Liu, Y., Williams, B. R., Sen, G. C., Silverman,

- R. H., et al. (2003). Apoptosis and interferons: Role of interferon-stimulated genes as mediators of apoptosis. *Apoptosis*, 8(3), 237-249.
- [70] Stark, G., Kerr, I., Williams, B., Silverman, R., & Schreiber, R. (1998). How cells respond to interferons. *Annual Review of Biochemistry*, 67(1), 227-264.
- [71] Darnell, J. E., Kerr, I. M., & Stark, G. R. (1994). Jak-STAT pathways and transcriptional activation in response to IFNs and other extracellular signaling proteins. *Science*, 264(5164), 1415-1421.
- [72] Kandasamy, A., & Schulz, R. (2009). Glycogen synthase kinase-3beta is activated by matrix metalloproteinase-2 mediated proteolysis in cardiomyoblasts. *Cardiovascular Research*, 83(4), 698-706.
- [73] Takimoto, E., & Kass, D. (2006). Role of oxidative stress in cardiac hypertrophy and remodeling. *Hypertension*, 49(2), 241-248.
- [74] Siwik, D., & Colucci, W. (2004). Regulation of matrix metalloproteinases by cytokines and reactive oxygen/nitrogen species in the myocardium. *Heart Failure Reviews*, 9(1), 43-51.
- [75] Sorescu, D., & Griendling, K. (2002). Reactive oxygen species, mitochondria, and NAD(P)H oxidases in the development and progression of heart failure. *Congestive Heart Failure*, 8(3), 132-140.
- [76] Spinale, F. G. (2007). Myocardial matrix remodeling and the matrix metalloproteinases: Influence on cardiac form and function. *Physiological Reviews*, 4(87), 1285-1342.
- [77] Ovechkin, A., Tyagi, N., Rodriguez, W., Hayden, M., Moshal, K., & Tyagi, S.

- (2005). Role of matrix metalloproteinase-9 in endothelial apoptosis in chronic heart failure in mice. *Journal of Applied Physiology*, 99(6), 2398-2405.
- [78] Li, Y. Y., Feng, Y. Q., Kadokami, T., McTiernan, C. F., Draviam, R., Watkins, S. C., et al. (2000). Myocardial extracellular matrix remodeling in transgenic mice overexpressing tumor necrosis factor alpha can be modulated by anti-tumor necrosis factor alpha therapy. *Proceedings of the National Academy of Sciences of the United States of America*, 97(23), 12746-12751.
- [79] Li, S., Li, X., & Rozanski, G. (2003). Regulation of glutathione in cardiac myocytes. *Journal of Molecular and Cellular Cardiology*, 35(9), 1145-1152.
- [80] Barhoumi, R., Bailey, R. H., & Burghardt, R. C. (1995). Kinetic analysis of glutathione in anchored cells with monochlorobimane. *Cytometry*, 19(3), 226-234.
- [81] Deneke, S. (2000). Thiol-based antioxidants. *Current Topics in Cellular Regulation*, 36(36), 151-180.
- [82] Meister, A., & Anderson, M. (1983). Glutathione. *Annual Review of Biochemistry*, 52(1), 711-760.
- [83] Sen, C. (2000). Cellular thiols and redox-regulated signal transduction. *Current Topics in Cellular Regulation*, 36(36), 1-30.
- [84] Verma, A., Hill, M., Bhayana, S., Pichardo, J., Singal, P.K. (1997). Role of glutathione in acute myocardial adaptation. *Adaptation Biology and Medicine*, (1), 399-408.
- [85] Ceconi, C., Bernocchi, P., Boraso, A., Cargnoni, A., Pepi, P., Curello, S., et al. (2000). New insights on myocardial pyridine nucleotides and thiol redox state in ischemia and reperfusion damage. *Cardiovascular Research*, 47(3), 586-594.

- [86] Vlamis Gardikas, A., & Holmgren, A. (2002). Thioredoxin and glutaredoxin isoforms. *Protein Sensors and Reactive Oxygen Species, PT A, Selenoproteins and Thioredoxin*, 347, 286-296.
- [87] Myers, M. L., Bolli, R., Lekich, R. F., Hartley, C. J., & Roberts, R. (1985). Enhancement of recovery of myocardial function by oxygen free-radical scavengers after reversible regional ischemia. *Circulation*, 72(4), 915-921.
- [88] Jolly, S. R., Kane, W. J., Bailie, M. B., Abrams, G. D., & Lucchesi, B. R. (1984). Canine myocardial reperfusion injury. Its reduction by the combined administration of superoxide dismutase and catalase. *Circulation Research*, 54(3), 277-285.
- [89] Werns, S. W., Shea, M. J., Driscoll, E. M., Cohen, C., Abrams, G. D., Pitt, B., & Lucchesi, B. R. (1985). The independent effects of oxygen radical scavengers on canine infarct size reduction by superoxide dismutase and not catalase. *Circulation Research*, 56(6), 895-898.
- [90] McCord, J. M., & Fridovich, I. (1969). Superoxide dismutase. an enzymic function for erythrocyte hemocuprein (hemocuprein). *Journal of Biological Chemistry*, 244(22), 6049-6055.
- [91] Nagy, N., Malik, G., Fisher, A., & Das, D. (2006). Targeted disruption of peroxiredoxin 6 gene renders the heart vulnerable to ischemia-reperfusion injury. *American Journal of Physiology. Heart and Circulatory Physiology*, 291(6), H2636-H2640.
- [92] Fisher, A., Dodia, C., Feinstein, S., & Ho, Y. (2005). Altered lung phospholipid

- metabolism in mice with targeted deletion of lysosomal-type phospholipase A2. *Journal of Lipid Research*, 46(6), 1248-1256.
- [93] Manevich, Y., & Fisher, A. (2005). Peroxiredoxin 6, a 1-cys peroxiredoxin, functions in antioxidant defense and lung phospholipid metabolism. *Free Radical Biology Medicine*, 38(11), 1422-1432.
- [94] Wang, X., Phelan, S., Forsman Semb, K., Taylor, E., Petros, C., Brown, A., et al. (2003). Mice with targeted mutation of peroxiredoxin 6 develop normally but are susceptible to oxidative stress. *Journal of Biological Chemistry*, 278(27), 25179-25190.
- [95] Fellstrom, B., & Zezina, L. (2001). Apoptosis: Friend or foe? *Transplantation Proceedings*, 33(3), 2414-2416.
- [96] Kumar, D., & Jugdutt, B. I. (2003). Apoptosis and oxidants in the heart. *Journal of Laboratory and Clinical Medicine*, 142(5), 288-296.
- [97] Lee, Y., & Gustafsson, A. (2009). Role of apoptosis in cardiovascular disease. *Apoptosis*, 14(4), 536-548.
- [98] Eaton, J., & Qian, M. (2002). Molecular bases of cellular iron toxicity. *Free Radical Biology Medicine*, 32(9), 833-840.
- [99] Cooper, J. M., & Schapira, A. H. V. (2003). Friedreich's ataxia: Disease mechanisms, antioxidant and coenzyme Q10 therapy. *BioFactors*, 18(1-4), 163-171.
- [100] Sayen, M. R., Gustafsson, A., Sussman, M., Molkenin, J., & Gottlieb, R. (2003).

Calcineurin transgenic mice have mitochondrial dysfunction and elevated superoxide production. *American Journal of Physiology. Cell Physiology*, 284(2), C562-C570.

- [101] Kubota, T., McTiernan, C. F., Frye, C. S., Slawson, S. E., Lemster, B. H., Koretsky, A. P., et al. (1997). Dilated cardiomyopathy in transgenic mice with cardiac-specific overexpression of tumor necrosis factor-alpha. *Circulation Research*, 81(4), 627-635.
- [102] Bryant, D., Becker, L., Richardson, J., Shelton, J., Franco, F., Peshock, R., et al. (1998). Cardiac failure in transgenic mice with myocardial expression of tumor necrosis factor-alpha. *Circulation*, 97(14), 1375-1381.
- [103] Li, P., Nijhawan, D., Budihardjo, I., Srinivasula, S. M., Ahmad, M., Alnemri, E. S., et al. (1997). Cytochrome c and dATP-dependent formation of apaf-1/caspase-9 complex initiates an apoptotic protease cascade. *Cell*, 91(4), 479-489.
- [104] Acehan, D., Jiang, X., Morgan, D., Heuser, J., Wang, X., & Akey, C. (2002). Three-dimensional structure of the apoptosome: Implications for assembly, procaspase-9 binding, and activation. *Molecular Cell*, 9(2), 423-432.
- [105] Pacher, P., & Szab, C. (2007). Role of poly(ADP-ribose) polymerase 1 (PARP-1) in cardiovascular diseases: The therapeutic potential of PARP inhibitors. *Cardiovascular Drug Reviews*, 25(3), 235-260.
- [106] Ashkenazi, A., & Dixit, V. (1998). Death receptors: Signaling and modulation. *Science*, 281(5381), 1305-1308.
- [107] Ronnebaum, S., & Patterson, C. (2010). The FoxO family in cardiac function and dysfunction. *Annual Review of Physiology*, 72(1), 81-94.

- [108] Sengupta, A., Molkenin, J., Paik, J., DePinho, R., & Yutzey, K. (2011). FoxO transcription factors promote cardiomyocyte survival upon induction of oxidative stress. *Journal of Biological Chemistry*, 286(9), 7468-7478.
- [109] Fu, Z., & Tindall, D. J. (2008). FOXOs, cancer and regulation of apoptosis. *Oncogene*, 27(16), 2312-2319.
- [110] Gurusamy, N., & Das, D. (2009). Autophagy, redox signaling, and ventricular remodeling. *Antioxidants Redox Signalling*, 11(8), 1975-1988.
- [111] Cuervo, A. (2004). Autophagy: Many paths to the same end. *Molecular and Cellular Biochemistry*, 263(1/2), 55-72.
- [112] Juhasz, G., & Neufeld, T. (2006). Autophagy: A forty-year search for a missing membrane source. *PLoS Biology*, 4(2), 136-164.
- [113] Pattingre, S., Espert, L., Biard Piechaczyk, M., & Codogno, P. (2008). Regulation of macroautophagy by mTOR and beclin 1 complexes. *Biochimie*, 90(2), 313-323.
- [114] Bruno, P., Calastretti, A., Priulla, M., Asnaghi, L., Scarlatti, F., Nicolin, A., et al. (2007). Cell survival under nutrient stress is dependent on metabolic conditions regulated by akt and not by autophagic vacuoles. *Cellular Signalling*, 19(10), 2118-2126.
- [115] Goswami, S., & Das, D. (2006). Autophagy in the myocardium: Dying for survival? *Experimental and Clinical Cardiology*, 11(3), 183-188.
- [116] Takagi, H., Matsui, Y., & Sadoshima, J. (2007). The role of autophagy in mediating cell survival and death during ischemia and reperfusion in the heart. *Antioxidants Redox Signalling*, 9(9), 1373-1381.
- [117] Baehrecke, E. (2005). Autophagy: Dual roles in life and death? *Nature*

*Reviews.Molecular Cell Biology*, 6(6), 505-510.

- [118] Codogno, P., & Meijer, A. J. (2005). Autophagy and signaling: Their role in cell survival and cell death. *Cell Death and Differentiation*, 12 Suppl 2, 1509-1518.
- [119] Scarlatti, F., Granata, R., Meijer, A. J., & Codogno, P. (2009). Does autophagy have a license to kill mammalian cells? *Cell Death and Differentiation*, 16(1), 12-20.
- [120] Hamacher Brady, A., Brady, N. R., Logue, S. E., Sayen, M. R., Jinno, M., Kirshenbaum, L. A., et al. (2007). Response to myocardial ischemia/reperfusion injury involves Bnip3 and autophagy. *Cell Death and Differentiation*, 14(1), 146-157.
- [121] Matsui, Y., Takagi, H., Qu, X., Abdellatif, M., Sakoda, H., Asano, T., et al. (2007). Distinct roles of autophagy in the heart during ischemia and reperfusion: Roles of AMP-activated protein kinase and beclin 1 in mediating autophagy. *Circulation Research*, 100(6), 914-922.
- [122] Yan, L., Vatner, D., Kim, S., Ge, H., Masurekar, M., Massover, W., et al. (2005). Autophagy in chronically ischemic myocardium. *Proceedings of the National Academy of Sciences of the United States of America*, 102(39), 13807-13812.
- [123] Hamacher Brady, A., Brady, N., & Gottlieb, R. (2006). Enhancing macroautophagy protects against ischemia/reperfusion injury in cardiac myocytes. *Journal of Biological Chemistry*, 281(40), 29776-29787.
- [124] De Meyer, G. R. Y., & Martinet, W. (2009). Autophagy in the cardiovascular system. *Biochimica Et Biophysica Acta.Molecular Cell Research*, 1793(9), 1485-1495.

- [125] Decker, R. S., & Wildenthal, K. (1980). Lysosomal alterations in hypoxic and reoxygenated hearts. I. ultrastructural and cytochemical changes. *The American Journal of Pathology*, 98(2), 425-444.
- [126] Matsui, Y., Kyoji, S., Takagi, H., Hsu, C., Hariharan, N., Ago, T., et al. (2008). Molecular mechanisms and physiological significance of autophagy during myocardial ischemia and reperfusion. *Autophagy*, 4(4), 409-415.
- [127] Bogoyevitch, M. A., Gillespie Brown, J., Ketterman, A. J., Fuller, S. J., Ben Levy, R., Ashworth, A., et al. (1996). Stimulation of the stress-activated mitogen-activated protein kinase subfamilies in perfused heart. p38/RK mitogen-activated protein kinases and c-jun N-terminal kinases are activated by ischemia/reperfusion. *Circulation Research*, 79(2), 162-173.
- [128] Yousefi, S., Perozzo, R., Schmid, I., Ziemiecki, A., Schaffner, T., Scapozza, L., et al. (2006). Calpain-mediated cleavage of Atg5 switches autophagy to apoptosis. *Nature Cell Biology*, 8(10), 1124-1132.
- [129] Pyo, J., Jang, M., Kwon, Y., Lee, H., Jun, J., Woo, H., et al. (2005). Essential roles of Atg5 and FADD in autophagic cell death: Dissection of autophagic cell death into vacuole formation and cell death. *Journal of Biological Chemistry*, 280(21), 20722-20729.
- [130] Tu, V., Bahl, J., & Chen, Q. (2002). Signals of oxidant-induced cardiomyocyte hypertrophy: Key activation of p70 S6 kinase-1 and phosphoinositide 3-kinase. *The Journal of Pharmacology and Experimental Therapeutics*, 300(3), 1101-1110.
- [131] Dufner, A., & Thomas, G. (1999). Ribosomal S6 kinase signaling and the control

- of translation. *Experimental Cell Research*, 253(1), 100-109.
- [132] Arad, M., Seidman, C., & Seidman, J. G. (2007). AMP-activated protein kinase in the heart: Role during health and disease. *Circulation Research*, 100(4), 474-488.
- [133] da-Silva, C., Jarzyna, R., Specht, A., & Kaczmarek, E. (2006). Extracellular nucleotides and adenosine independently activate AMP-activated protein kinase in endothelial cells: Involvement of P2 receptors and adenosine transporters. *Circulation Research*, 98(5), e39-e47.
- [134] Motoshima, H., Goldstein, B., Igata, M., & Araki, E. (2006). AMPK and cell proliferation-AMPK as a therapeutic target for atherosclerosis and cancer. *Journal of Physiology*, 574(1), 63-71.
- [135] Horman, S., Beauloye, C., Vertommen, D., Vanoverschelde, J., Hue, L., & Rider, M. (2003). Myocardial ischemia and increased heart work modulate the phosphorylation state of eukaryotic elongation factor-2. *Journal of Biological Chemistry*, 278(43), 41970-41976.
- [136] Terai, K., Hiramoto, Y., Masaki, M., Sugiyama, S., Kuroda, T., Hori, M., et al. (2005). AMP-activated protein kinase protects cardiomyocytes against hypoxic injury through attenuation of endoplasmic reticulum stress. *Molecular and Cellular Biology*, 25(21), 9554-9575.
- [137] Hwang, J., Kwon, D., Park, O., & Kim, M. (2008). Resveratrol protects ROS-induced cell death by activating AMPK in H9c2 cardiac muscle cells. *Genes Nutrition*, 2(4), 323-326.
- [138] Adolphe, J., Whiting, S., Juurlink, B. H. J., Thorpe, L., & Alcorn, J. (2010). Health

effects with consumption of the flax lignan secoisolariciresinol diglucoside. *British Journal of Nutrition*, 103(7), 929-938.

- [139] Carreau, C., Flouriot, G., Bennetau Pelissero, C., & Potier, M. (2008). Enterodiol and enterolactone, two major diet-derived polyphenol metabolites have different impact on ERalpha transcriptional activation in human breast cancer cells. *The Journal of Steroid Biochemistry and Molecular Biology*, 110(1-2), 176-185.
- [140] Prasad, K. (2000). Antioxidant activity of secoisolariciresinol diglucoside-derived metabolites, secoisolariciresinol, enterodiol, and enterolactone. *International Journal of Angiology*, 9(4), 220-225.
- [141] Juurlink, B. H. (2001). Therapeutic potential of dietary phase 2 enzyme inducers in ameliorating diseases that have an underlying inflammatory component. *Canadian Journal of Physiology and Pharmacology*, 79(3), 266-282.
- [142] Wang, W., Liu, L. Q., Higuchi, C. M., & Chen, H. (1998). Induction of NADPH : Quinone reductase by dietary phytoestrogens in colonic Colo205 cells. *Biochemical Pharmacology*, 56(2), 189-195.
- [143] Prasad, K. (1997). Hydroxyl radical-scavenging property of secoisolariciresinol diglucoside (SDG) isolated from flax-seed. *Molecular and Cellular Biochemistry*, 168(1-2), 117-123.
- [144] Prasad, K. (2000). Oxidative stress as a mechanism of diabetes in diabetic BB prone rats: Effect of secoisolariciresinol diglucoside (SDG). *Molecular and Cellular Biochemistry*, 209(1-2), 89-96.
- [145] Prasad, K. (2009). Flaxseed and cardiovascular health. *Journal of Cardiovascular Pharmacology*, 54(5), 369-377.

- [146] Penumathsa, S., Koneru, S., Thirunavukkarasu, M., Zhan, L., Prasad, K., & Maulik, N. (2007). Secoisolariciresinol diglucoside: Relevance to angiogenesis and cardioprotection against ischemia-reperfusion injury. *The Journal of Pharmacology and Experimental Therapeutics*, 320(2), 951-959.
- [147] Weatherall, D. J., & Clegg, J. B. (1996). Thalassemia--a global public health problem. *Nature Medicine*, 2(8), 847-849.
- [148] Barton, J. C., & Bertoli, L. F. (1996). Hemochromatosis: The genetic disorder of the twenty-first century. *Nature Medicine*, 2(4), 394-395.
- [149] Ballas, S. K. (2001). Iron overload is a determinant of morbidity and mortality in adult patients with sickle cell disease. *Seminars in Hematology*, 38(1 Suppl 1), 30-36.
- [150] Weatherall, D., & Clegg, J. (2001). Inherited haemoglobin disorders: An increasing global health problem. *Bulletin of the World Health Organization*, 79(8), 704-712.
- [151] Liu, P., & Olivieri, N. (1994). Iron overload cardiomyopathies: New insights into an old disease. *Cardiovascular Drugs and Therapy*, 8(1), 101-110.
- [152] Prasad, K. (1997). Hydroxyl radical-scavenging property of secoisolariciresinol diglucoside (SDG) isolated from flax-seed. *Molecular and Cellular Biochemistry*, 168(1-2), 117-123.
- [153] Gao, X., Campian, J., Qian, M., Sun, X., & Eaton, J. (2009). Mitochondrial DNA damage in iron overload. *Journal of Biological Chemistry*, 284(8), 4767-4775.
- [154] Khaper, N., Bryan, S., Dhingra, S., Singal, R., Bajaj, A., Pathak, C., et al. (2010). Targeting the vicious inflammation-oxidative stress cycle for the management of heart failure. *Antioxidants Redox Signalling*, 13(7), 1033-1049.

- [155] Torre Amione, G., Kapadia, S., Lee, J., Bies, R. D., Lebovitz, R., & Mann, D. L. (1995). Expression and functional significance of tumor necrosis factor receptors in human myocardium. *Circulation*, *92*(6), 1487-1493.
- [156] Nishio, R., Matsumori, A., Shioi, T., Ishida, H., & Sasayama, S. (1999). Treatment of experimental viral myocarditis with interleukin-10. *Circulation*, *100*(10), 1102-1108.
- [157] Bartfay, W. J., Butany, J., Lehotay, D. C., Sole, M. J., Hou, D., Bartfay, E., et al. (1999). A biochemical, histochemical, and electron microscopic study on the effects of iron-loading on the hearts of mice. *Cardiovascular Pathology*, *8*(6), 305-314.
- [158] Pucheu, S., Coudray, C., Tresallet, N., Favier, A., & de Leiris, J. (1993). Effect of iron overload in the isolated ischemic and reperfused rat heart. *Cardiovascular Drugs and Therapy*, *7*(4), 701-711.
- [159] Otto Duessel, M., Aguilar, M., Moats, R., & Wood, J. (2007). Antioxidant-mediated effects in a gerbil model of iron overload. *Acta Haematologica*, *118*(4), 193-199.
- [160] Nordberg, J., & Arnér, E. S. (2001). Reactive oxygen species, antioxidants, and the mammalian thioredoxin system. *Free Radical Biology Medicine*, *31*(11), 1287-1312.
- [161] Kalinina, E. V., Chernov, N. N., & Saprin, A. N. (2008). Involvement of thio-, peroxi-, and glutaredoxins in cellular redox-dependent processes. *Biochemistry*, *73*(13), 1493-1510.
- [162] Rzymiski, T., Milani, M., Pike, L., Buffa, F., Mellor, H. R., Winchester, L., et al.

(2010). Regulation of autophagy by ATF4 in response to severe hypoxia.  
*Oncogene*, 29(31), 4424-4435.